ÉCOLE DE TECHNOLOGIE SUPÉRIEURE
UNIVERSITÉ DU QUÉBEC

MÉMOIRE PAR ARTICLES PRÉSENTÉ À
L'ÉCOLE DE TECHNOLOGIE SUPÉRIEURE

COMME EXIGENCE PARTIELLE
À L'OBTENTION DE LA
MAÎTRISE EN GÉNIE MÉCANIQUE
M. Ing.

PAR
Yan BOURGEOIS

RAFFINEMENT D'UNE NOUVELLE PLAQUE TROCHANTERIENNE À L'AIDE DE LA MÉTHODE PAR ÉLÉMENTS FINIS

MONTRÉAL, LE 17 DÉCEMBRE 2010

PRÉSENTATION DU JURY

CE MÉMOIRE A ÉTÉ ÉVALUÉ

PAR UN JURY COMPOSÉ DE :

M. Yvan Petit, directeur de mémoire
Département de génie mécanique à l'École de technologie supérieure

M. Partick Terriault, président du jury
Département de génie mécanique à l'École de technologie supérieure

M. Carl-Éric Aubin, membre du jury
Département de génie mécanique à l'École Polytechnique de Montréal

IL A FAIT L'OBJET D'UNE SOUTENANCE DEVANT JURY ET PUBLIC

LE 13 DÉCEMBRE 2010

À L'ÉCOLE DE TECHNOLOGIE SUPÉRIEURE

REMERCIEMENTS

Je voudrais d'abord remercier mon directeur de maîtrise Yvan Petit pour son appui tout au long de ma maîtrise. Pour m'avoir permis de faire surchauffer un nombre considérable de processeurs. Pour m'avoir donné de la latitude dans mon projet. Pour avoir cru en moi et m'avoir fait confiance durant tout ce temps.

Merci à Vladimir Brailovski de m'avoir accueilli dans ses locaux et d'avoir supporté le projet dans son ensemble par son soutien financier, sont appui moral et son esprit critique.

Merci à Yannick Baril pour ce travail d'équipe. Son expérience et ses conseils ont grandement été appréciés.

Merci aux gens du LIO à l'Hôpital du Sacré-Cœur pour tous ces midis de frisbee et de poker. Merci aussi de toujours m'avoir considéré comme un des vôtres même si j'étais physiquement au LAMSI.

Merci aux gens du LAMSI pour tous ces midis de badminton. Merci aussi de toujours m'avoir considéré comme un des vôtres même si je n'étais pas un membre du LAMSI.

Merci à tous mes partenaires d'escalade qui ont fait en sorte que je puisse me libérer l'esprit durant ces soirées ou ces matins de grimpe.

Merci à mes parents de m'avoir supporté tout le long de mes études et de mes projets…

RAFFINEMENT D'UNE NOUVELLE PLAQUE TROCHANTERIENNE À L'AIDE DE LA MÉTHODE PAR ÉLÉMENTS FINIS

Yan BOURGEOIS

RÉSUMÉ

Le détachement du grand trochanter (GT) peut se produire suite à une fracture ou une ostéotomie. Dans tous les cas, il est impératif de repositionner le fragment et de le stabiliser. Plusieurs techniques de cerclage à l'aide de fils ou de câbles ont été développées dans le passé. De nos jours, les systèmes de plaque et câble sont généralement utilisés pour assurer le maintien du grand trochanter. Or ces systèmes montrent des problématiques de maintien qui peuvent porter en échec la guérison osseuse. Dans le but de réduire cette problématique, un nouveau concept (Y3), utilisant une plaque avec vis et câbles, a été développé dans le cadre d'un stage de recherche antérieure effectué par le candidat.

Les objectifs de ce nouveau système sont d'abord de réduire les mouvements entre le GT et le fémur, mais aussi de fournir un profil le plus bas possible. Un « profil bas » a pour avantage de diminuer la friction entre les muscles et la plaque pouvant ainsi diminuer les risques de bursite et de douleur. La géométrie en « Y » de la plaque contourne la protubérance du GT favorisant un « profil bas ». Or, les dimensions utilisées pour la conception initiale de la plaque semblent être surdimensionnées. L'objectif de ce mémoire est le raffinement des dimensions de la plaque Y3 à l'aide de la méthode par éléments finis.

Le modèle est composé de la partie proximale du fémur avec une ostéotomie du GT et la plaque Y3 utilisant des vis pour maintenir le grand trochanter. En accord avec les essais expérimentaux, la base du fémur est encastrée et des charges sont appliquées sur la tête fémorale et le GT simultanément. Une analyse de la sensibilité des différentes régions de la plaque Y3 sur les déplacements du GT a d'abord été effectuée pour orienter les étapes itératives de raffinement. Par la suite, le modèle a été utilisé pour raffiner les dimensions de la plaque.

La comparaison entre les résultats expérimentaux et numériques a montré que les mouvements du grand trochanter par rapport au fémur vont dans la même direction. Par contre, les déplacements du modèle numérique sont plus faibles que l'expérimentation. Les simplifications du modèle numérique sont probablement à l'origine de cette rigidité. L'étude de sensibilité a permis de déterminer que la région qui lie les branches supérieures à la branche inférieure de l'implant est la plus critique pour les déplacements du grand trochanter. Le raffinement de la plaque, réalisé en 5 itérations, a permis de réduire son épaisseur de 5% pour la région critique et entre 25% et 33% pour les autres régions. Cette diminution pourrait avoir un impact appréciable sur la douleur des patients et sur la probabilité de complication.

Mots-Clés : trochanter, éléments finis, système de rattachement

REFINEMENT OF A NOVEL TROCHANTERIC PLATE USING FINITE ELEMENT MODEL

Yan BOURGEOIS

ABSTRACT

Greater trochanter (GT) detachment can occur following a fracture or an osteotomy. In all cases, it is imperative to fix the fragment. In the past, different wires or cables cerclage technique were used. Nowadays, cable grip systems are usually used to maintain the GT. But these systems show important issues which can lead to bone healing failure. In order to reduce these problems, a novel concept (Y3) of GT reattachment, using a plate with cable and screw, was developed by the candidate in previous work.

The objective of the Y3 system is to reduce the movement between the GT and the femur but also to provide a low profile. A low profile presents the advantage of decreasing the friction between the muscles and the plate helping, reducing bursitis and pain. The "Y" shape of the plate avoiding the GT protuberance is a key element for its low profile. However, the initial concept of Y3 plate seems to be overdesign. The objective of this thesis is to further refine the Y3 plate design using finite elements method.

The model represents the femur's proximal part with a GT osteotomy and the Y3 plate fixed using screws to maintain the GT. In concordance with experiments used to validate the model, the lower extremity of the femur is fixed and loads are simultaneously applied to the femoral head and the GT. A sensitivity study of different Y3 plate regions to the GT displacements was first achieved to prepare the iterative refinement steps. The model was then used to refine the plate's size and shape.

Validation results suggest a good agreement between experimental and numerical displacement. Numerical simulations predict displacements in the same direction but smaller in amplitude than experiments. The presence of over-constraints due to reducing assumptions may explain in part the rigid behavior of the model. The results show that the most critical region for GT displacement is where the superior and inferior branches merge together. The plate refinement, completed in 5 iterations, allowed a thickness reduction of 5% in the most critical region and between 25% and 33% for other regions. This decrease in size could have a favorable impact on pain and complication for patients.

Keywords: trochanter, finite elements, reattachment system

TABLE DES MATIÈRES

LISTE DES TABLEAUX

Page

LISTE DES FIGURES

Page

LISTE DES ABRÉVIATIONS, SIGLES ET ACRONYMES

CAD	Computer assisted design
CFI	Canadian Foundation for Innovation
CGZ	Système *Cable grip* de la compagnie Zimmer
CT	Computed tomography
FEM	Finite element model
FQRNT	Fond Québecois de la Recherche sur la Nature et les Technologies
GT	Grand trochanter
GTR	Greater trochanter reattachement
LHS	Locking head screws
MÉF	Modèle par éléments finis
NA	Normal angle
NSERC	Natural Science and Engineering Council
RCRA	Registre canadien des remplacements articulaires
RCSYS	Reference coordinates system
ROI	Region of interest
RP	Reference point
SDRB	Standard deviation of rigid body
SF	Security factor
WA	Wide angle

LISTE DES SYMBOLES ET UNITÉS DE MESURE

DISPF	Percent change in GT displacement from the initial design (%)
MODF	Percent change in cross-section area (%)
P1	Load apply on femoral head (N)
P2	Load apply on greater trochanter (N)
SENF	Sensitivity index (%/%)

INTRODUCTION

Le remplacement de l'articulation de la hanche, aussi appelé arthroplastie de la hanche, consiste à remplacer la tête fémorale par une prothèse et à insérer une cupule dans l'acétabulum. Une complication commune à cette intervention est la fracture du grand trochanter (GT) (Pritchett, 2001). Une ostéotomie du GT est aussi effectuée lors de certaines révisions d'arthroplastie de la hanche pour faciliter l'enlèvement de la prothèse primaire. Dans les deux cas (fracture ou ostéotomie), il est impératif que le GT soit remis en place et maintenu en position. Pour ce faire, les chirurgiens favorisent l'utilisation des systèmes de fixation incluant la combinaison d'une plaque et de câbles. Or, les présents systèmes semblent avoir des problèmes de stabilité dans la direction antéropostérieure lors de mouvements complexes tel que la levée d'une chaise. Un manque de stabilité produisant des mouvements relatifs importants entre le fémur et le fragment du GT peut causer la non-union du fragment (Poitout, 2004).

Un nouveau système de maintien du GT (Y3) utilisant des vis, des câbles et une géométrie particulière en forme de « Y » a été développé afin de minimiser les déplacements du GT dans la direction antéropostérieure. En plus de réduire les déplacements antéropostérieurs, le système Y3 favorise un « profil bas » comparativement au système *Cable Grip* de la compagnie *Zimmer* en contournant la protubérance du GT. Ce « profil bas » permettrait de réduire le frottement avec les muscles diminuant ainsi les risques de bursite et la douleur ressentie par les patients. Or, les dimensions de conception initiale de la plaque Y3 sont basées sur des valeurs plus conservatrices que les systèmes présentement utilisés. Ainsi, il pourrait être possible de modifier les dimensions de la plaque afin d'obtenir un profil encore plus réduit du système Y3.

L'objectif de ce mémoire est de raffiner la conception de la plaque Y3 afin de renforcer les parties critiques et d'assouplir les autres de façon à réduire prioritairement l'épaisseur de la plaque. Pour ce faire, un modèle par éléments finis (MÉF), représentant les expérimentations effectuées lors de l'étude de (Baril *et al.*, 2010a), sera développé et validé. De plus, pour permettre un raffinement efficace, une étude de sensibilité des différentes régions de la plaque sur les mouvements du GT sera effectuée.

La Figure 0.1 présente la structure du mémoire. Les flèches pointillées montrent les relations entre les articles en annexes et les articles dans le corps du texte. Dans un premier temps, une revue de la littérature générale permettra de mettre en relief la problématique, les solutions présentement disponibles, le système Y3 et de discuter des présents modèles numériques de plaques fémorales. Dans un deuxième temps, la méthodologie et les résultats seront présentés à l'aide de deux articles (premier auteur) et supportés par deux articles (coauteur) présentés en annexe. Le premier article, décrit le MÉF ainsi qu'une étude de sensibilité de la stabilité du GT au changement de dimensions de la plaque Y3 alors que le deuxième article décrit le raffinement de la plaque Y3. Enfin, une discussion des résultats sera effectuée et une conclusion clôturera le mémoire.

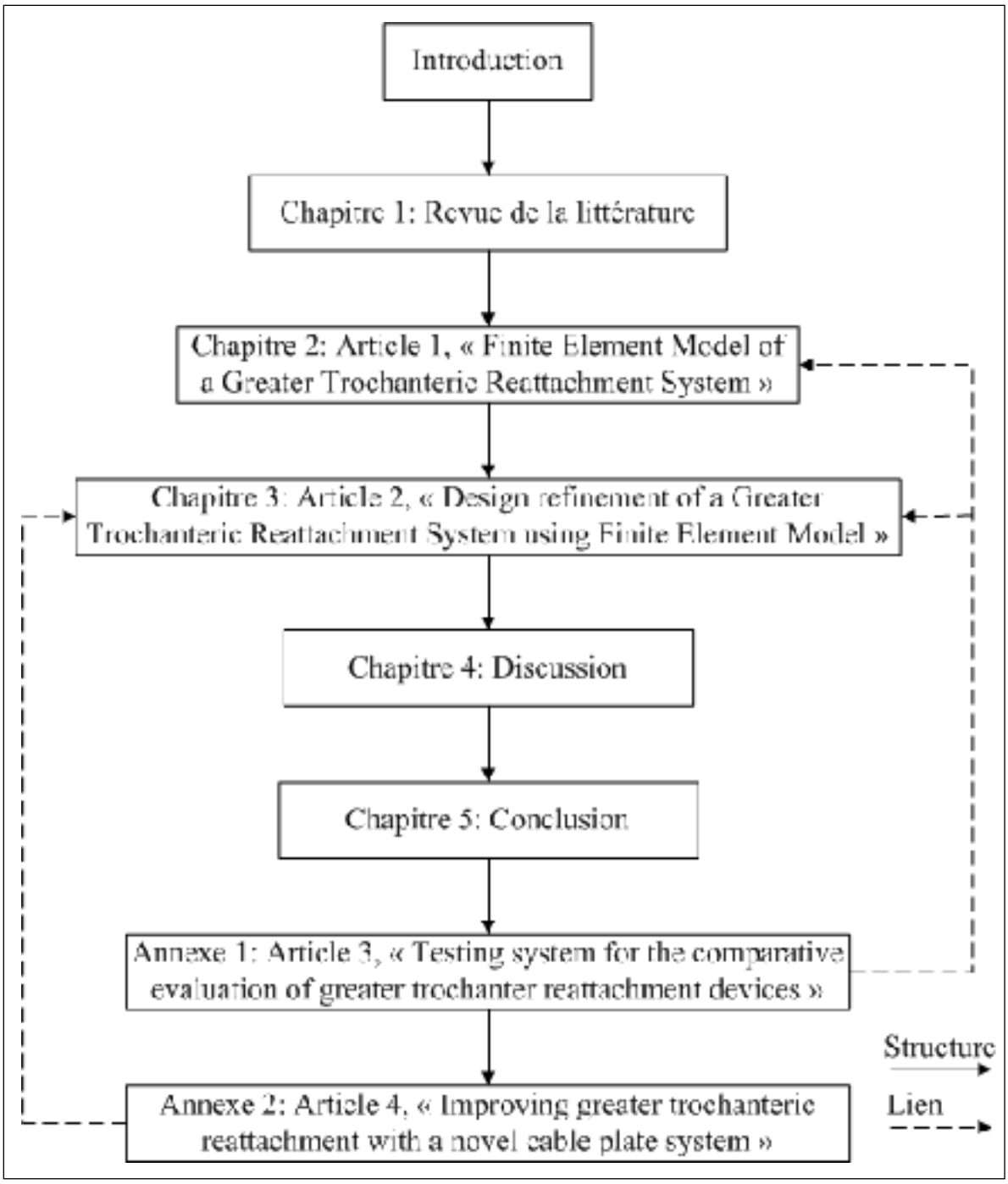

Figure 0.1 Structure du mémoire

CHAPITRE 1

REVUE DE LITTÉRATURE

1.1 Anatomie fonctionnelle de la hanche

L'articulation de la hanche peut se caractériser comme une articulation sphéroïde où la tête fémorale, située dans la partie proximale du fémur, est liée à l'os coxal par sa cavité acétabulaire (Figure 1.1). Il s'agit de l'articulation synoviale offrant la plus grande amplitude de rotation dans tous les plans de l'espace.

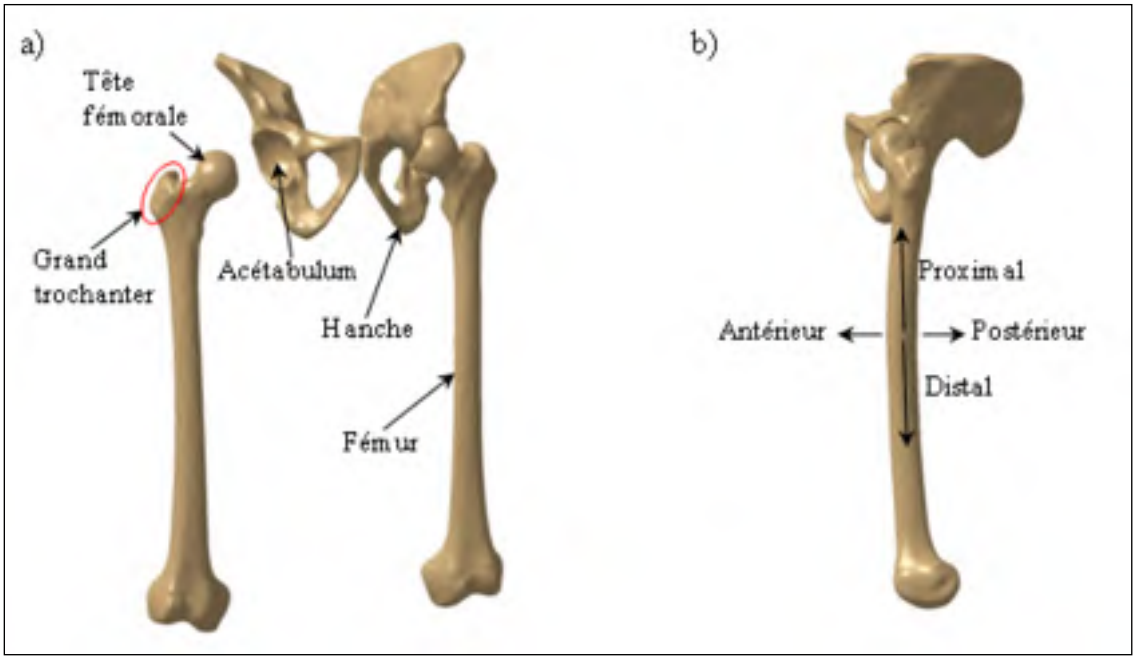

Figure 1.1 a) Région anatomique b) Terminologie spatiale

Différent muscles importants pour le mouvement de la hanche trouvent leur origine sur l'os iliaque et s'insèrent sur le fémur au niveau du grand trochanter (GT) (Figure 1.2). Le moyen fessier et le petit fessier ont comme principale fonction d'assurer le mouvement d'abduction de la hanche mais ils sont aussi sollicités lors des mouvements de flexion et de rotation

interne-externe de la hanche. Ces muscles très puissants peuvent exercer des efforts sur le GT et la tête fémorale de l'ordre de 1 à 3 fois le poids du corps (Heller *et al.*, 2005).

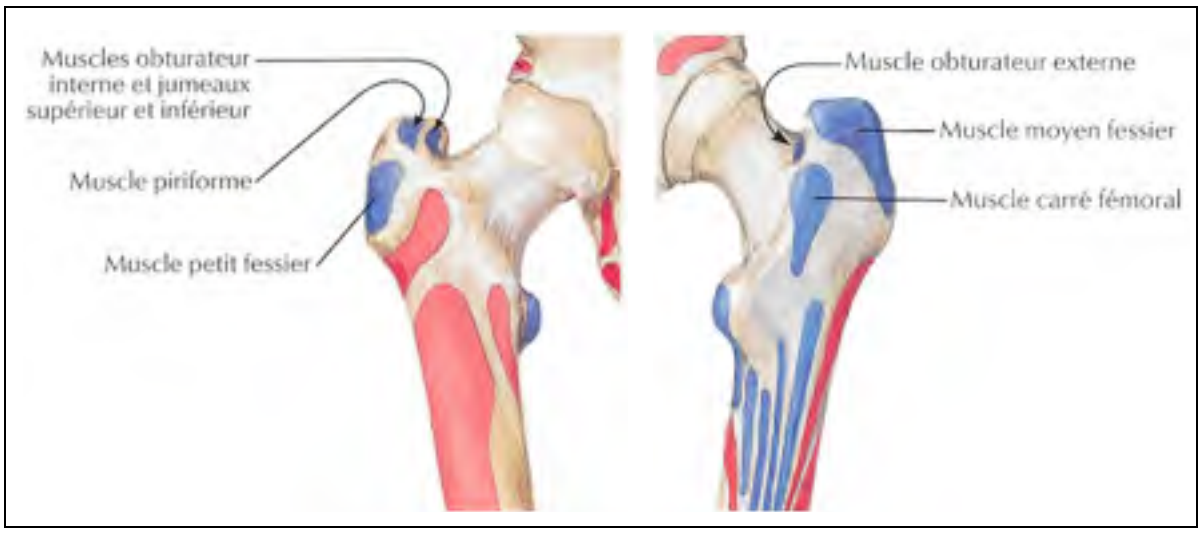

Figure 1.2 Insertion musculaire de la région du GT
Tirée de Netter (2007, pp. 490-491)

1.2 Arthroplastie de la hanche

Selon le Rapport annuel de 2008-2009 du Registre canadien des remplacements articulaires (RCRA) (Institut canadien d'information sur la santé, 2009), 24 253 arthroplasties de la hanche ont été pratiquées en 2006-2007. Cette intervention chirurgicale consiste à remplacer la tête fémorale par une prothèse fémorale et à insérer une cupule dans l'acétabulum (Figure 1.3). Les étapes de cette opération consistent d'abord à faire une incision et couper les muscles afin d'accéder à la partie proximale du fémur. Par la suite, une dislocation de l'articulation de la hanche permet d'accéder à l'acétabulum et à la tête fémorale. L'acétabulum est alors alésé à la dimension de la cupule qui est ensuite fixée. La tête fémorale est retirée du fémur à l'aide d'une scie rotative ou alternative. Un système de râpes permet de former la cavité où la prothèse fémorale y sera ajustée ou cimentée. Il est aussi possible qu'une ostéotomie du GT soit effectuée pour faciliter le positionnement de l'implant (Amstutz, Mai et Schmidt, 1984; Bal *et al.*, 2006; Berry et Muller, 1993; Chin et Brick, 2000;

Lakstein *et al.*, 2009; Nutton et Checketts, 1984). De plus, une complication commune à cette étape est la fracture du grand trochanter (Pritchett, 2001). S'il y a eu détachement du GT, celui-ci est repositionné et rattaché, puis l'articulation est repositionnée et la plaie est refermée.

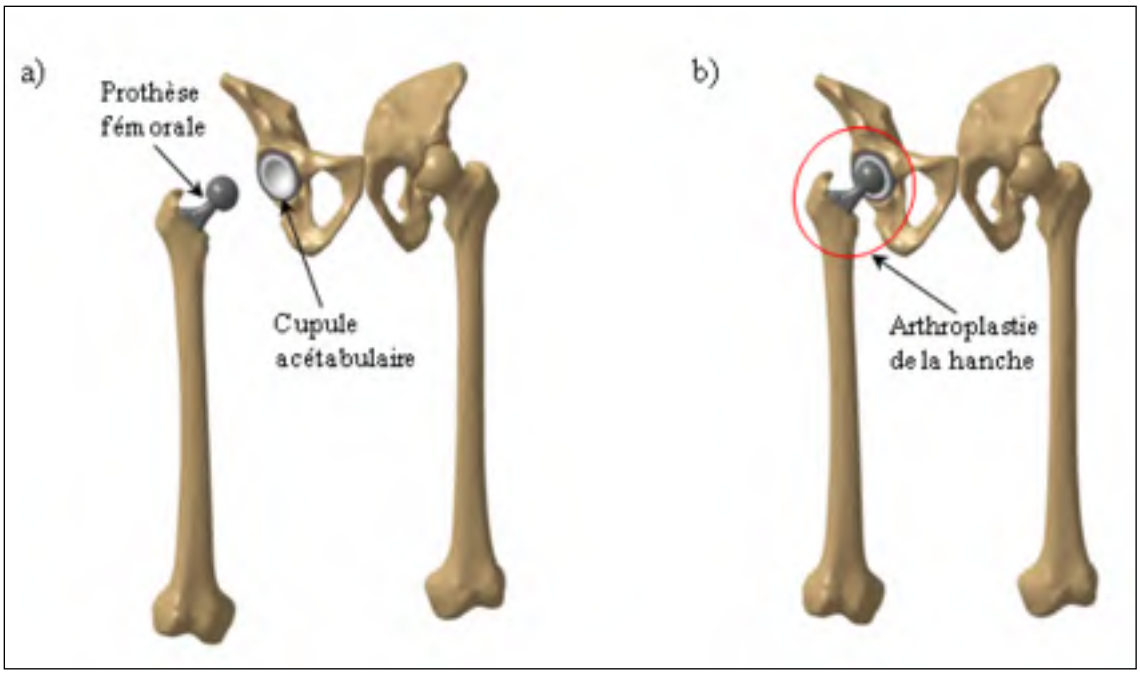

Figure 1.3 a) Composantes de l'arthroplastie de la hanche b) Résultat de l'arthroplastie de la hanche

Selon le RCRA, 13.6 % des arthroplasties de la hanche en 2006-2007 étaient des révisions (Institut canadien d'information sur la santé, 2009). La révision de la hanche peut être nécessaire lors que l'usure des composantes mécaniques nuit au bon fonctionnement de l'articulation ou s'il y a décèlement de la prothèse. La procédure de révision de l'arthroplastie de la hanche s'apparente à la chirurgie primaire, mais l'opération d'ostéotomie de la tête fémorale est remplacée par le retrait de la prothèse. Pour ce faire, les chirurgiens procèdent généralement à une ostéotomie du GT (Figure 1.4). La longueur de l'ostéotomie peut varier selon l'approche du chirurgien et la qualité de l'os disponible lors de la révision. La Figure 1.4a illustre une ostéotomie du GT dite classique alors que la Figure 1.4b est une

ostéotomie étendue du GT (Archibeck *et al.*, 2003). La prothèse fémorale est alors remplacée par une prothèse généralement plus longue et la cupule acétabulaire est aussi remplacée par une composante compatible à la nouvelle prothèse. Finalement, le GT est rattaché, l'articulation est repositionnée et la plaie est refermée.

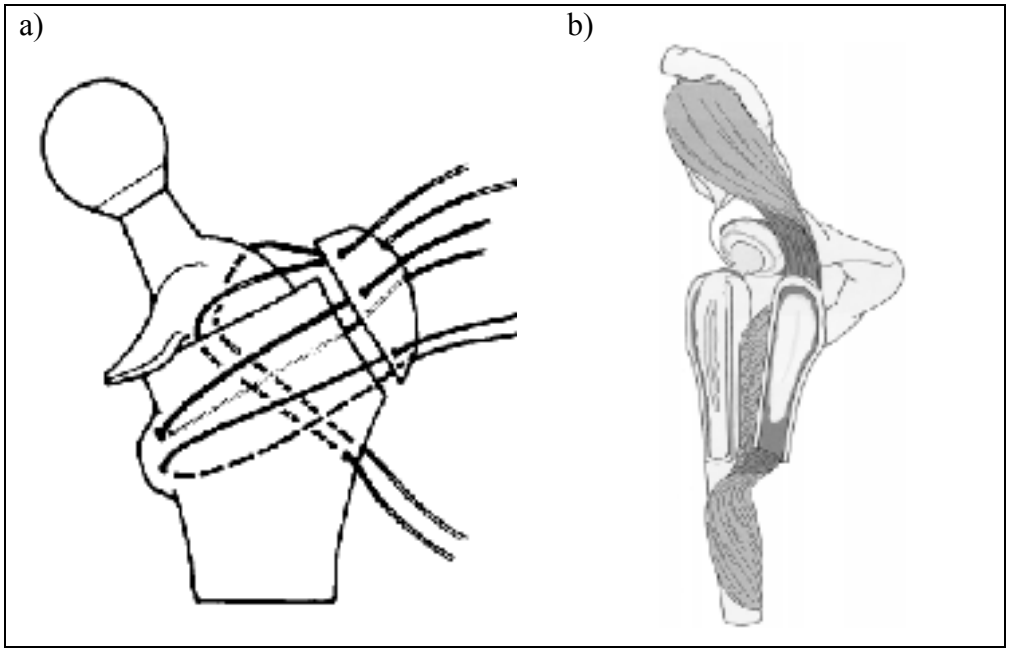

Figure 1.4 a) Ostéotomie classique b) Ostéotomie étendue
a) Tirée de Bal et Harris (1998, p. 30) b) Tirée de Chen et al. (2000, p. 1216)

1.3 Fixation du grand trochanter

Au début des arthroplasties de la hanche, le rattachement du GT n'était pas considéré comme étant problématique car le temps de réadaptation des patients était beaucoup plus long (Charnley, 1979) que maintenant. Selon le RCRA, la durée de réadaptation est passée de 8 jours à 5 jours en moyenne entre 1997 et 2007 (Institut canadien d'information sur la santé, 2009). Le temps de réadaptation étant trop petit pour que le fragment du GT soit remodelé au fémur, il est primordial que le système de fixation utilisé soit en mesure de le stabiliser adéquatement.

Les premières méthodes de maintien du GT consistaient à faire un cerclage (Figure 1.5) à l'aide de fils métalliques ou de câbles (Bal *et al.*, 2006). Plusieurs méthodes de cerclage ont été développées utilisant entre un et quatre fils ou câbles. De plus, le cerclage peut être transversal (Figure 1.5a), axial (Figure 1.5b) ou une combinaison des deux (Figure 1.5c) (Amstutz, Mai et Schmidt, 1984; Bal *et al.*, 2006; Bal, Maurer et Harris, 1998; Berry et Muller, 1993; Chin et Brick, 2000; Lakstein *et al.*, 2009; Markolf, Hirschowitz et Amstutz, 1979; Nicholson, Mulcahy et Fenelon, 2001; Nutton et Checketts, 1984; Plausinis *et al.*, 2003; Schutzer et Harris, 1988).

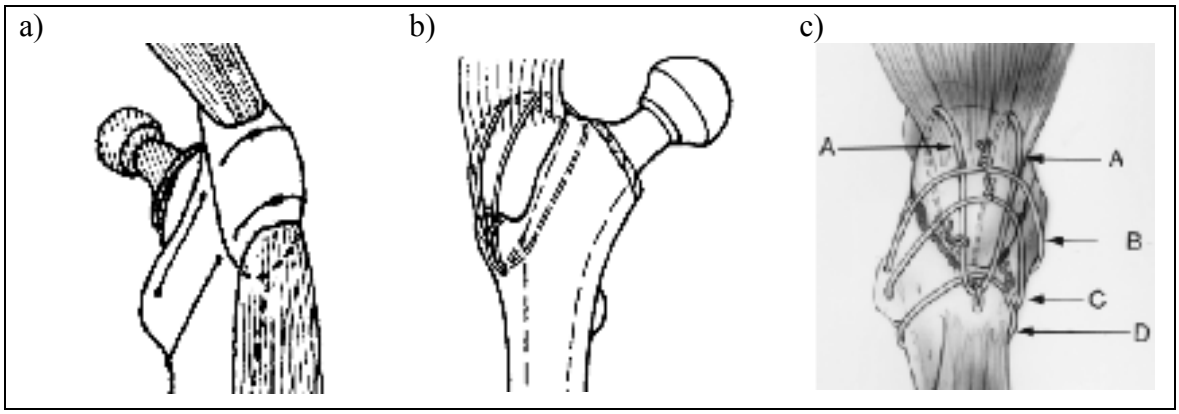

Figure 1.5 a) Cerclage transversal b) Cerclage axial c) Cerclage combiné
a) Tirée de Bal et al. (2006, p. 60) b) Tirée de Berry et Muller (1993, p. 157)
c) Tirée de Chin et Brick (2000, p. 403)

Or, dans les années 80, un groupe de chercheurs a développé une nouvelle méthode de fixation à l'aide d'un système composé d'une plaque et de câbles (Figure 1.6) (Dall et Miles, 1983). La plaque possède des crochets qui sont insérés par impact dans l'os cortical. Le système est ensuite maintenu en place à l'aide de deux câbles qui encerclent le fémur. Une tension de 357 N est généralement appliquée à l'aide d'un outil spécialement conçu pour le serrage de ces câbles. Par la suite, plusieurs systèmes de fixation de type « Cable Grip » inspirés du système de Dall et Miles ont été proposés par les compagnies telles que *Zimmer et Biomet.* (Koyama *et al.*, 2001; Zarin, Zurakowski et Burke, 2009)

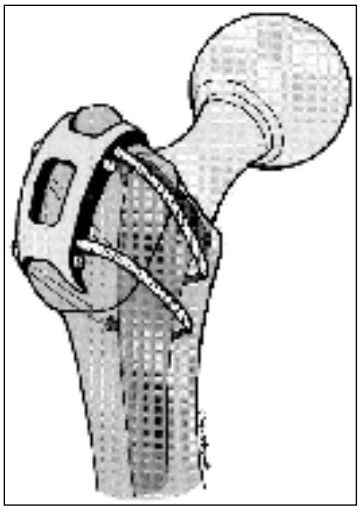

Figure 1.6 Système plaque et câble
Tirée de Hersh et al. (1996, p. 321)

Des études ont montré que les systèmes de plaque et câbles sont plus efficaces que le cerclage (Dall et Miles, 1983; Heller *et al.*, 2005). Ces études ont fait la comparaison entre différents types de fixation du GT avec cerclage et le système de plaque et câbles *Dall-Miles*. Les résultats ont montré que, pour un même chargement, les déplacements du système *Dall-Miles* étaient inférieurs pour la direction antéropostérieure et verticale. Or, même si les systèmes de plaque et câbles sont plus performants que le cerclage, il reste encore de nombreux cas problématiques. Des études cliniques incluant entre 62 et 251 patients ayant subit un rattachement du GT à l'aide du système *Dall-Miles* ont montré qu'entre 9 % et 31 % des patients présentaient des problèmes de non-union et qu'entre 10 % et 19 % des problèmes de bris (Barrack et Butler, 2005; Koyama *et al.*, 2001; McCarthy *et al.*, 1999).

1.4 Système Y3

Pour pallier aux problèmes des présents systèmes de plaque et câbles, une nouvelle conception d'un système de maintien du GT (Y3) utilisant des câbles et des vis a été proposée. Cette nouvelle plaque possède une géométrie unique en forme de « Y » (Figure 1.7) favorisant l'immobilisation du GT dans la direction antéropostérieure, qui semble être problématique dans les systèmes actuels. Des cas cliniques relevés par le chirurgien G. Yves Laflamme semblaient montrer une migration du fragment dans la direction antérieure. Deux

hypothèses principales ont été émises pour expliquer ce déplacement. La première serait que les crochets des plaques impactés dans le GT, qui ont une approche très latérale, ne maintiendraient pas suffisamment le fragment dans la direction antéropostérieure. La deuxième serait que la friction des câbles avec l'os et les tissus mous ne serait pas suffisante pour maintenir la rotation de la plaque, ce qui pourrait produire des mouvements indésirables dans la direction antéropostérieure.

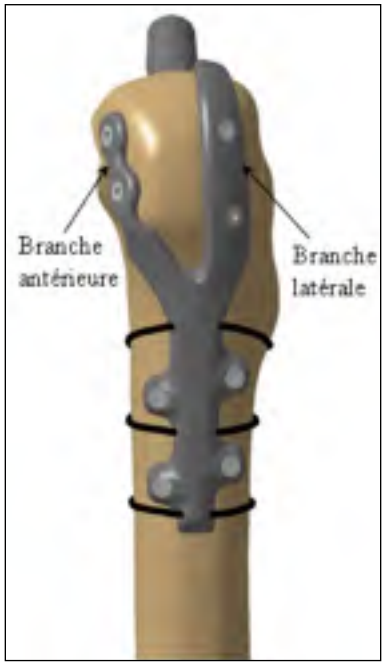

Figure 1.7 Système Y3

La conception du système Y3 a été développée dans l'objectif que la branche antérieure résiste aux mouvements antéropostérieurs alors que la branche médiale résiste aux mouvements proximaux-distaux du grand trochanter. L'utilisation de vis à tête autobloquante en ajout aux câbles a pour but de rigidifier l'assemblage, mais aussi de réduire le mouvement de rotation de la plaque. La section des branches de la plaque Y3 possède une forme concave pour augmenter son moment d'inertie. Ainsi, il est possible de réduire l'épaisseur des branches sans compromettre la rigidité du système. De ce fait, la plaque Y3 permet d'offrir

une conception à « profil bas » pouvant contribuer à la diminution de la douleur des patients et permettant de réduire les risques de tendinites, bursites, etc.

Une étude comparative, effectuée à l'aide d'un plan expérimental factoriel fractionnaire, a permis de montrer l'avantage de la plaque Y3 dans la direction antéropostérieur. L'étude, effectuée par Baril et al. (ANNEXE II) propose la comparaison entre le système *Cable Grip* de la compagnie *Zimmer* (CGZ) et le nouveau système Y3. Pour vérifier la stabilité du fragment du GT dans les deux directions, soit antéropostérieur et proximal-distal dans le plan de coupe du GT, deux types de chargements ont été effectués. Le premier chargement, stimulant les déplacements proximaux-distaux, représente la montée d'escalier selon l'étude de Heller et al. (2005). Le deuxième chargement, favorisant le déplacement antéropostérieur, est une adaptation de l'étude de Heller et al. (2005) et Charnley et al. (1979) pour représenter le lever d'une chaise. Les résultats de cette étude montrent qu'il n'y a aucune différence significative entre les déplacements du GT pour le système CGZ et le système Y3 pour le premier cas de chargement. Par contre, une diminution significative des déplacements du GT a été observée pour le deuxième cas de chargement en faveur du système Y3. Ainsi l'étude de Baril et al. (ANNEXE II) suggère que l'objectif de conception du système Y3, qui est de réduire l'instabilité antéropostérieure, est atteint. Bien que le système Y3 possède déjà une conception à bas profil comparativement au système CGZ (Figure 1.8), il pourrait être possible de réduire davantage le profil, car la largeur des branches conférée à la plaque Y3 est plus importante que les systèmes présentement utilisés.

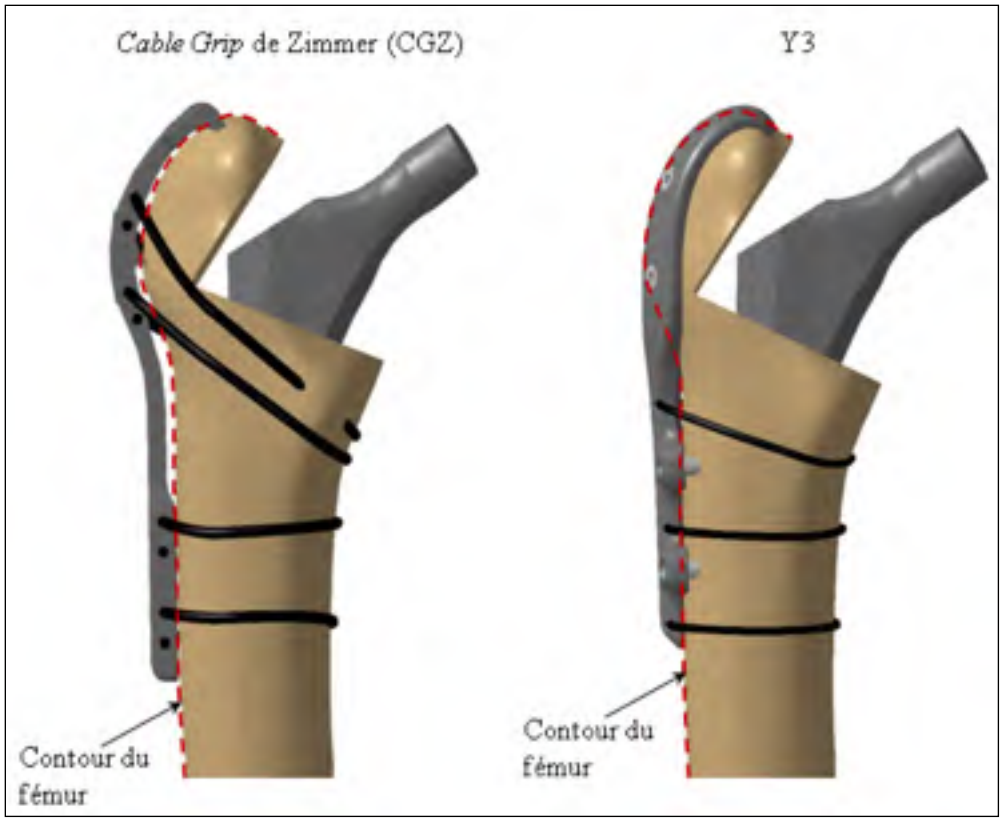

Figure 1.8 Comparaison de profil des plaques CGZ et Y3

Une meilleure compréhension du comportement du système Y3 dans le maintien du fragment du GT est nécessaire pour raffiner la conception de la plaque Y3 en enlevant la matière non nécessaire dans les régions moins importantes et en l'ajoutant aux endroits critiques. Afin d'éviter les coûts, le temps et la complexité de la mesure des déformations de la plaque en une multitude de points pour effectuer l'évaluation expérimentale des différents raffinements de plaque Y3, l'utilisation d'un MÉF est désignée. L'élaboration d'un MÉF demande la détermination de conditions limites et de stratégies de modélisation rigoureuses. Or, la littérature connue jusqu'à maintenant ne présente aucun MÉF d'aucun système de maintien du GT. Par contre, différentes études par MÉF ont été effectuées sur des plaques de maintien immobilisant des fragments d'os ayant subi une fracture ou une ostéotomie. Ces modèles peuvent fournir des informations considérables pour la détermination des conditions limites et des stratégies de modélisation.

1.5 MÉF de plaques et vis

Dans la littérature connue, quatre études pertinentes utilisant des MÉF pour étudier la fixation de systèmes de plaque et vis ont été retenues. Chen et al. (2004), Tai et al. (2009) et Peleg et al. (2006) ont étudié la fixation de fractures proximales du fémur alors que Cegonino et al (2004) se sont intéressé aux fractures distales du fémur. L'étude s'apparentant le plus à celle présentée dans ce mémoire est une analyse par MÉF de différents traitements pour des fractures fémorales distales effectués par Cegonino et al. (2004). Ces études portant sur des sujets non reliés à celui du mémoire, les conclusions des études ne sont pas rapportées, seulement la méthodologie des MÉF sera discutée.

L'étude présentée par Cegonino et al. (2004) fait la comparaison entre trois systèmes différents de maintien de fracture fémorale distale dont deux utilisent un système de plaque et des vis (Figure 1.9) tandis que le dernier utilise un système avec une tige interne (Figure 1.7c).

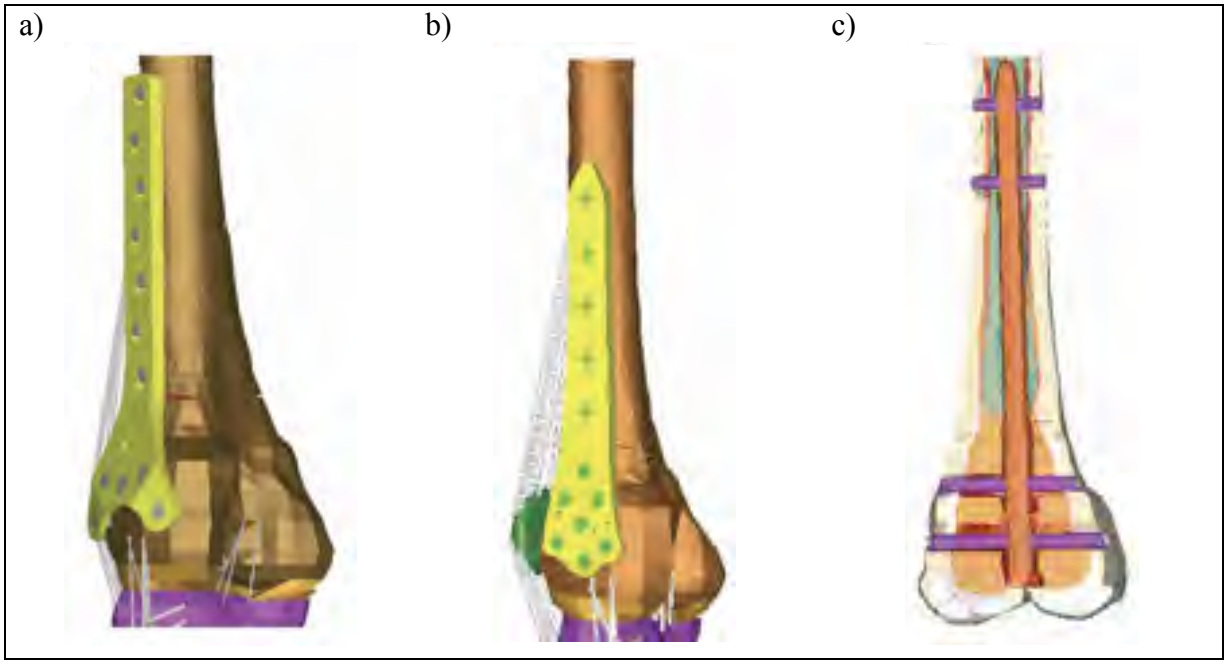

Figure 1.9 a) Plaque et vis type 1 b) Plaque et vis type 2 c) Système tige interne
Tirée de Cegonino et al. (2004, pp. 248, 249)

Dans cette étude, la géométrie du fémur provient de la numérisation par tomodensitométrie d'un fémur cadavérique féminin de 76 ans. Les propriétés mécaniques conférées à l'os sont isotropiques, mais une distinction entre l'os cortical et spongieux est prise en compte. Les modules d'élasticité proviennent d'une étude externe effectuée par Evans (1976) qui a réalisé des essais de tension sur des échantillons d'os d'un radius cadavérique d'un sujet mâle de 45 ans. Le maillage utilise des éléments briques, dont l'ordre des équations n'est pas précisé. Le contact entre les vis et l'os utilise des liaisons nœud à nœud, par contre le type de liaison entre les vis et la plaque n'est pas précisé. Un contact sans friction est défini entre les os du fragment et du fémur. L'analyse est basée sur les contraintes de Von-Mises et les déplacements relatifs entre le fémur et le fragment. Les déplacements relatifs sont seulement considérés dans l'axe de la partie centrale du fémur, c'est-à-dire que seulement la distance axiale entre le fragment et le fémur est analysée, les déplacements tangentiels ne sont pas pris en compte.

Chen et al. (2004) analysent différents types de fixation de la tête fémorale suite à un affaissement causé par une ostéonécrose. L'étude compare huit différents modes de fixation de la tête fémorale, faisant varier le type et le nombre de vis qui maintiennent la tête fémorale (Figure 1.10).

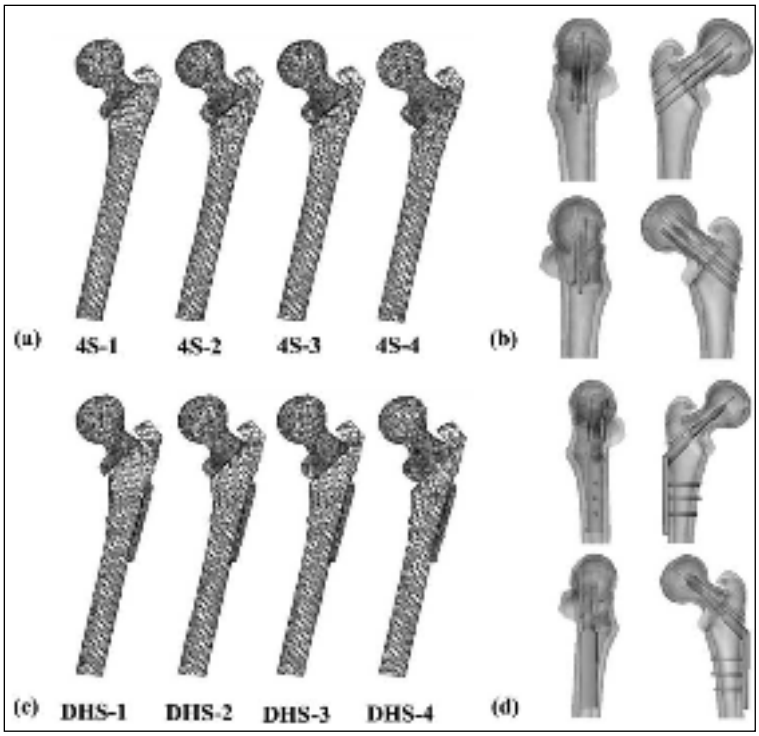

Figure 1.10 Modèle de Chen
Tirée de Chen et al. (2004, p. 257)

La géométrie du fémur utilisée dans le modèle provient d'une tomodensitométrie d'un fémur synthétique de la compagnie *Sawbones*. Les propriétés mécaniques conférées au fémur, tirées des données du fabricant des os synthétiques, sont isotropiques et une distinction entre les propriétés de l'os cortical et l'os spongieux est prise en compte. Le maillage utilise des éléments tétraédriques à 10 nœuds et la simulation est effectuée à l'aide du logiciel *Mentat 2000*. Les contacts entre l'os et les vis sont considérés comme étant totalement liés. Par contre, les contacts entre la plaque et l'os ainsi qu'entre le fémur et le fragment utilisent un coefficient de friction de 0,3 basé sur l'étude de Mann et al. (1995). L'analyse fait une étude comparative de la distribution des contraintes de Von-Mises pour les huit différentes configurations de fixation.

Tai et al. (2009) étudient le repositionnement de la tête fémorale suite à une déformation ou une mauvaise formation. L'opération consiste à faire une ostéotomie pour ensuite replacer la tête fémorale à une position anatomique. La tête fémorale est maintenue à l'aide d'une plaque et de 4 à 6 vis selon les configurations étudiées (Figure 1.11).

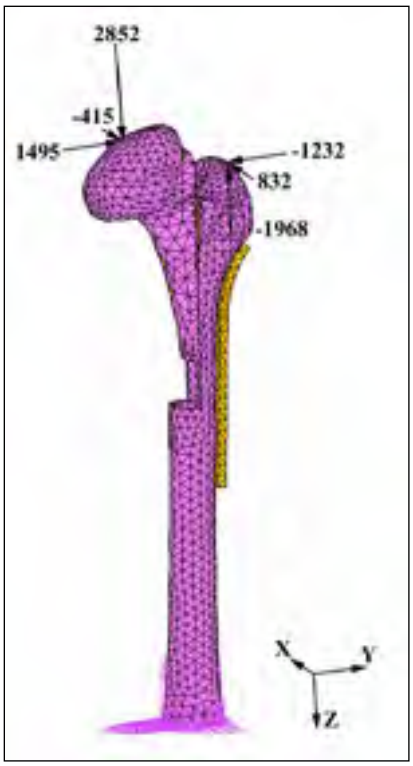

Figure 1.11 Modèle de Tai
Tirée de Tai et al. (2009, p. 117)

Une étude comparative est effectuée sur quatre longueurs d'ostéotomie et quatre variations de nombre de vis soit : 2 proximales / 2 distales, 2 proximales / 3 distales, 3 proximales / 2 distales et 3 proximales / 3 distales. Le modèle propose une reconstruction numérique, à l'aide d'un tomodensitomètre, d'un fémur cadavérique provenant d'un patient mâle de 25 ans. Les propriétés mécaniques attribuées au fémur sont isotropiques et une distinction entre l'os spongieux et cortical est considérée. Les valeurs proviennent de l'étude de Brown, Way et Ferguson (1981) qui ont évalué mécaniquement les propriétés mécaniques sur des échantillons d'os cubiques de sujets adultes provenant de la tête fémorale réséqué suite à une

arthroplastie de la hanche ou une autopsie. Le maillage utilise des éléments tétraédriques à 10 nœuds. La liaison entre les vis et l'os est modélisée par un contact lié dont un seuil de 1 700N limite l'adhérence des vis basée sur l'étude d'arrachement de vis vertébrale de Huang et al. (2003). Pour le contact entre le fragment du GT et le fémur, un contact lié est aussi utilisé, mais le seuil de détachement est fixé à 100 MPa sans toutefois expliquer la provenance de cette valeur. L'analyse est effectuée à l'aide de la distribution des contraintes de Von-Mises et le déplacement vertical de la tête fémorale.

Peleg et al. (2006) font la comparaison de deux types de fixation intertrochantérique suite à une fracture (Figure 1.12).

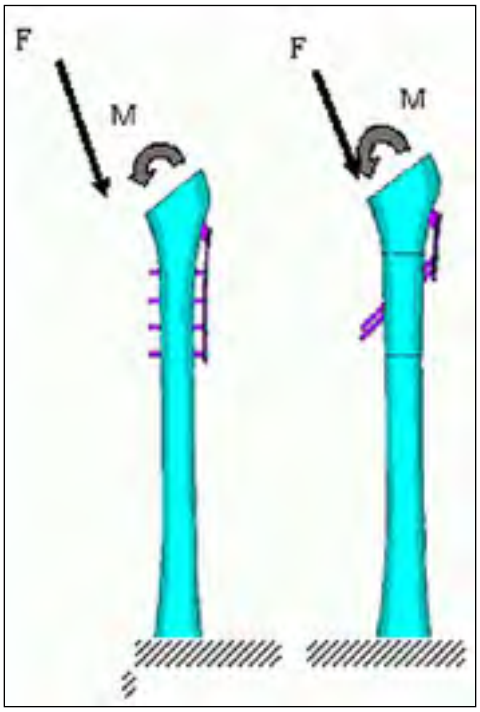

Figure 1.12 Modèles de Peleg
Tirée de Peleg et al (2006, p. 966)

La géométrie du fémur provient d'un spécimen générique obtenu par tomodensitométrie. Seul l'os cortical a été utilisé pour la modélisation du fémur et des propriétés isotropiques ont été attribuées, sans toutefois indiquer les valeurs attribuées et leur provenance. Le maillage utilise des éléments hexagonaux dont l'ordre des équations est inconnu. La simulation, générée à l'aide du logiciel *Ansys*, utilise un algorithme de Newton-Raphson pour la résolution. Les contacts entre les vis et l'os sont définis comme totalement liés et aucun contact entre la plaque et le fémur n'est généré. De plus, aucune modélisation de la tête fémorale fracturée n'est effectuée, une force de 3 fois le poids du corps est appliquée directement sur l'implant. L'analyse compare la distribution des contraintes de Von-Mises dans la plaque et dans l'os du fémur pour les deux types de fixation.

Les différentes études ressorties utilisent une méthodologie similaire. La géométrie du fémur est générée à partir de la tomodensitométrie dans tous les cas. De cette façon, il est possible de définir deux matériaux différents pour l'os cortical et l'os spongieux ainsi que de considérer les cavités à l'intérieur du fémur. Tous, sauf Chen et al. (2004), utilisent des spécimens cadavériques pour générer la géométrie du fémur. Les modèles composites de la compagnie Sawbones représentent le plus fidèlement possible les propriétés mécaniques et géométriques d'un fémur humain. Heiner (2008) a étudié les propriétés du fémur composite (génération 4) de la compagnie Sawbones et a conclu qu'elles s'approchent des propriétés d'un fémur humain. Ces modèles synthétiques sont moins dispendieux et plus reproductibles que les spécimens cadavériques. Par contre, il faut prendre en considération que ce ne sont pas toutes les propriétés de l'os qui sont similaires. Seuls les modules d'élasticité et les limites élastiques ont été comparés dans l'étude de Heiner (2008). Il n'est donc pas possible de considérer que les autres propriétés telles que la friction, la dureté ou la résistance en fatigue sont comparables.

Le maillage « élément brique » utilisé par Gegonino et al.(2004), ainsi que Peleg et al (2006), a le désavantage d'avoir une inadéquation plus importante entre le modèle géométrique et le maillage, surtout concernant les formes arrondies telles que le fémur. De ce fait, Tai et al. (2009) et Chen et al. (2004) ont utilisé un maillage tétraédrique à 10 nœuds qui est plus facile à générer par les logiciels et qui s'adapte mieux aux géométries arrondies. En complément, une étude sur le type d'élément utilisé pour la modélisation d'un fémur, effectué par Viceconti et al. (1998), a montré qu'un maillage structuré donne une plus grande précision, mais demande beaucoup de temps humain pour la définition du maillage. Il a également montré que le maillage non structuré utilisant des éléments tétraédriques donne de bons résultats et est facile à générer (Viceconti *et al.*, 1998). De plus, Polgar et al. (2001) ont fait une étude sur l'ordre des équations de maillage et la taille de mailles à utiliser pour la modélisation d'un fémur avec des éléments tétraédriques. Ils ont montré qu'un maillage tétraédrique du deuxième ordre, possédant des éléments d'une taille moyenne de 5 mm, offrait une différence en dessous de 1 % avec l'expérimentation. Ainsi, il est possible avec un maillage tétraédrique approprié de bien modéliser le comportement d'un fémur tout en limitant les distorsions géométriques.

Les études utilisant des plaques et vis définissent les vis comme un cylindre sans modéliser les filets. Le type de liaison utilisé varie d'une étude à l'autre, mais tous s'apparentent à un contact totalement lié. Cegonino et al. (2004) utilisent des liaisons nœuds à nœuds, ce qui est une définition un peu plus rigide que le contact lié avec un algorithme par pénalité. Tai et al. (2009) utilisent un contact collé avec une définition d'arrachement. L'utilisation d'un seuil d'arrachement pourrait être pertinent dans la définition des contacts vis-os mais les essais expérimentaux présentés par Baril et al. (2010), voir ANNEXE II, sur le système Y3 ne présentent aucun arrachement de vis. L'utilisation d'un seuil d'arrachement ne semble donc pas nécessaire dans le contexte de la présente étude.

Chen et al. (2004) sont les seuls à définir un contact pour la liaison entre la plaque et l'os cortical. Ce contact utilise un coefficient de friction de 0,3 basé sur l'étude Mann et al. (1991). Or cette étude (Mann *et al.*, 1991) détermine le coefficient de friction à utiliser pour une prothèse fémorale cimentée. Il a déterminé le coefficient de friction à utiliser entre la prothèse fémorale et l'os spongieux, pour un modèle numérique, en croisant les résultats avec des données expérimentales d'une prothèse fémorale cimentée avec du polyméthacrylate de méthyle (Mann *et al.*, 1991). De ce fait, il semble inapproprié d'utiliser un coefficient de friction de 0,3 entre une plaque et l'os cortical sur la base de ces résultats seulement.

Pour le contact entre le fragment de l'os et le fémur, chaque étude utilise une définition différente. L'utilisation d'un seuil de séparation tel que défini dans l'article de Tai et al. (2009) ne semble pas pertinente pour représenter un fragment d'os. Il est très difficile de déterminer la limite d'adhésion du fragment avec le fémur. Chen et al. (2004) utilisent un contact avec frottement ayant le même coefficient de friction (0,3) que le contact entre la plaque et l'os, se référant toujours à la même étude (Mann *et al.*, 1991), ce qui apparaît inadéquat. Il est difficile de bien déterminer le coefficient de friction pour ce type de contact. Ainsi, il semble plus adéquat d'utiliser un contact sans friction tel que défini dans l'étude de Cegonino et al. (2004).

1.6 Études d'optimisation de concepts de plaques à l'aide de MÉF

Des quatre études par MÉF, sur les systèmes de plaques et vis fémoraux, aucune ne fait l'analyse du comportement d'une plaque ou son raffinement. Par contre, deux autres études proposent l'optimisation d'un concept par MÉF. La première étude, effectuée par Pappas, Young et Lee (2006), porte sur l'analyse par MÉF d'une nouvelle plaque fémorale (Mennen 3) pour les fractures péri-prosthétiques.

L'étude comparative entre la plaque Mennen et Mennen 3 (Figure 1.13) optimise la conception de la nouvelle plaque.

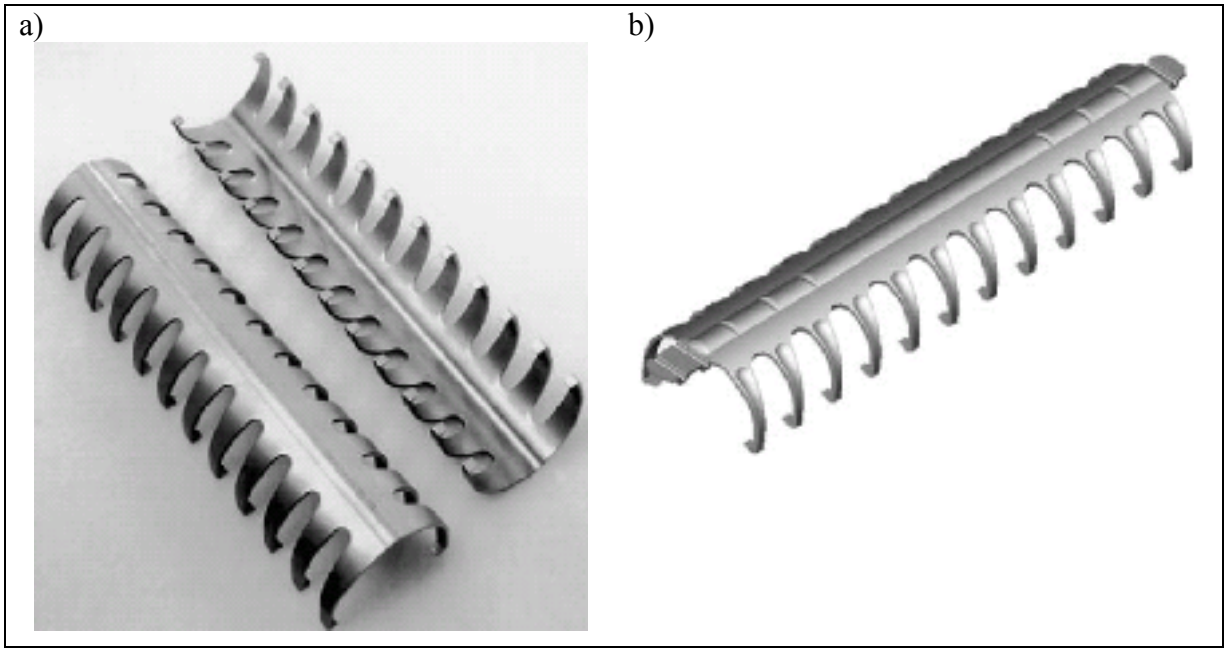

Figure 1.13 a) Plaque Mennen b) Plaque Mennen3
Tirée de Pappas, Young et Lee (2006, pp. 776, 781)

Les simulations par le MÉF utilisent la géométrie de la plaque sans modéliser le fémur. Les conditions limites sont celles des essais expérimentaux qui consistent en deux appuis à 12 mm des extrémités de la plaque et deux forces ponctuelles appliquées de façon symétrique avec une distance de 110 mm entre elles (Figure 1.14).

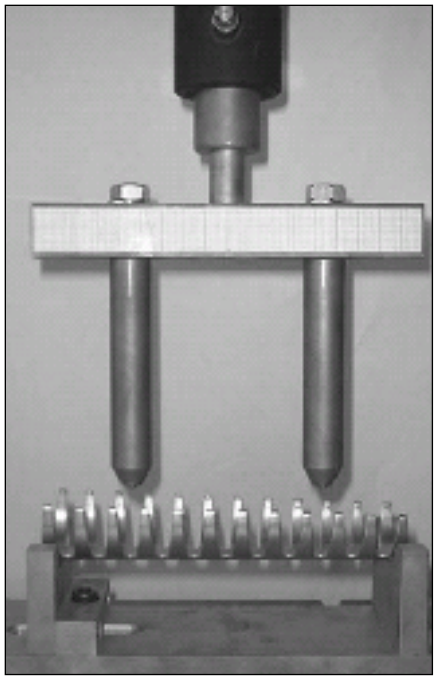

Figure 1.14 Montage expérimental de l'étude de Pappas
Tirée de Pappas, Young et Lee (2006, p. 778)

La flexion générée par ces conditions limites est mesurée et un seuil de 10 mm basé sur l'étude de Noorda et Wuisman (2002) permet de déterminer la force maximale qui peut être appliquée sur la plaque. Dans cette étude, les auteurs mentionnent que le changement géométrique de la plaque Mennen vers la plaque Mennen 3 est effectué par optimisation, or les zones optimisées et les algorithmes d'optimisation ne sont pas mentionnés. Bien que les résultats montrent une nette amélioration entre la plaque Mennen et Mennen 3, une augmentation d'environ 850 N dans le chargement maximal, aucun résultat ne montre qu'il y a eu une optimisation de concept.

La deuxième étude, réalisée par Elkholy (1995), fait l'optimisation du diamètre des vis et l'épaisseur de la plaque pour quatre configurations de vis d'un système de maintien de la tête fémorale. La fonction objectif a pour but de minimiser le poids de la plaque et a comme borne la limite élastique de l'acier inoxydable. Par contre, le MÉF utilisé pour l'optimisation

suppose de grandes simplifications (Figure 1.15). Le modèle simplifie la géométrie de la plaque, des vis et du fémur à l'aide d'éléments à une dimension (élément beam).

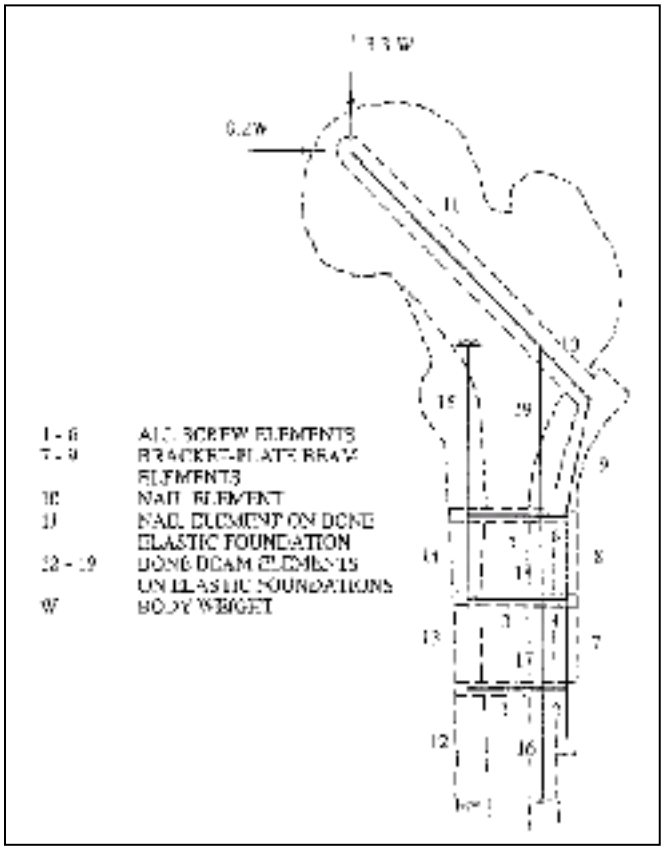

Figure 1.15 Modèle numérique d'Elkholy
Tirée de Elkholy (1995, p. 222)

À la lumière de ces deux études, un modèle tridimensionnel avec modification complexe de géométrie, tel que l'étude de Pappas, Young et Lee, rend difficile l'utilisation de paramètres de modification et l'optimisation d'une conception. C'est probablement pour cette raison que l'étude sur la plaque Mennen a été orientée plus sur une comparaison de concept qu'une optimisation. Pour effectuer une optimisation, il faut souvent simplifier énormément la modélisation tel que proposé par l'étude d'Elkholy (1995).

1.7 Résumé des objectifs

La revue des connaissances montre que le détachement du GT est généralement dû à une complication de l'arthroplastie de la hanche ou à une révision de la hanche. Les différents systèmes de maintien du grand trochanter de type « Cable grip » développés jusqu'à maintenant présentent des lacunes dans le maintien du GT. Le système de maintien Y3 a été développé dans le but de réduire les problématiques liées à la fixation du GT. Une des propriétés du système Y3 est son « profil bas » qui favorise une diminution de la friction entre les muscles et la plaque. Bien que le profil de la plaque Y3 soit assuré par le contournement de la partie protubérante du GT, il pourrait être envisageable de le diminuer davantage en amincissant la plaque tout en gardant le même niveau de déplacement du GT par rapport au fémur. En effet, la comparaison des aires de section des branches de la plaque Y3 et de la plaque CGZ suggère que les dimensions de la plaque Y3 sont surestimées.

La littérature connue jusqu'à maintenant contient peu d'études qui optimisent les dimensions de plaques et aucune ne porte sur des plaques trochantériennes. Les études, trouvées dans la littérature, visant à améliorer la conception de plaques, utilisent des MÉF. Les MÉF de plaque attachent un ou des fragments du fémur et présentent plusieurs simplifications permettant d'obtenir une solution convergente et un temps de résolution raisonnable. L'ensemble des modèles utilise des propriétés isotropes de l'os. Ils simplifient également la modélisation des vis par un cylindre qui est fixé à l'os et la plaque. Les contacts entre les fragments d'os est le point divergent entre toutes les études, chacune utilise des artifices différents pour définir ces contacts.

Ainsi, l'objectif principal de cette étude est de raffiner les dimensions du système de rattachement Y3 pour favoriser un « profil bas ».

Pour ce faire, les objectifs spécifiques de cette étude sont :

- le développement et la validation d'un MÉF représentant un fémur avec une ostéotomie du GT dont le rattachement est assuré à l'aide du système Y3;
- l'étude de la sensibilité des déplacements du GT en fonction de la modification de section de différentes régions de la plaque;
- le raffinement des dimensions de la plaque Y3 afin de favoriser un « profil bas » sans augmenter les déplacements du GT par rapport au fémur.

CHAPITRE 2

ARTICLE 1 « FINITE ELEMENT MODEL OF A GREATER TROCHANTERIC REATTACHMENT SYSTEM »

Y. Bourgeois[1-2], Y. Petit[1-2] and Y. G-Laflamme[2]

[1]École de Technologie Supérieure, 1100 Notre-Dame Ouest, Montréal, Canada

[2]Hôpital du Sacré-Coeur, 5400 boulevard Gouin Ouest, Montréal, Canada

Cet article a été publié dans: 32nd Annual International Conference of the IEEE Engineering in Medecine and Biology Society
Buenos Aires, Argentina, August 31 - September 4, 2010

RÉSUMÉ

Cet article étudie, à l'aide d'un MÉF de l'assemblage du système Y3, la sensibilité des différentes régions de la plaque Y3 sur les déplacements du GT. Le MÉF simule le rattachement du GT à l'aide de la plaque Y3 avec des vis autobloquantes. La condition de chargement du GT tente de simuler un type de chargement complexe qui s'apparente au lever d'une chaise. Le MÉF est validé à l'aide de données expérimentales préliminaires qui utilisent les mêmes conditions de chargement. La description du montage expérimental se réfère à l'étude de Baril et al. (2010b) présentée dans l'ANNEXE I.

La validation du modèle montre que la direction des mouvements du GT est concordante entre les résultats expérimentaux et numériques. L'étude de sensibilité montre que la région la plus sensible aux déplacements est celle qui lie les branches proximales à la branche distale de la plaque.

Le candidat est l'auteur principal de cet article publié dans le « *Conference proceedings of the IEEE Engineering in Medicine and Biology Society »*. Il a réalisé le développement et les simulations du MÉF. Il a aussi fait les essais expérimentaux nécessaires pour la validation du modèle. Il a effectué l'analyse des résultats et la rédaction de l'article.

ABSTRACT

Detachment of greater trochanter (GT) is generally associated with hip arthroplasty complications and needs for repositioning and fixation. A new GT reattachment system (Y3) was proposed to reduce GT displacements in anterior-posterior direction to decrease non-union issues. The goal of this study is to develop and validate a FEM of the Y3 GTR system. FEM validation suggests a good concordance between numerical and experimental GT displacements. Sensitivity study show that the transition between proximal and distal branches of Y3 design is the most influent part on all GT displacements. The anterior branch affects more anterior-posterior displacements and rotation while the posterior branch affects more proximal displacements and rotation. This study provides an improved understanding of the influence of Y3 geometry on GT displacements.

2.1 INTRODUCTION

Detachment of greater trochanter (GT) could occur after hip arthroplasty. Bone reduction for femoral implantation favors fissuring and fracture of GT. GT osteotomy is also necessary during revision hip arthroplasty. GT Reattachment (GTR) can be achieved by cerclage wires or cable grip systems. Although cable grip systems are more stable then cerclage wires (Barrack et Butler, 2005; Hersh *et al.*, 1996), non-union and cable breakage remain important issues (Barrack et Butler, 2005; Koyama *et al.*, 2001; McCarthy *et al.*, 1999).

In order to reduce these problems a new design of GTR system (Y3) using self-locking screws and cables is proposed (Figure 2.1). The premise of Y3 GTR system is to prevent anterior-posterior as well as distal-proximal GT displacements from its special Y shaped anterior and lateral branches. Minimized GT displacements would reduce non-union and fiber union issues.

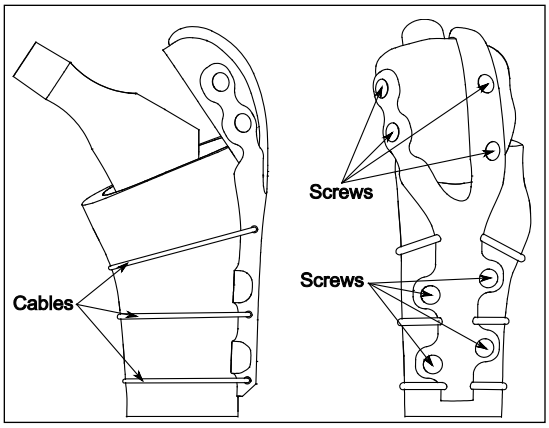

Figure 2.1 Y3 Greater Trochanteric Reattachement System

A detailed evaluation of the contribution of Y3 refinements to GT stabilization is complex. Finite element modeling (FEM) is a reliable method to simulate changes in plate geometry and to assess its load-displacement behavior. The objective of this study is to develop and validate a FEM of the Y3 GTR system.

2.2 Methods

2.2.1 Numerical simulations

The initial geometry was defined from computerized tomography (CT) scans of a 4th generation composite femur (*Sawbones)* and a computer assisted design (CAD) model of the Y3 GTR system. A CAD software (Catia V5) was then used to numerically perform: a) the arthroplasty cut and GT osteotomy, b) implantation of the femoral implant and c) Y3 GTR positioning using screw fixation (Figure 2.2).

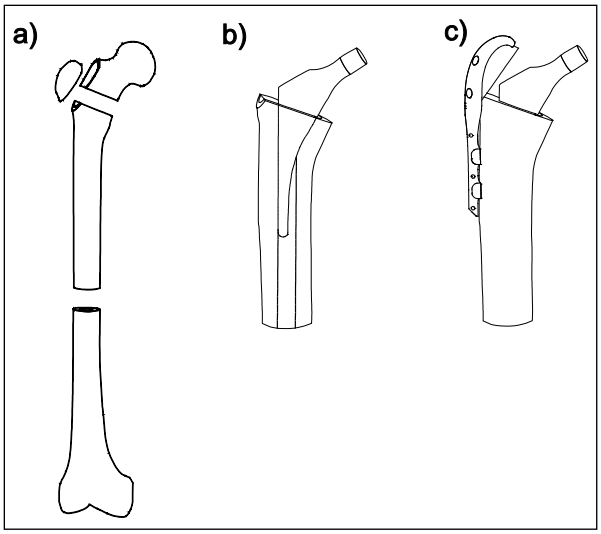

Figure 2.2 CAD modeling steps of the GTR-Femur assembly

The FEM mesh, generated with Catia V5, is composed of 10 nodes tetrahedral elements, as recommend for femoral FEM (Polgar, Viceconti et O'Connor, 2001). FEM mesh parameters and material properties are summarized in Table 2.1. Mesh size is defined by average element length whereas mesh sag is the maximum geometric deviation between CAD and FEM mesh. FEM mesh refinement of Y3 plate was performed by adjusting the minimum and maximum general length of elements. Convergence of mesh refinement was considered when a variation less than 8% of the maximum displacement of the GT relative to the femur was observed.

Table 2.1 FEM Material and mesh properties

Components	Material	Young Modulus (MPa)	Mesh Size (mm)	Mesh sag (mm)
Scews	Stanless steel *	193000	1	0.1
Plate	Titanium alloy *	110000	2	1
Prothesis	Titanium alloy*	110000	3	1
Femoral cortical bone	Cortical bone**	16900	5	2.5
GT cortical bone	Cortical bone**	16900	3	1
Femoral cancellous bone	Cancellous bone**	155	4	1
GT cancellous bone	Cancellous bone**	155	2.5	1

*ASM International (ASM-International et Granta-Design, 2010)

**Properties from Sawbones (Pacific Research Laboratories, 2009)

Connections between the locking head screws (LHS) and the Y3 plate were defined as fixed joints whereas the LHS to femur interactions were modeled with bounded contacts. Bounded contacts tied the nodes to the connected surface even though fixed joint constrains the relative movements of 2 bodies along their respective coordinate systems. Bounded contacts were also used between the cortical and the cancellous bone. Frictionless contacts were defined between the GT and femur.

Loads and boundary conditions applied to the FEM are illustrated in Figure 2.3. All displacements were fixed at the distal nodes of the femur model.

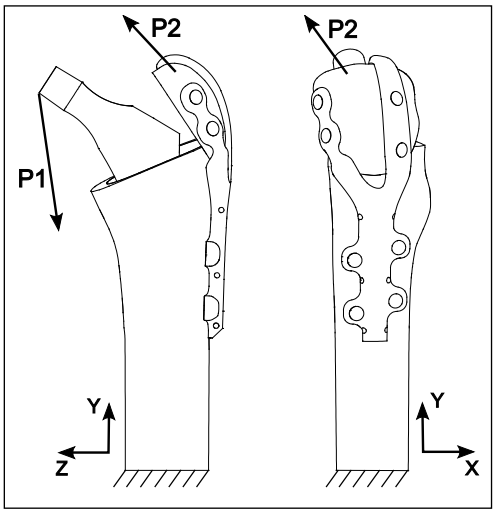

Figure 2.3 FEM loading and boundary conditions

Femoral head (P1) and GT (P2) forces (Table 2.2) were applied to simulate rising from a chair. To do so, P1 and P2 magnitude and orientation were defined based on the data of Heller et al. (2005) and Charlney (1979). However, the load magnitude corresponds to 75% of the reaction forces found by Heller et al. (2005) due to physical limitations of the setup.

Table 2.2 Loads applied to the femur (P1) and the GT (P2)

Application point	Magnitude (N)	Directional vectors		
		X	Y	Z
P1	2400	0.16	-0.96	-0.24
P2	650	-0.50	0.60	0.63

FEM simulations were made using *Ansys Workbench* software *(ANSYS inc., Canonsburg, PA, USA).* A non linear Newton-Raphson algorithm with force convergence criteria was used to solve the static equilibrium problem.

Relative displacements between the GT and the femur were assessed using rigid body assumptions. Four nodes were selected on the GT and the femur to define the rigid bodies and their relative movement was calculated with a custom-made Matlab algorithm adapted from Petit, Aubin et Labelle (2004). The assumption of rigid body movements was used to allow a better comparison with experimental measurements. Rigid body GT displacements and rotations compute were generated five times with different combinations of node selection to assess the variability of the rigid body measurements.

2.2.2 Experimental simulations

The experimental model also used a composite femur Sawbones model. A cutting guide was used to achieve GT osteotomy, femoral head cut and femoral length repeatable and comparable to the numerical model (Figure 2.2a). The femoral prosthesis cavity was prepared with a conventional rasp. The femoral prosthesis (Secur-Fit Max, Stryker) was then press fitted in the cavity (Figure 2.2b). GT was reattached to the femur using the Y3 GTR system (Figure 2.2c). Fixation of the femur on the test bench was done by cementing the distal extremity of femur in a fixed steel tubing (Figure 2.4).

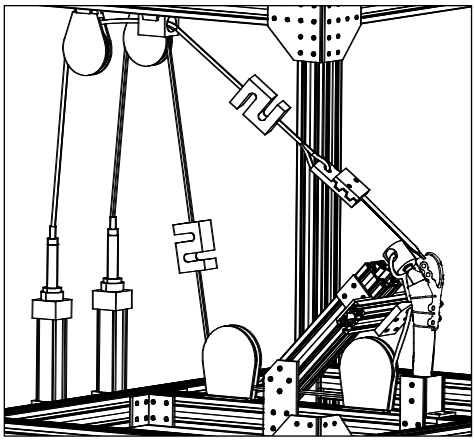

Figure 2.4 Experimental setup

Loading conditions were the same as for numerical simulations (Table 2.2). The femoral head (P1) and GT (P2) forces were applied using two hydraulic pistons through cables and pulleys (Figure 2.4). P1 was applied first up to the maximum in 2 seconds ramp. Then, P2 was also applied in a 2 seconds ramp. A dwell time of 5 seconds was respected before P2 and P1 were sequentially unloaded in 2 seconds ramps. Applied forces were measured during experiments with 2 load cells (LC101-500 and 4448 N, LC101-1k, Omega Engineering Inc, Stamford, CT, USA) installed on the transmission cables. A total of three identical trials were performed.

Four landmarks were placed on the GT and on the proximal extremity of the femur, close to the femoral cut, and tracked using a video camera (GRAS-20S4M-C, Point Grey Research, Richmond, BC, Canada) positioned with a field of view on the GT cut. Relative GT-femur displacements were calculated with the assumption of rigid movements using the same algorithm as for numerical simulations.

2.2.3 FEM Validation and sensitivity studies

A reference point (RP) located at the distal extremity of the GT was defined (Figure 2.5) for the comparison of relative femur-GT displacements between experimental and numerical simulations. Displacement components of the RP are given in a reference coordinate system (RCSYS) located at RP. The Xr-Yr plane of RCSYS was defined by the GT osteotomy cut plane and the Yr axis is coincident with the femoral shaft longitudinal axis (Figure 2.5).

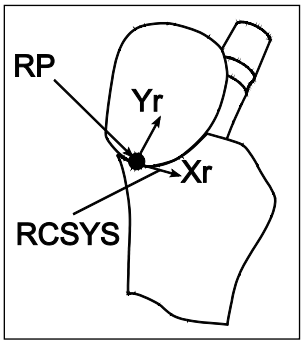

Figure 2.5 GT rigid body references

Sensitivity of the FEM to a change in the cross-section area of the Y3 plate without any modification of its general shape (position of branches, screws or cables) was assessed for each region of interest (ROI) defined in Figure 2.6. Xr, Yr GT displacements and rotation were defined as dependant variables for this sensitivity study. A sensitivity index (SENF) was defined as the ratio between the percent change in cross-section area (MODF) of the ROI and the percent change in GT displacement from the initial design (DISPF):

$$\text{SENF} = \frac{\text{DISPF}}{\text{MODF}} \tag{2.1}$$

In this sensitivity study, MODF ranged between 8 and 44% and DISPF ranged between 2 and 18%.

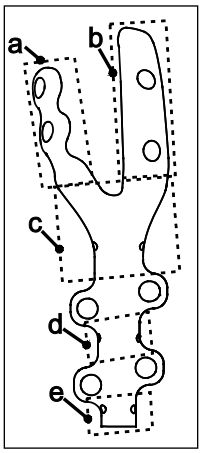

Figure 2.6 Y3 plate regions of interest (ROI)

2.3 Results

The Plate FEM mesh refinements converged after two iterations with a maximum displacements variation of 0.65%. The final minimum and maximum element length are 2mm and 3mm respectively for a total of 14 028 elements.

Comparison of GT displacements between experimental and numerical simulations is summarized in Table 2.3. Displacements of the RP are coherent for both models: anterior

displacement (Xr negative), proximal displacement (Yr positive) and positive rotation. However, the amplitude of GT displacements in Xr and Yr axes is more important during experimental simulations, except for the rotation that is larger in numerical simulations.

Table 2.3 Experimental vs. numerical rigid body movements

	Xr (mm) [Range*]	**Yr (mm) [Range*]**	**Rotation (deg) [Range*]**
Experimental	-1.66 [0.27]	0.83 [0.11]	0.52 [0.16]
Numerical	-0.47 [0.07]	0.51 [0.10]	0.84 [0.23]
Deviation	72 %	38 %	62 %

** Difference between minimum and maximum*

Sensitivity results for rotation, Xr and Yr axis displacement are summarized in Table 2.4.

Table 2.4 FEM Sensitivity to a change in ROI cross-section area

ROI (Figure 2.6)	**SENF (%/%)**		
	Xr	**Yr**	**Rotation**
a	1.15	0.49	1.39
b	0.69	1.35	1.19
c	1.81	1.41	2.25
d	0.71	1.28	0.27
e	0.04	0.05	0.04

Y3 plate ROI *c* influences the most and ROI *e* has no effect on all displacements. ROI *a* is the second important for Xr displacements while ROIs *b* and *d* have a less important effect. In Yr direction, ROI *b*, *c* and *d* have a similar impact and ROI *a* have a lower impact. Only ROI *a*, *b* and *c* really affected rotations.

2.4 Discussion

In this study, a mesh refinement convergence criteria of 8% based on rigid body displacements was used. This led to a low calculation time consuming FEM. The same mesh was used for all analyses since the plate geometry did not change significantly. No mesh refinement has been performed for the femoral prosthesis model since it was only introduced in the FEM to transfer loads on the femur. Although femur deformation was not the subject of this study, it may influence GT displacements. Thus, femur mesh size was defined in accordance with previous studies (Polgar, Viceconti et O'Connor, 2001; Viceconti *et al.*, 1998).

The comparison between experimental and numerical simulation results shows that GT displacement directions are similar. This may imply that GT displacements from the FEM are coherent with the experimental model. On the other hand, magnitudes of displacements differ between experimental and numerical simulations. This can be explained partially by the simplifications inherent to the FEM approach. As for examples, connections between screws, bone and plate (rigid contacts) are stiffer in the FEM than in experimentation. Also, no contact has been defined between the plate and the femur based on preliminary simulations. Frictionless contacts have been used between GT and femur while the friction is probably not negligible in reality. Nevertheless, the magnitude of displacements was not relevant for the sensitivity of the FEM to changes in cross-section area of the plate ROIs since a relative comparison was performed to identify ROIs having the most important effect.

Results show that cross-section of ROI *c* is the most critical region on the Y3 plate. Actually, this ROI is located at the transition between the GT and femoral part. From a mechanical stand point, ROI *c* could be seen as the embedment of a beam upon which flexion is applied. Consequently the inertia of ROI *c* along its lateral axis should greatly affect the strength of Y3 plate along the Xr axis and rotation. This is also relevant for ROIs *a* and *b* but their impact was found to be less critical. Displacements along the Yr axis have three evenly

important ROI (*b*, *c* and *d)*. These may be conceptualized as rectangular beam submitted to an axial load, which are equally affected by thickness and width.

2.5 Conclusion

Important non-union and breakage issues have been reported with the actual cable grip systems. The Y3 plate has been designed to reduce displacements of the GT. A FEM was developed and comparison of GT displacements between numerical and experimental simulations was performed to assess the validity of the FEM. Results suggest that GT displacements are concordant between numerical and experimental simulations although the magnitude was different.

Sensitivity of GT displacements to changes in the Y3 geometric design of several regions of interest was also assessed. The results show that the part of Y3 GTR acting as a link between the GT and the femur was the most influent on all displacements out of the five regions of interest. The branches overlapping the GT also had significant effects on GT displacements and rotations. The anterior branch affects more anterior-posterior displacements and rotation while the posterior branch affects more proximal displacements and rotation as it was anticipated during the initial Y3 GTR design.

This study gives a better understanding of the influence of local changes in geometry of the Y3 GTR system on GT displacements. The proposed FEM allowed modifying the geometry of Y3 GTR system and evaluate its effect on GT displacements. This sophisticated tool will allow in future studies to compare and optimize different designs of GTR using several criteria such as reducing material where not needed, reinforce critical zone or reduce the profile of the implant.

2.6 Acknowledgment

This research was funded in part by the Natural Science and Engineering Council (NSERC), Fond Québecois de la Recherche sur la Nature et les Technologies (FQRNT) and the Canadian Foundation for Innovation (CFI). The authors also thank Yannick-Vincent Baril for his technical assistance during experimental tests.

2.7 References

C.K. Hersh, R.P. Williams, L.W. Trick, D. Lanctot, and K. Athanasiou, "Comparison of the mechanical performance of trochanteric fixation devices," *Clin Orthop Relat Res*, (no. 329), pp. 317-25, Aug 1996.

R.L. Barrack and R.A. Butler, "Current status of trochanteric reattachment in complex total hip arthroplasty," *Clin Orthop Relat Res*, vol. 441, pp. 237-42, Dec 2005.

K. Koyama, F. Higuchi, M. Kubo, T. Okawa, and A. Inoue, "Reattachment of the greater trochanter using the Dall-Miles cable grip system in revision hip arthroplasty," *J Orthop Sci*, vol. 6, (no. 1), pp. 22-7, 2001.

J.C. McCarthy, J.V. Bono, R.H. Turner, T. Kremchek, and J. Lee, "The outcome of trochanteric reattachment in revision total hip arthroplasty with a Cable Grip System: mean 6-year follow-up," *J Arthroplasty*, vol. 14, (no. 7), pp. 810-4, Oct 1999.

K. Polgar, M. Viceconti, and J.J. O'Connor, "A comparison between automatically generated linear and parabolic tetrahedra when used to mesh a human femur," *Proceedings of the Institution of Mechanical Engineers, Part H (Journal of Engineering in Medicine)*, vol. 215, (no. H1), pp. 85-94, 2001.

ASM-International and Granta-Design. 2010. Materials for Medical Devices Database. http://products.asminternational.org/meddev/index.aspx. Accessed: march 29, 2010

Pacific Research Laboratories (2009). "Composite Bones." Retrieved March 28, 2009, from http://www.sawbones.com/products/bio/composite.aspx.

M.O. Heller, G. Bergmann, J.P. Kassi, L. Claes, N.P. Haas, and G.N. Duda, "Determination of muscle loading at the hip joint for use in pre-clinical testing," *J Biomech*, vol. 38, (no. 5), pp. 1155-63, May 2005.

S.J. Charnley, *Low friction arthroplasty of the hip*, Berlin: Sprigner-Verlag, 1979.

Y. Petit, C.-É. Aubin, and H. Labelle, "Spinal shape changes resulting from scoliotic spine surgical instrumentation expressed as intervertebral rotations and centers of rotation," *Journal of Biomechanics*, vol. 37, (no. 2), pp. 173-180, 2004.

M. Viceconti, L. Bellingeri, L. Cristofolini, and A. Toni, "A comparative study on different methods of automatic mesh generation of human femurs," *Medical Engineering & Physics*, vol. 20, (no. 1), pp. 1-10, 1998.

CHAPITRE 3

ARTICLE 2 « DESIGN REFINEMENT OF A GREATER TROCHANTERIC REATTACHMENT SYSTEM USING FINITE ELEMENT MODEL »

Y. Bourgeois[1-2], Y. Petit[1-2] and Y. G-Laflamme[2]

[1]École de Technologie Supérieure, 1100 Notre-Dame Ouest, Montréal, Canada

[2]Hôpital du Sacré-Coeur, 5400 boulevard Gouin Ouest, Montréal, Canada

Cet article a été soumis à la revue : Computer Methods in Biomechanics and Biomedical Engineering

RÉSUMÉ

L'article porte sur le raffinement d'une plaque trochantérienne à l'aide d'un MÉF. Le modèle comporte un fémur avec une ostéotomie du GT qui est rattaché à l'aide du système d'attache Y3 utilisant des vis à tête autobloquantes. La simulation utilise deux types de chargement pour le GT, soit un chargement correspondant à la montée d'escalier et au lever d'une chaise. Les résultats numériques ont été validés à l'aide de résultats expérimentaux qui proviennent de l'étude de Baril et al. (2010a) présentée à l'ANNEXE II alors que la validation du montage expérimental se réfère à l'article en ANNEXE I (Baril *et al.*, 2010b). Les résultats expérimentaux utilisent les mêmes conditions que le modèle numérique à l'exception que les essais du montage expérimental utilisent des câbles en CoCr en plus des vis à tête autobloquante.

La validation du modèle numérique a permis de déterminer que la direction du mouvement du GT est concordante avec les essais expérimentaux. Or la grandeur des déplacements est généralement plus faible pour les essais numériques. Le raffinement, généré en cinq itérations, produit une plaque dont le volume est diminué de 29%. Les contraintes de Von-Mises sont situées près des deux trous proximaux de la branche fémorale de l'implant et sont

légèrement sous le seuil de 500 MPa établi pour respecter un facteur de sécurité minimal de 1,6 pour la limite élastique et 1,3 en fatigue.

Le candidat est l'auteur principal de cet article soumis pour publication dans la revue *Computer Methods in Biomechanics and Biomedical Engineering*. Il a généré le MÉF et réalisé l'ensemble de l'étude de raffinement du système de fixation du grand trochanter. Il a aussi réalisé l'analyse des résultats et la rédaction de l'article sous la supervision des co-auteurs.

ABSTRACT

Greater trochanteric reattachment (GTR) is generally needed after an osteotomy or a fracture. Cable grip systems have been reported high complication rates. Recent experiments on a new GTR (Y3) design suggest the potential to reduce such complications. One feature of the Y3 GTR is its low profile, which reduces the risk of bursitis and pain. However, a previous sensitivity study (Bourgeois, Petit et Laflamme, 2010) suggests that the initial design of the Y3 GTR is overdesigned in different regions. This study aims to further refine the Y3 GTR design for a lower profile. A finite element model (FEM) was developed and validated for this refinement study. Design iterations resulted in thickness decreases of between 5 and 33%. Maximum Von-Mises stresses were located close to the proximal cable holes, and were 312 MPa and 498 MPa for stair climbing and sit-to-stand loading scenarios respectively. Lower thickness offers a low profile for bursitis and pain reduction.

3.1 Introduction

The detachment of the greater trochanter (GT) is a common complication with hip arthroplasty. Removal of the femoral head and neck for stem implantation favors the fissuring and fracture of the GT. GT osteotomy is also performed in revision hip arthroplasty to improve exposure. All these procedures require GT repositioning and attachment. Cerclage wires, and more recently cable grip systems, can be used for GT Reattachment

(GTR). Even the second generation trochanteric system, which incorporates a plate, reports disappointing complication rates, with 9-31% non-union and 10-19% breakage (Barrack et Butler, 2005; Koyama *et al.*, 2001; McCarthy *et al.*, 1999).

Furthermore, the bulkiness of the plate in the trochanter region leads to a significant increase in abductor pain, hardware impingement, and bursitis (Jarit *et al.*, 2007; McCarthy *et al.*, 1999; Takahira *et al.*, 2010). A novel GTR design (Y3) using self-locking screws and cables is proposed (Figure 3.1) in an attempt to restore the abductor function more consistently than is possible with the cable system that has been available until now (Petit, Laflamme et Bourgeois, Summited (2008)).

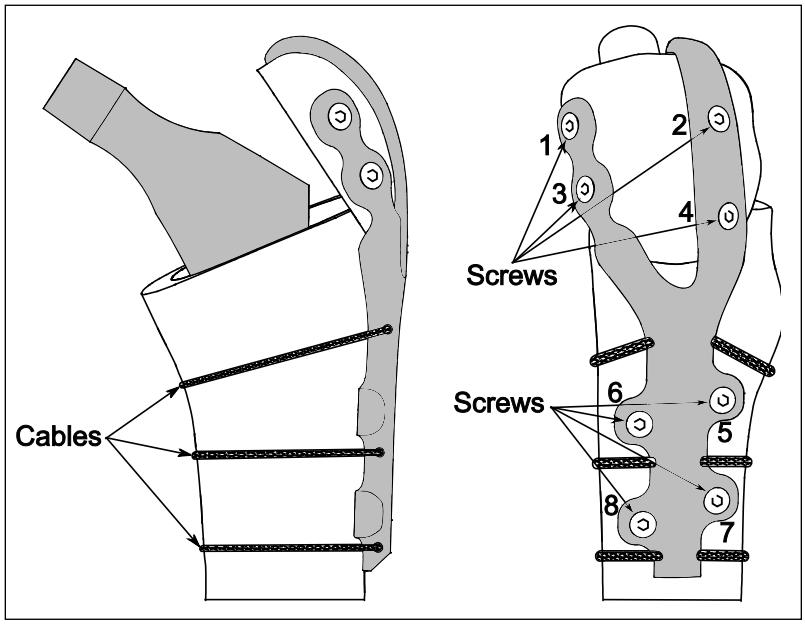

Figure 3.1 Y3Greater Trochanteric Reattachement System

In a previous experimental comparative study, (Baril *et al.*, 2010a) demonstrated that the Y3 GTR offers better stability in the anterior-posterior direction and equivalent stability in the superior-inferior direction versus a commercially available system. Since the trochanter is subjected to repetitive sliding of the fascia lata, a low-profile implant is desirable in order to minimize the risk of bursitis and pain. By reducing the thickness of the plate, this may also reduce the Y3 plate rigidity, which could help avoid stress shielding problems, such as

osteopenia and bone necrosis (Ganesh, Ramakrishna et Ghista, 2005; Tonino *et al.*, 1976). Previous finite element analyses have identified Y3 plate regions of interest having the greatest effect on GT displacements and suggest reducing the cross-section area of the proximal and distal branches, where GT displacements are less affected (Bourgeois, Petit et Laflamme, 2010).

The objective of this study is to reduce the thickness and cross-section area of the Y3 plate, using a finite elements model (FEM), without increasing GT displacements relative to the femur.

3.2 Material and Methods

3.2.1 Numerical model

The geometric model was obtained from computed tomography (CT) scans of a 4th generation composite femur (*Sawbones®,* Pacific Research Laboratories Inc., Vashon, WA). The arthroplasty cut (Figure 3.2a), GT osteotomy (Figure 3.2a), femoral implantation (Figure 2b) and Y3 plate positioning using locking-screws (Figure 3.2c) were done using computer assisted design (CAD) software (Catia V5, Dassault Systèmes, Montreal, Canada).

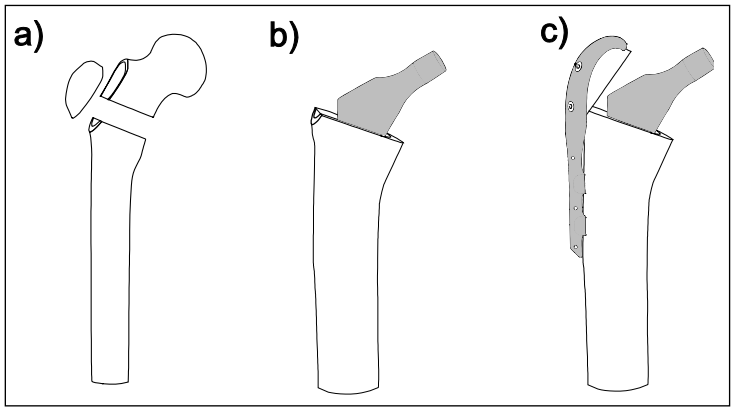

Figure 3.2 CAD modeling steps of the GTR and Femur assembly: a) Arthroplasty cuts, b) femoral implant installation,

c) Y3 plate positioning and fixation with self-locking screws.

The FEM mesh, generated with the Advanced Meshing Tools of Catia V5, was composed of 10-node tetrahedral elements, as recommended for femoral FEM (Polgar, Viceconti et O'Connor, 2001). Mesh generation was defined with two parameters: mesh size and mesh sag. The mesh size was defined as the average element length while the mesh sag was the maximum geometric deviation between the CAD model and the FEM mesh. The meshing parameters and material properties defined in the model are described in Table 3.1. The mesh was then transferred to ANSYS *Workbench* software *(ANSYS* Inc., *Canonsburg, PA, USA)*. The mesh refinement of the Y3 plate was performed by adjusting the minimum and maximum general element lengths. Mesh refinement convergence was considered to be achieved when a less than 5% variation of the maximum contour displacement of the GT relative to the femur and a less than 10% variation of maximal Von-Mises stress were observed. The criterion for maximal contour displacement variation was based on the standard deviation of a rigid body calculation (Baril *et al.*, 2010b; Petit, Aubin et Labelle, 2004). Calculations were performed using a least-squares singular value decomposition method in order to determine the geometric transformation of rigid body movement. The maximal Von-Mises stress criterion corresponds to a variation of 50 MPA.

Table 3.1 FEM Material and mesh properties

Components	**Material**	**Young Modulus (MPa)**	**Mesh Size (mm)**	**Mesh sag (mm)**
Scews	Stanless steel *	193000	1	0.1
Plate	Titanium alloy * (Ti-6Al-4V)	110000	2	1
Prosthesis	Titanium alloy*	110000	3	1
Femoral cortical bone	Cortical bone**	16900	5	2.5
GT cortical bone	Cortical bone**	16900	3	1

Femoral cancellous bone	Cancellous bone**	155	4	1
GT cancellous bone	Cancellous bone**	155	2.5	1

*ASM International (ASM-International et Granta-Design, 2010)

**Properties from Sawbones (Heiner, 2008)

Symmetric bonded contacts were used between the locking-screws and the femur as well as between the cortical and the cancellous bone. Symmetric bounded contacts allow the coupling of contact nodes and connected surfaces in both directions. Frictionless symmetric contacts were used between the GT and the femur on osteotomy surfaces. Frictionless contacts allow tangential movement and node separation from the connected surface, but no penetration is allowed. Fixed joints were used to connect the locking-screw head to the Y3 plate holes. The definition of these fixed joints constrains the relative movements of the 2 bodies in their respective coordinate systems.

The loads and boundary conditions applied to the FEM are illustrated in Figure 3.3. All displacements were fixed on the distal nodes of the femur model to represent embedment.

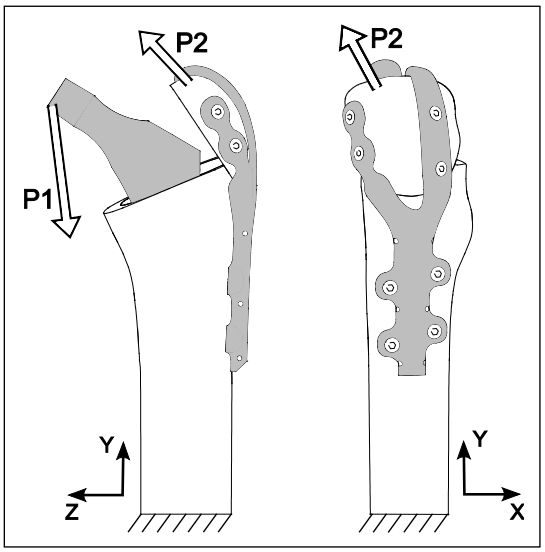

Figure 3.3 FEM loading and boundary conditions

Femoral head (P1) and GT (P2) forces (Figure 3.3) were applied simultaneously. Two cases of P2 were used: $P2^1$, normal angle (NA), was applied to represent the stair climbing critical load case, while $P2^2$, wide angle (WA), was used to represent the critical load when rising from a chair. These forces were the same as those used experimentally by Baril et al. (2010a).

Table 3.2 Loads applied to the femur (P1) and the GT (P2)

Application force	Magnitude (N)	Directional vectors		
		X	Y	Z
P1	2400	0.16	-0.24	-0.96
$P2^1$	650	-0.34	0.73	0.60
$P2^2$	650	-0.50	0.63	0.60

A non-linear Newton-Raphson algorithm with force convergence criteria was used to solve the static equilibrium problem. GT displacements relative to the femur were calculated using the assumption of rigid body movements. Four nodes were chosen on the GT and the femur to define the rigid bodies. Their relative movements were calculated using a custom-made Matlab algorithm adapted from Petit et al. (2004). Rigid body measurements were performed five times to assess their variability.

3.3 Experimentation

Two 4th generation composite femurs (*Sawbones*®, Pacific Research Laboratories Inc. Vashon, WA) were used for experimental testing. The femoral cuts were similar to the numerical model (Figure 3.2a) and were performed with the help of a cutting guide. The femoral prosthesis cavity was prepared with a conventional rasp and a femoral prosthesis (Secur-Fit Max®, Stryker, Mahwah, NJ) was press-fitted into the cavity (Figure 3.2b). The GT was reattached with a Y3 plate, locking-screws and Co-Cr cables. Plate installation was performed according to the following sequence:

1) Screws attaching the Y3 plate to the femoral shaft through holes 5 and 6 (Figure 3.1) were inserted.

2) Cables were tightened at 355N and re-tightened from proximal to distal.

3) Locking-screws were inserted in all remaining holes.

The experimental testing apparatus was previously described by Baril et al. (2010b), and the sameloading conditions applied to the numerical model were used in the experimental model (Table 3.2). Loads P1 and P2 were applied simultaneously, with a 2-second ramp and a dwell of 5 seconds observed before unloading with a 2-second ramp. A total of three identical trials were performed.

The same rigid body movement algorithm used for numerical simulations was used to calculate GT displacements relative to the femur.

3.4 Validation

The GT movement relative to the femur was analyzed at a reference point (RP) located at the distal extremity of the GT (Figure 3.4). The displacement direction was given by a referential coordinate system (RCSYS) located at the RP. The Xr-Yr plane was defined by the GT osteotomy plane and the Yr axis direction across the femoral shaft longitudinal axis (Figure 3.4). The displacement of the GT at the RP in the Xr, Yr axes and rotation in the Xr-Yr plane defined the rigid body movement in the osteotomy plane.

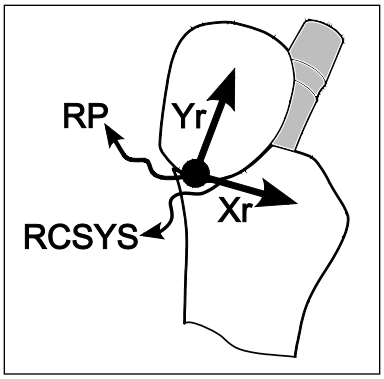

Figure 3.4 GT rigid body reference point (RP) and reference coordinate system (RCSYS)

3.5 Y3 Plate Refinement Methodology

The Y3 plate refinement was aimed at reducing its cross-section area without causing any change to its general shape (position of branches, screws or cables). The plate thickness and width were independently changed for each region of interest (ROI) shown in Figure 3.5.

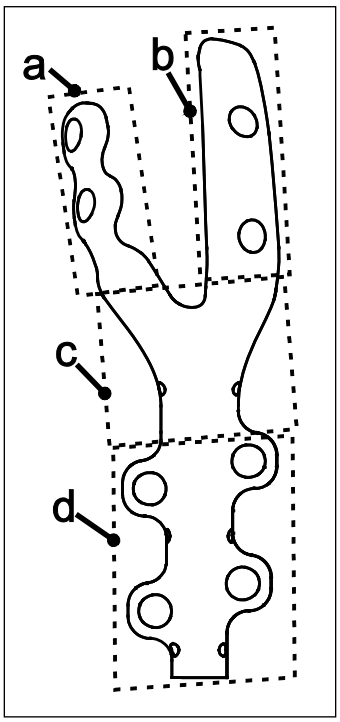

Figure 3.5 Y3 plate regions of interest (ROI)

Figure 3.6 shows the decision tree used to achieve the Y3 design refinement. For every design iteration, simulation results were compared to the initial FEM simulation. Simulation output data was verified based on two criteria:

1) The maximum contour displacement (Figure 3.7) must be smaller or equal to the initial movement result, incremented by a standard deviation to compensate for the rigid body assumption. The maximum contour displacement was defined by the larger displacement along the coincident contour between the GT and the femur from unloaded to loaded state.

2) Von-Mises stresses must be smaller than, but be as close as possible to 500 MPa, which corresponds to a security factor (SF) of 1.6 on the yield stress and of 1.3 on the endurance limit after $3x10^6$ cycles (ASM-International et Granta-Design, 2010) (~1 year walking (Tudor-Locke, Hart et Washington, 2009) for the Titanium alloy used in this study.

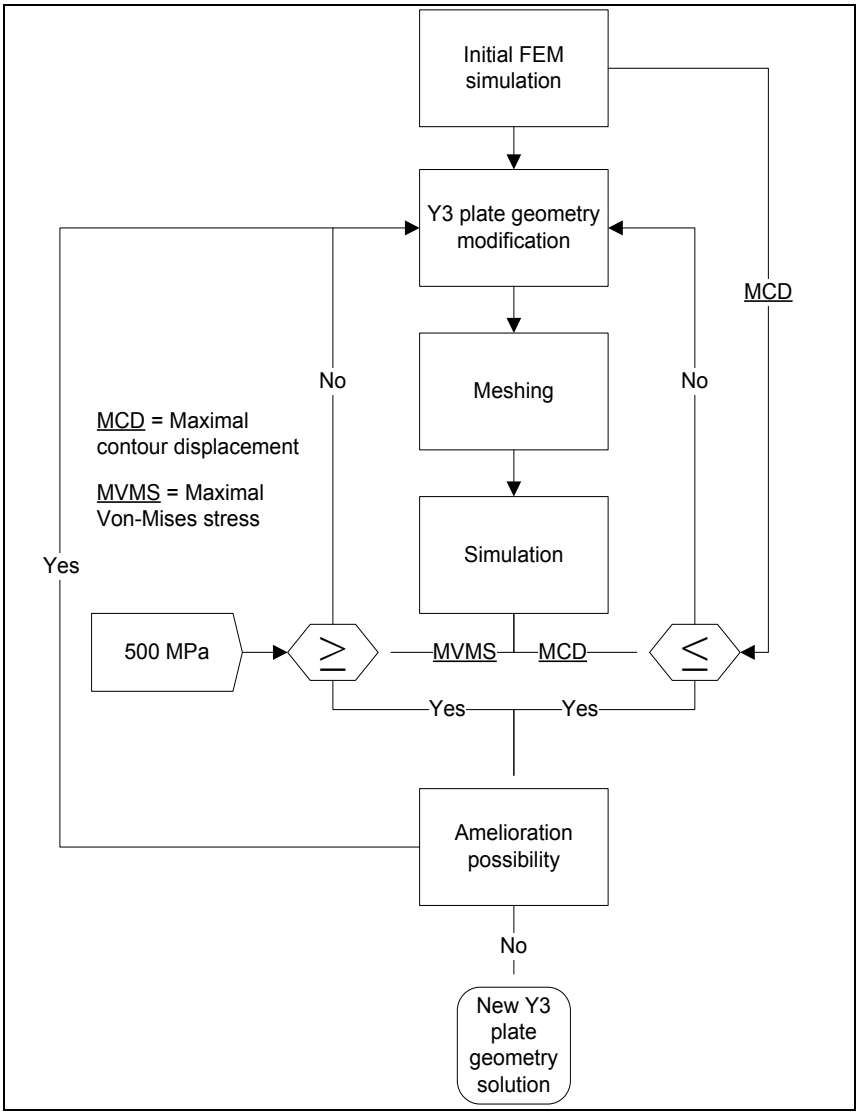

Figure 3.6 Y3 Design refinement decision tree

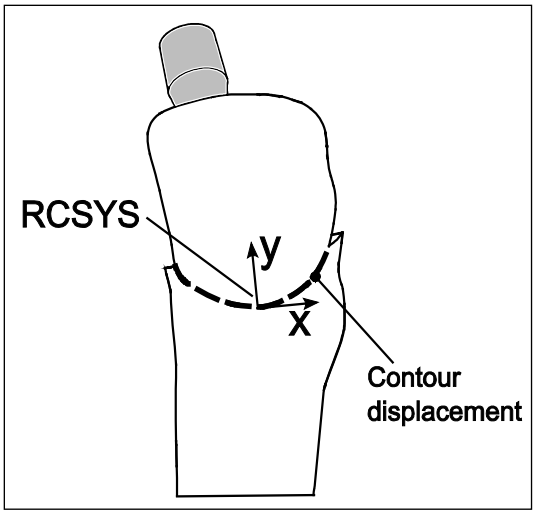

Figure 3.7 Contour displacement

If one or both criteria were not reached for the two loading cases (NA and WA), the Y3 plate geometry was modified, re-meshed and the simulations were repeated. Otherwise, the next step consisted in considering improvement possibilities. Based on a previous study, Bourgeois et al. (2010) determined the influence of modifying each of the ROI on GT displacements. This criterion was used to qualitatively assess whether the Von Mises Stress criterion is suboptimal for all ROI with a low or a moderate influence on the GT displacements. The design refinement was considered to be completed when there was no possibility for additional improvement.

3.6 Results

After convergence, the Y3 plate mesh consists of a total of 43,637 elements with minimum and maximum element lengths of 0.75 mm and 2mm, respectively. The Y3 plate mesh refinement converged after five iterations using NA and WA loading cases. The change in the maximal Von-Mises stress was less than 2.3% and 0.6%, and was less than 0.6% and 0.2% for maximal contour displacement, using NA and WA respectively. The comparison of the GT displacements between experimental and numerical simulations is summarized in Table 3.3.

Table 3.3 Experimental and numerical rigid body movements

	Normal angle (NA)			Wide angle (WA)		
	Xr (mm) [Range*]	**Yr (mm) [Range*]**	**Rotation (deg) [Range*]**	**Xr (mm) [Range*]**	**Yr (mm) [Range*]**	**Rotation (deg) [Range*]**
Experimental	-0.75 [0.17]	0.71 [0.13]	0.81 [0.34]	-0.77 [0.24]	0.74 [0.43]	0.54 [0.60]
Numerical	-0.33 [0.08]	0.53 [0.11]	0.49 [0.24]	-0.49 [0.07]	0.49 [0.10]	0.86 [0.23]
Deviation	57 %	25 %	40 %	37 %	35 %	58 %

** Difference between minimum and maximum*

RP displacements manifested a concordant direction between experimental and numerical models. Along the Xr axis, the GT RP moved anteriorly relative to the femur (negative direction) for NA and WA loading cases. Along the Yr axis, displacements were in the proximal direction (positive) in all cases. Positive rotations (counterclockwise) were also concordant between numerical and experimental models. Discrepancies in displacements ranging between 25% and 58% were observed. All displacements observed experimentally were larger than numerical results, except for the GT rotation in WA loading.

To perform the Y3, design refinement thresholds were determined. The maximal contour displacement threshold was defined from the initial design simulation results and a confidence interval corresponding to one standard deviation of rigid body (SDRB) assumption. The result was a maximal contour displacement threshold of 1.33 mm and 2.04 mm for the NA and WA respectively since SDRB was 0.11 mm and 0.16 mm for the NA and WA respectively. Refinement iteration results are summarized in Figure 3.8.

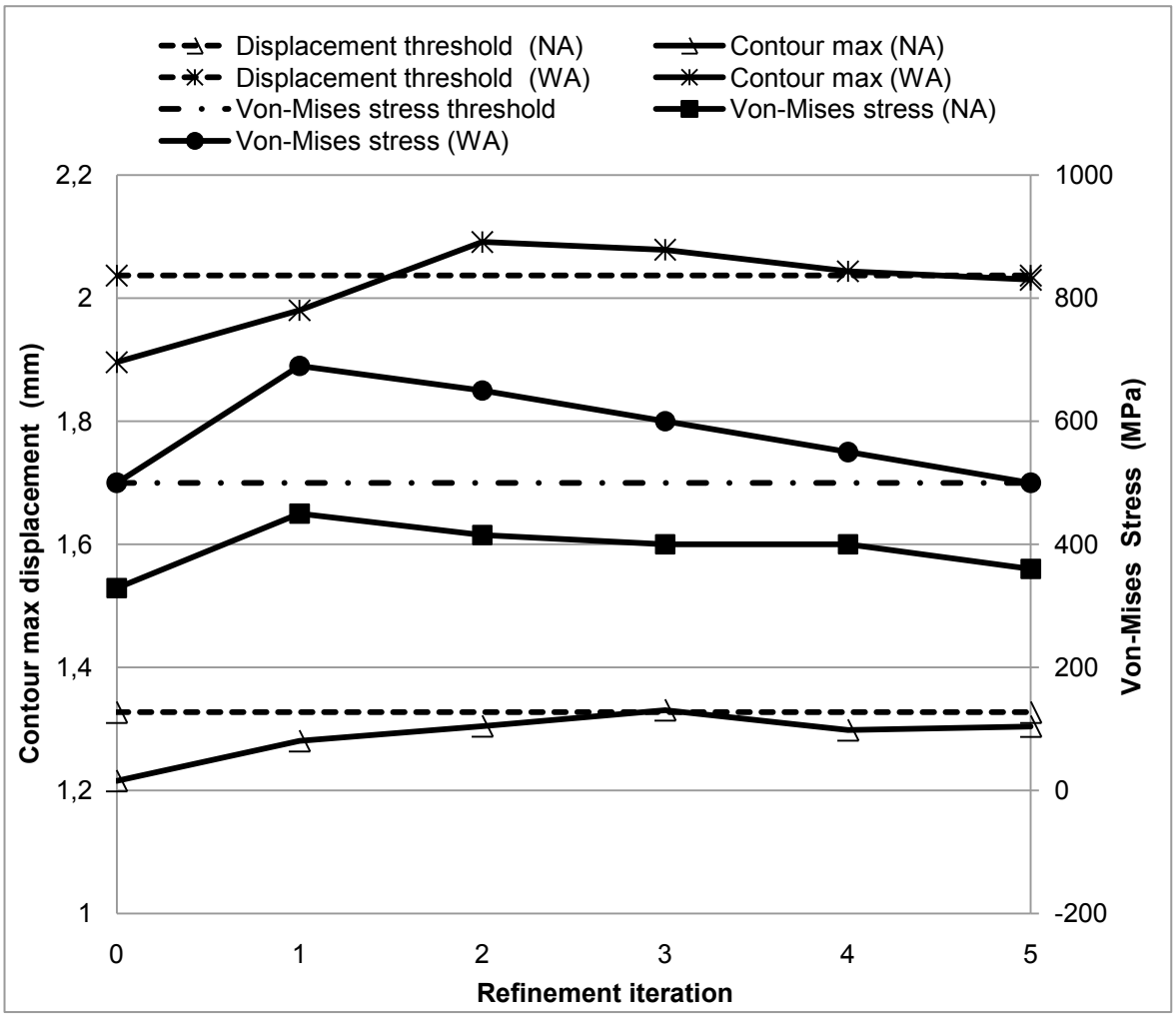

Figure 3.8 Design refinement results

The change in design between the initial (0) and final iteration (5) resulted in a 29% material reduction. Figure 3.9 shows specific geometrical changes for all regions of interest.

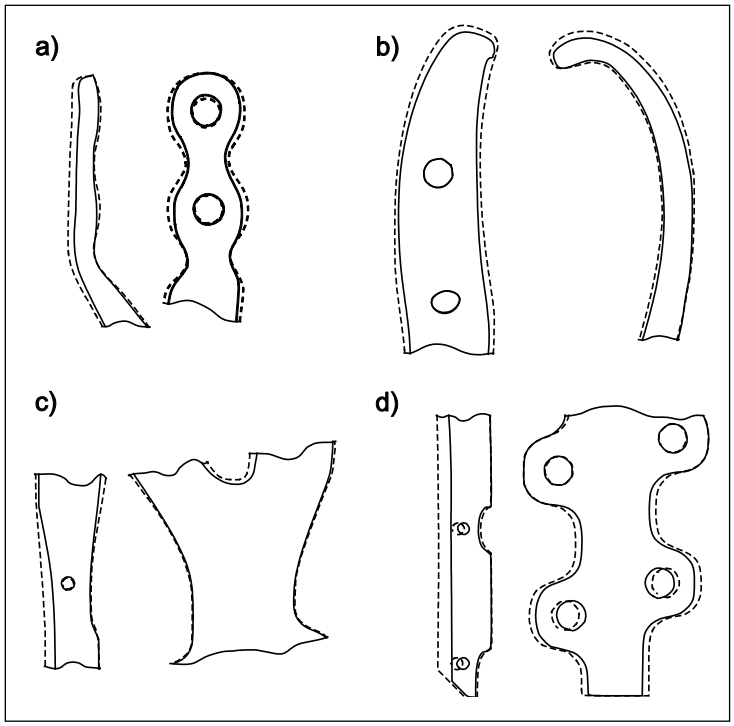

Figure 3.9 Change in shape of the Y3 plate after design refinement

The thickness of ROI *a* (Figure 3.9a) was reduced by 33% and its width by 17%. The ROI *b* (Figure 3.9b) saw a 25% reduction in its thickness and an 8% reduction in its width. The ROI *c* (Figure 3.9c) thickness was 5% smaller, but its width increased by 7%. ROI *d* (Figure 3.9d) ended with a smaller thickness and width – by 30% and 8% respectively.

The maximal Von-Mises stresses for the refined design were 364 MPa for NA and 498 MPa for WA. In both loading cases, maximal Von-Mises stresses were located around the first two proximal cable holes (Figure 3.10).

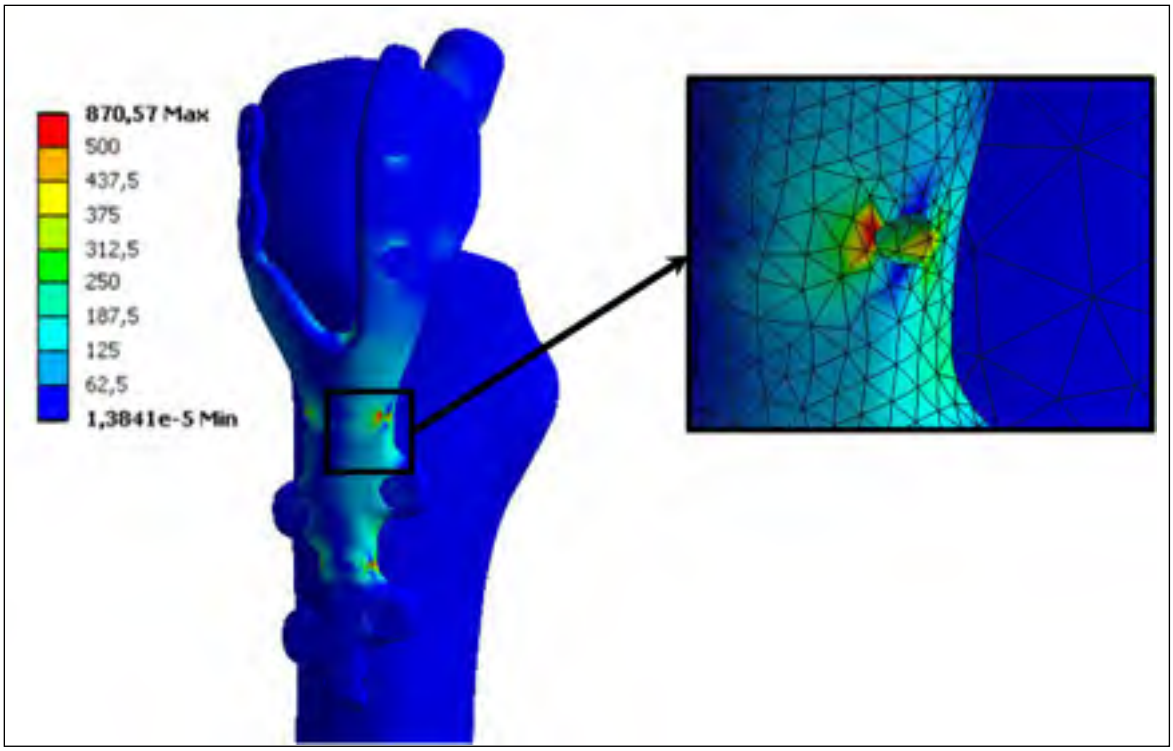

Figure 3.10 Von-Mises stress distribution (In this image, red zone is associated to numerical stress concentration not taken into consideration in the analysis)

3.7 Discussion

In this study, refined mesh parameters were used for the initial geometry and for all refinement iterations. Mesh refinements were not performed on the femoral prosthesis because their displacements and stresses were not considered crucial for this study. The femoral implant was modeled only to provide a realistic load transfer to the femur. Although femoral displacement and stresses were not directly analyzed in this study, femur deformations may have an impact on GT movements. To ensure the validity of femur deformation results, the mesh size was defined in accordance with previous studies (Polgar, Viceconti et O'Connor, 2001; Viceconti *et al.*, 1998).

Rigid body GT movement direction was in agreement between experimental and numerical results, which may imply that the FEM adequately reproduces the experimental behavior of

the GT. On the other hand, differences were observed in the magnitude of movement between the two models. Modeling assumptions can partly explain the generally higher stiffness of FEM as compared to the experimental model. For instance, bonded contacts used for screw connections in bone and the fixed joints between the plate and the screws provided a stiffer screw-bone connection than the experimental model. Frictionless contacts were also used between the femur and GT while friction behavior is most likely not negligible in reality. Further, the experimental model included Co-Cr cables in addition to screws, while the FEM only included screw fixations to reduce convergence problems. Nevertheless, the differences observed should not affect the conclusions of this study due to its comparative nature.

The width of ROI *c* was increased in this refinement study in order to reduce the GT rotation. This is in accordance with a previous study on the effects of ROI (Bourgeois, Petit et Laflamme, 2010) suggesting that reducing ROI *c* may have an important effect on GT displacements. The cross-section areas of ROI *a*, *b* and *d* saw the greatest reductions. For all ROI, except for ROI *c*, the thickness was reduced by 1.9 to 3.8 times the width. This significant thickness reduction greatly contributes to the realization of the low profile objective of Y3 plate refinement in an attempt to reduce the risk of bursitis and pain. It is important to note that thickness reduction was also limited by geometric constraints. For example, locking screws need minimal thickness for the locking head. In such cases, Von-Mises stress augmentation was obtained by reducing the width. Increased Von-Mises stresses indicate a reduced rigidity of the implant, which fosters a decrease in bone stress shielding (Tonino *et al.*, 1976).

Maximal Von-Mises stresses were located close to the two proximal cable holes of ROI *d*. Although the maximal Von-Mises stresses were below the target limit (500 MPa), further implementation of cables in the FEM may affect the constraints in this area. Forthcoming analyses will be performed to ensure the maximal Von-Mises stress criterion will still be respected when cables are included in the construct, although this should be the case from a

mechanical stand point. Adding cables in the construct should distribute the loads between screws and cables and decrease bending moments in the plate.

3.8 Conclusion

This study presents the refinement of a new GTR system composed of a Y-shaped plate and locking screws using FEM in an attempt to provide a low profile design without compromising GT stability.

FEM validation suggests that the GT rigid body movements observed were in line with experimental results: the movement of RP in Xr, Yr axis and rotation were in the same direction. Design refinement iterations allowed convergence to the specified criteria within five iterations. The cross-section area of ROI *a*, *b* and *d* saw the greatest reductions and ROI *c* saw a slightly reduction in thickness and a slight increase in width. These results were in agreement with a previous study on the influence of the geometry of the ROI on GT displacements. Generally, the overall thickness was importantly reduced, in keeping with the reduced profile design target aimed at decreasing the risk of bursitis and pain.

The Y3 refined plate resulting from this FEM study is thinner and more flexible then the initial one. Next steps will include testing the refined plate in synthetic and cadaveric specimens to confirm its stability and strength. Subsequently, the Y3 plate will be adapted for clinical follow-up studies.

3.9 Acknowledgment

This research was funded in part by the Natural Science and Engineering Council (NSERC), the Fonds Québecois de la Recherche sur la Nature et les Technologies (FQRNT) and the Canadian Foundation for Innovation (CFI). The authors also thank Yannick-Vincent Baril for his technical assistance during experimental tests and Dominic Boisclair for his editorial help.

3.10 Reference

Bourgeois Y., Petit Y. and Laflamme Y.G. 2010. Finite Element Model of a Greater Trochanteric Reattachment System. Proceedings of the 32nd Annual International Conference of the IEEE EMBS; August 31 - September 4; Buenos Aires, Argentina, 3936-3929.

Barrack R.L. and Butler R.A. 2005. Current status of trochanteric reattachment in complex total hip arthroplasty. Clin Orthop Relat Res. 441:237-242.

Koyama K., Higuchi F., Kubo M., Okawa T. and Inoue A. 2001. Reattachment of the greater trochanter using the Dall-Miles cable grip system in revision hip arthroplasty. J Orthop Sci. 6(1):22-27.

McCarthy J.C., Bono J.V., Turner R.H., Kremchek T. and Lee J. 1999. The outcome of trochanteric reattachment in revision total hip arthroplasty with a Cable Grip System: mean 6-year follow-up. J Arthroplasty. 14(7):810-814.

Jarit G.J., Sathappan S.S., Panchal A., Strauss E. and Di Cesare P.E. 2007. Fixation systems of greater trochanteric osteotomies: Biomechanical and clinical outcomes. Journal of the American Academy of Orthopaedic Surgeons. 15(10):614-624.

Takahira N., Itoman M., Uchiyama K., Takasaki S. and Fukushima K. 2010. Reattachment of the greater trochanter in total hip arthroplasty: the pin-sleeve system compared with the Dall-Miles cable grip system. International Orthopaedics. 34(6):793-797.

Petit Y., Laflamme G.Y. and Bourgeois Y. Submitted (2008). Orthopaedic fixation component and method. Canadian Intellectual Property Office. Patent No. CA 2643678.

Baril Y., Bourgeois Y., Brailovski V., Duke K., Laflamme Y.G. and Petit Y. Submitted (2010). Improving greater trochanteric reattachment with a novel cable plate system. Clinical Biomechanics.

Tonino A., Davidson C., Klopper P. and Linclau L. 1976. Protection from stress in bone and its effects. Experiments with stainless steel. J Bone Joint Surg Br. 58(1):107-113.

Ganesh V., Ramakrishna K. and Ghista D. 2005. Biomechanics of bone-fracture fixation by stiffness-graded plates in comparison. Biomed Eng Online. [Internet]. [cited 2010 August 28]; 4:46. Available from: http://www.biomedical-engineering-online.com/content/4/1/46

Polgar K., Viceconti M. and O'Connor J.J. 2001. A comparison between automatically generated linear and parabolic tetrahedra when used to mesh a human femur. Proceedings of the Institution of Mechanical Engineers, Part H (Journal of Engineering in Medicine). 215(H1):85-94.

Petit Y., Aubin C-É and Labelle H. 2004. Spinal shape changes resulting from scoliotic spine surgical instrumentation expressed as intervertebral rotations and centers of rotation. Journal of Biomechanics. 37(2):173-180.

Baril Y., Bourgeois Y., Brailovski V., Duke K., Laflamme Y.G. and Petit Y. Forthcoming 2010. Testing system for the comparative evaluation of greater trochanter reattachment devices. Experimental Techniques.

ASM-International and Granta-Design [Internet]. 2010. Materials for Medical Devices Database; [cited 2010 March 29]. Available from: http://products.asminternational.org/meddev/index.aspx.

Heiner AD. 2008. Structural properties of fourth-generation composite femurs and tibias. J Biomech. 41(15):3282-3284.

Tudor-Locke C., Hart T.L. and Washington T.L. 2009. Expected values for pedometer-determined physical activity in older populations. International Journal of Behavioral Nutrition and Physical Activity. 6:59.

Viceconti M., Bellingeri L., Cristofolini L. and Toni A. 1998. A comparative study on different methods of automatic mesh generation of human femurs. Medical Engineering & Physics. 20(1):1-10.

DISCUSSION

Ce projet avait pour objectif de raffiner le concept de la plaque Y3 afin de réduire son profil. Un « profil bas » a l'avantage de diminuer la friction entre la plaque et les muscles favorisant une diminution de douleur pour les patients. Pour ce faire, un MÉF a été développé et validé à l'aide d'essais expérimentaux. Une étude de sensibilité a permis de déterminer l'impact de modifier les dimensions de la plaque sur les déplacements du GT. Les résultats de l'étude de sensibilité ont contribué au raffinent de la plaque Y3 afin d'en réduire le profil.

La validation du modèle numérique avec les essais sur modèles *Sawbones* a été effectuée, pour les deux articles, à l'aide de deux expérimentations différentes. Les résultats expérimentaux présentés dans le premier article ont été obtenus en utilisant un système de fixation utilisant des vis autobloquantes. Par ailleurs, les résultats expérimentaux du deuxième article ont été obtenus avec un système de fixation incluant des vis et des câbles en CoCr. La comparaison entre le modèle expérimental et le modèle numérique effectuée dans les deux articles montre qu'il y a concordance dans l'orientation du mouvement du GT. La similitude de direction de déplacement du fragment, à grand angle (WA), entre les résultats expérimentaux des deux articles montre que l'ajout des câbles ne change pas le comportement du fragment. Par contre, pour les essais qui incluent les câbles, il y a diminution des déplacements de 54% et 10% dans les axes Xr et Yr respectivement. Les déplacements Xr et Yr du modèle numérique sont entre 35% et 72% plus rigides que les expérimentations. Ainsi, il est possible de penser que la modélisation des câbles n'apporterait pas de contribution importante dans les déplacements du GT du modèle numérique.

La comparaison entre l'expérimentation et le modèle numérique, réalisée dans les deux articles, montre également que le MÉF est plus rigide, sous-estimant les déplacements du point de référence (sauf pour la rotation). Cette rigidité peut s'expliquer en partie par le comportement des contacts liant les vis à l'os et à la plaque. Le type de contact « totalement lié » utilisé pour modéliser la liaison entre les vis et l'os ne semble pas représenter fidèlement

le cas expérimental. En expérimentation, si la vis applique une force tangentielle (Ft) seulement, la moitié du cylindre devrait fournir un effort de réaction (Fr) (Figure 3.11a). Par contre, par la définition du contact du modèle numérique, la force de réaction (Fr) sera répartie sur toute la surface du trou (Figure 3.11b). Ainsi, la pression de réaction du modèle numérique serait plus faible que le modèle expérimental ce qui engendrait une déformation locale plus petite dans le modèle numérique, donc moins de déplacement. Il est aussi possible qu'un mouvement relatif entre la vis et l'os soit présent dans le modèle expérimental et pas dans le modèle numérique.

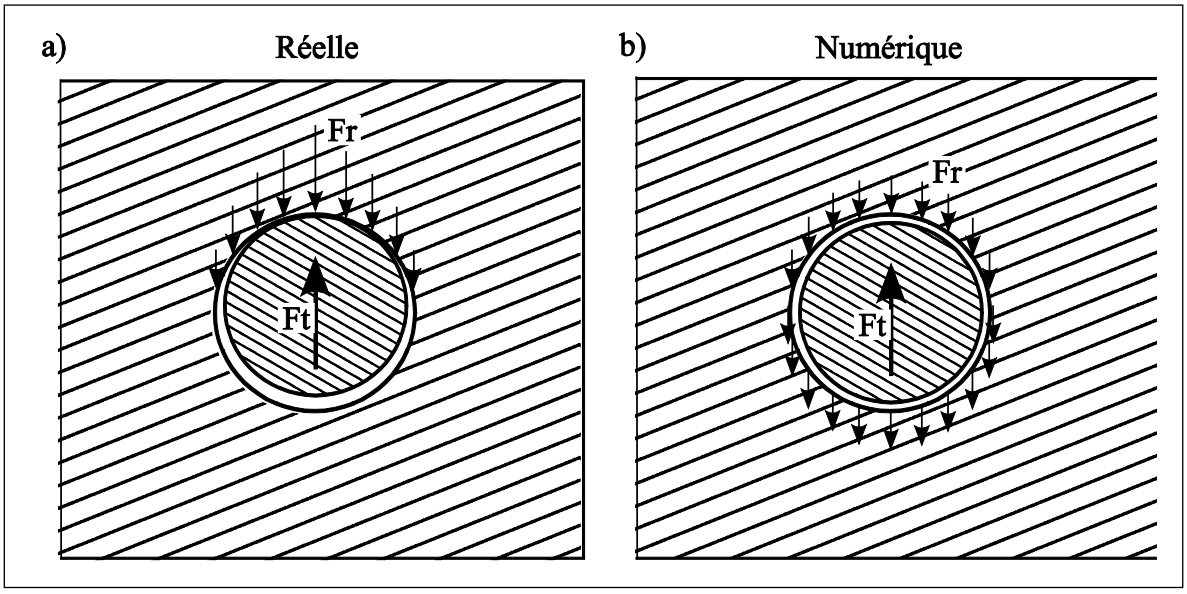

Figure 3.11 a) Force de réaction d'un charment transversale réelle aux vis b) Force de réaction d'un chargement transversal numérique aux vis

En ce qui concerne les rotations, il a été observé que les rotations sont plus grandes dans le modèle numérique comparativement à l'expérimentation. Cela peut s'expliquer par le fait que la friction entre le GT et le fémur a été considérée comme nulle, ce qui n'est pas le cas dans les essais expérimentaux. Il est possible que cette simplification augmente les rotations du GT comparativement aux essais avec modèles *Sawbones*. L'ajout d'un coefficient de friction entre le GT et le fémur pourrait être inclut dans le modèle. Bien que l'ajout de cette friction implique peu d'effort d'adaptation et une légère augmentation du temps de calcul, la

caractérisation du coefficient de friction entre l'os spongieux et l'os cortical d'un modèle Sawbones est nécessaire. Aucune étude déterminant le coefficient de friction entre deux fragments d'os Sawbones n'a été trouvée dans la littérature et très peu d'études du coefficient de friction d'os cadavérique, hydraté et non hydraté, ont été publiées (Von Fraunhofer, Schaper et Seligson, 1985). Ainsi, les nombreuses simplifications du MÉF tendent à rigidifier le modèle et à sous-estimer les déplacements observés expérimentalement. Pour cette raison, il n'est pas possible de considérer les résultats de façon absolue mais plutôt sur une base comparative avec le modèle initiale. De plus, les contraintes de Von-Mises n'étant pas validées expérimentalement, il est possible que les résultats ne soit pas le reflet exact des contraintes admise dans la plaque.

L'étude du premier article a permis de comprendre l'influence de la variation de section des différentes régions d'intérêt de la plaque sur les déplacements du GT. Il en ressort que les déplacements du GT sont plus sensibles pour la région *c*, reliant les deux branches proximales à la branche distale. La région *e* a été incluse dans la région *d* pour l'étude du deuxième article car elle a peu d'incidence sur les déplacements du GT. De plus, la région *e* est soumise aux mêmes limites géométriques que la région *d*; un minimum d'épaisseur et de largeur doit être conservé pour le passage des câbles. Le raffinement de la plaque Y3, présenté dans le deuxième article, montre une convergence des déplacements et des contraintes de Von-Mises sous les seuils établis. Le volume de la plaque Y3 raffinée est diminué de 29 % comparativement à la plaque initiale. La grande modification des régions *a*, *b* et *d* (de 25 % à 33 % pour l'épaisseur et de 8 % à 17 % pour la largeur) et la petite modification de la région *c* (5 % pour l'épaisseur et 7 % pour la largeur) est en accord avec les résultats du premier article indiquant qu'une modification de la région *c* affecterait les déplacements du GT de façon importante.

L'analyse des contraintes de Von-Mises effectuée dans le deuxième article montre un maximum dans la région des trous de passage des câbles proximaux (Figure 3.10). Les contraintes établies autour des trous présentent toutefois des points de singularité. Ces points

ont été déterminés comme points singuliers car leurs voisins présentaient des contraintes nettement inférieures (57%) même avec des raffinements de maillage. Ainsi, les résultats présentés font omission des contraintes de ces points singuliers et le maximum considère une moyenne des points autour du point singulier. Bien que la validation du modèle suggère que la modélisation des câbles a peu d'impact sur le comportement du fragment, il n'est pas possible d'en dire autant pour les contraintes induites par les câbles dans la plaque. Il n'est pas facile d'anticiper ce que les câbles pourraient changer aux contraintes près des trous. Il n'est donc pas possible d'affirmer avec certitude que le seuil de contrainte établi pour le raffinement de la plaque serait respecté. Il est vrai que l'ajout des câbles créerait un chargement dans la région des trous. Or, avec les câbles, les forces transmises à la plaque seraient mieux réparties car elles passeraient par les câbles et les vis. Ainsi, le moment de flexion pourrait être plus petit diminuant les contraintes dans la plaque. Il serait judicieux, dans une prochaine étude, de faire des simulations incluant la modélisation des câbles pour confirmer que les câbles n'augmentent pas les contraintes près des trous.

Il pourrait être avantageux de produire un modèle comportant des paramètres de modification de géométrie avec une régénération automatique du maillage et des conditions limites afin d'automatiser et d'accélérer le processus itératif. Ce type de modèle faciliterait la réalisation d'une optimisation et pourrait être utilisé dans un processus d'adaptation finale de la plaque en vue de sa production à grande échelle. Ce genre de modèle ouvre aussi la porte à différentes études connexes. Il pourrait être utilisé pour étudier de nouvelles versions ou configurations de la plaque Y3. Par exemple, une version allongée de la plaque pourrait être utilisée pour fixer une fracture de la diaphyse en périphérie d'une prothèse fémorale, problèmes fréquents pour lesquels le concept de la plaque Y3 pourrait possiblement s'avérer avantageux comparativement aux solutions actuelles. Le modèle pourrait aussi être adapté pour étudier des cas plus complexes de fractures multiples du GT.

De plus, la plaque étant conçue pour être formée à la géométrie spécifique du fémur lors de la chirurgie, l'étude d'une déformation plastique et de ses effets sur sa résistance pourrait être pertinente. Ultimement, il serait possible de faire une étude de personnalisation de plaque dont le modèle numérique serait une base de calcul pour en évaluer la performance. Une première étape de numérisation pourrait générer le modèle du fémur. Une seconde étape permettrait le positionnement et l'adaptation de la plaque spécifiquement pour le fémur du patient. Par la suite, le modèle permettrait de produire rapidement des résultats de stabilité du fragment et de contraintes induites dans la plaque. Une fois la plaque validée avec le modèle numérique, celle-ci pourrait être produite en alliage de titane par un procédé de fabrication en forme libre.

CONCLUSION

Le détachement du GT est une complication possible suite à l'arthroplastie de la hanche. Les systèmes de plaque et câbles présentement utilisés permettent de repositionner et de maintenir le GT. Or des problématiques importantes de bris, de non-union ou d'unions fibreuses liées à l'instabilité du fragment ont été rapportées avec les présents systèmes. Le nouveau système Y3 tente de pallier à ces problèmes en utilisant une géométrie particulière et en jumelant l'avantage de l'utilisation de câbles et de vis. De plus, sa conception offre un « profil bas » dans le but de réduire le frottement entre les tissus mous et la plaque pouvant diminuer la douleur des patients. Une étude expérimentale comparative a permis de montrer que le système de fixation Y3 semble mieux retenir les déplacements antéropostérieurs que le système *Cable Grip* de la compagnie *Zimmer*.

L'objectif général de la présente étude visait à raffiner la conception de la plaque Y3. Pour ce faire un MÉF a d'abord été développé et validé par comparaison avec des essais expérimentaux. Le MÉF a ensuite été utilisé pour évaluer la sensibilité des déplacements du GT selon le changement des dimensions de différentes régions. En fonction des résultats de l'étude de sensibilité, un raffinement dimensionnel de la plaque a été réalisé avec le MÉF.

La comparaison entre les données expérimentales et numériques a permis de valider le comportement du MÉF. Or la différence de grandeur des résultats a montré que le modèle numérique est généralement plus rigide que l'expérimentation. La simplification du contact entre les vis et l'os semble être le principal facteur expliquant cette rigidité accrue.

Le raffinement du concept a permis de réduire le volume de la plaque Y3 de 29 %. La région *c*, qui est la plus influente sur le déplacement du GT, a été la moins modifiée avec une diminution d'épaisseur de 5 % et une augmentation de 7 % de largeur. Les changements de géométrie ont favorisé « un profil » bas de la plaque tout en n'augmentant pas les déplacements du GT comparativement au concept initial. Les contraintes maximales de Von-

Mises sont légèrement sous le seuil des 500 MPa et se situent dans la région des deux trous proximaux. L'absence des câbles dans le MÉF ne permet pas de déterminer si les contraintes sont réellement sous le seuil des 500 MPa. L'ajout des câbles dans le modèle pourrait avoir pour effet d'augmenter les contraintes dans cette région. Ainsi, il serait adéquat, pour la suite du projet, d'ajouter les câbles dans le MÉF.

Le MÉF développé et validé dans le cadre de ce travail a permis de mieux comprendre l'importance des différentes régions de la plaque Y3. De plus, le raffinement effectué a diminué de façon importante l'épaisseur des régions qui ont un impact moindre sur les déplacements du GT. Enfin, il en résulte une plaque avec « un profil » plus bas tout en gardant un même maintien du GT. Cette amélioration du concept favorise une diminution de la douleur, des bursites et des risques de complication.

Il pourrait être avantageux d'automatiser la modification et la simulation du modèle permettant d'effectuer une optimisation des différents paramètres de conception et de faciliter les modifications dans le but d'une production à grande échelle de l'implant. Les simplifications du MÉF pourraient avoir un impact sur l'estimation des contraintes de Von-Mises. Il est donc possible que les contraintes admises dans la plaque expérimentalement diffèrent des contraintes calculées numériquement. Ainsi, des essais expérimentaux avec un système de détection des déformations permettraient de valider le modèle d'un point de vue déformation-contrainte ce qui serait un apport important comparativement à une validation de déplacement du fragment du GT.

Bien que plusieurs améliorations puissent être effectuées, le présent modèle pourrait facilement être utilisé dans des études de sensibilité du déplacement du GT pour mieux connaître les effets sur l'angle de coupe, l'orientation et l'amplitude d'application des forces externes, le coefficient de friction entre le fragment et le fémur, etc.

ANNEXE I

ARTICLE 3 « TESTING SYSTEM FOR THE COMPARATIVE EVALUATION OF GREATER TROCHANTER REATTACHMENT DEVICES »

Y. BARIL[1], Y. BOURGEOIS[1,3], V. BRAILOVSKI[1], K. DUKE[2], G. Y. LAFLAMME[3] AND Y. PETIT[1,3]

[1] École de technologie supérieure, Mechanical Engineering, Montréal, Québec, Canada

[2] University of Alberta, Mechanical Engineering, Edmonton, Alberta, Canada

[3] Hôpital Sacré-Coeur de Montréal, Research Center, Montréal, Québec, Canada

Cet article a été soumis dans la revue : Experimental Techniques

RÉSUMÉ

Cet article effectue la validation du montage expérimental de comparaison des systèmes de rattachement du GT. Une évaluation d'un système avec trois caméras sur des essais typiques de rattachement du GT permet de valider si la lecture des déplacements du GT est significative par rapport à l'erreur de mesure.

Les résultats montrent que les caméras dans les vues antérieure et postérieure obtiennent une erreur, due à la déformation du fémur, qui est trop importante pour capter les déplacements du GT lors du chargement simulant l'action musculaire. Ainsi, ces caméras sont invalidées pour ce type de mesure et seulement la caméra dans le plan de l'ostéotomie est retenue pour les essais.

CONTRIBUTION

L'auteur de ce mémoire a contribué à la conception, la fabrication et l'assemblage des composantes mécaniques du montage. Il a participé à l'intégration du système hydraulique du montage. Il a établi le protocole de préparation des spécimens Sawbones et a préparé les spécimens nécessaires pour la validation du montage. Il a également participé à la planification et au déroulement des essais de validation. Finalement, il a participé à l'analyse des résultats et à la rédaction de l'article.

ABSTRACT

The scope of this study is to propose and validate a specialized test bench that applies biaxial forces on an orthopaedic model of Greater Trochanter (GT) reattachment with integrated cable tension measurement. Stability of the GT fragment is evaluated using a custom tri-planar video movement analysis system with the first camera's Field of View (FOV) corresponding to the GT osteotomy plane and the second and third camera's FOVs corresponding to the median plane of the femur in frontal and posterior views, respectively. A typical experimentation and its critical analysis conclude the paper.

INTRODUCTION

Greater Trochanter fracture can result from hip replacement surgery complications. An osteotomy of the Greater Trochanter (GT) may also be requested during hip revision to allow for better exposure of the femur and easier removal of the femoral implant. Regardless of the source, cable-plate systems are currently preferred to cable cerclage for GT reattachment[1]. However, a significant number of complications are still reported with modern GT reattachment systems. The number of breakages is as much as 19% and trochanteric non-union occurs in 15% of GT reattachments[2].

Numerous biomechanical tests have been performed on various wire, cable and cable-plate GT reattachment systems. These tests were conducted to: compare cable systems[3,4], to understand the mechanics of the GT reattachment[5], or to evaluate novel osteotomy techniques[6,7].

A first limitation of the majority of the above-mentioned biomechanical studies consists of applying only abductor forces on the reattached GT, one of the exceptions being Bredbenner et al.[8] who considered the application of both trochanteric and femoral head forces using a cantilever arm which does not allow independent modulation of applied forces' intensity and direction. A second limitation of the majority of studies is to take displacement measurements in only one direction using traction machine transducers or mechanical extensometers. However, Schwab et al.[9] used a planar video motion analysis to track relative GT-femur sliding, whereas Schoeniger et al.[7] and Bredbenner et al.[8] used an Optotrak-motion measuring system (Northern Digital Inc, Waterloo, ON, CA) to analyze relative GT-femur movements.

An ideal test bench must simulate the application of physiological forces on an upper femur extremity: abductor forces acting on the GT fragment and body-weight forces acting on the femoral head. To simulate different hip movements, these forces should be controlled independently and their directions changed easily. Relative GT-femur movements, including in-plane sliding, tilting and out-of-plane GT-femur opening should be measured. A test bench that could monitor the progression of cable tension during testing would also be a valuable asset.

The test bench presented in this study is specifically designed for testing of GT fixation systems, but it can also be used to carry out studies of a wide range of proximal femoral fracture fixation systems. The test bench includes an original tri-planar motion analysis video system that was developed and installed on a customized hydraulic test bench. In this work,

both systems are described and a typical testing experiment is presented as an illustration of the capability of the developed system.

MATERIALS AND TESTING SYSTEM DESCRIPTION

FEMUR MODEL, REATTACHMENT DEVICE AND SPECIMEN PREPARATION

Biomechanical studies on the GT osteotomy used either cadaveric human bone [5,9] or polyurethane model[6,10]. In this study, to limit the interspecimen variability, polyurethane SawBone model of 4th generation (Pacific Research Laboratories Inc, Vashon Island, WA, USA) was used. It is accepted that this model mimics better the rigidity of the bone specimen than the previous 3rd generation model[11].

The greater trochanter and femoral head are here cut in a way to reproduce a fracture occurring after a hip replacement surgery or a worst case scenario during a revision surgery without the iliotibial band attached to the fragment. The Sawbones femur is subjected to three successive cuts (Figure 1a) with the help of a preparation jig made by rapid prototyping reproducing the Sawbones' shape and ensures its precise positioning. First, a transversal cut A-A is made with a hand saw medially in the femur body (1). Next, a trochanteric cut B-B is made severing the GT fragment (2). The third cut C-C allows the removal of the femoral head (3). The femur is than reamed allowing the implantation of a press-fit femoral implant (Stryker, Kalamazoo, MI, USA) (4) (Figure 1b). The distal part of the femur is embedded in a 50 mm wide square steel tube with polyester-based body filler (Bondo, 3M, GA, USA). The square tube is precisely positioned using the specialized prototyped preparation jig. Using a rotary tool, three recesses are made in the GT fragment to accommodate the plate teeth, which are then filled with polyester-based body filler. This technique makes possible the insertion of the plate teeth in the cortical bone which is impossible by its impaction in synthetic bone.

The GT fragment is reattached to the femur using the Cable-ready® cable grip system (Zimmer Inc., Warsaw, IN, USA), which consists of an integral long GT reattachment device -- plate (5) (Figure 1c) and four 1.8 mm diameter Cobalt-Chrome cables (not shown). The plate (5) teeth are imprinted in the filled recesses (see Figure 1b) to assure that the implant system and the GT fragment fit together. To simulate a usual clinical practice to increase the proximal cable stability, a 2 mm diameter hole is drilled medially through the lesser trochanter, allowing the first proximal cable to pass through it (Figure 1c). An abductor force application strap (6) is then fixed to the proximal region of the GT fragment using a screw attachment, with the possibility of free rotation about the screw axis. The GT fragment is now prepared for fixation with the Cable-ready® cable grip system.

TESTING SYSTEM

The testing system can be divided into three subsystems: a test bench, a computerized control-data acquisition system, and a motion-analysis video system designed to record GT fragment displacements. LabView software (LabView 8.6, National Instruments., Austin, TX, USA) controls the test bench using a real-time configured personal computer target as described in detail in Chartrand et al.[12].

TEST BENCH

As shown in Figure 2, two hydraulic cylinders (7) (1 1/8-MH-TF-4-D, Scheffer Corporation, Cincinnati, OH, USA) are connected to the model by a pair of transmission cables (8); the first (P1) is linked to the femoral head (12) and the second (P2) is linked to the GT fragment attachment strap (6). The forces P1 and P2 applied by the cylinders (7) are recorded by the load cells (9) and (11) (4448 N, LC101-1k and 2224 N, LC101-500, Omega Engineering Inc, Stamford, CT, USA) installed on the transmission cables. The transmission cables are redirected to the femoral head (12) and to the abductor force application strap (6) by pulleys and guides (10, 13). The direction of the P1 and P2 forces can be easily modified by changing the guides' positions (10, 13) using slide-screw systems.

In each attachment cable (14) of the GT reattachment system, shown in more detail in Figure 3a, a through-hole load cell (15) (889 N, LC8100-200-5, Omega Engineering Inc, Stamford, CT, USA), a crimping device (16) and a tensioning bracket (17) are installed to allow continuous measurement of the cable tension.

The Cable-Ready^{tm} plate is inserted in the molded GT recesses, and the GT and the plate are assembled and implanted on the femur. Each of the four attachment cables are passed through the plate (5), the tensioning bracket (17), the load washer (15) and the crimping device (16). The first proximal cable is also passed through the lesser trochanter hole (Figure 3a). Initially, the cables are slightly tightened using external tools, and then they are tensioned from the proximal (Cable 1) to the distal (Cable 4) up to a load of 355 N (80 lb) according to the manufacturer's instructions. Important variations of Cable 1's tension can be observed during this initial tightening procedure (Figure 3b). To stabilize the system, all of the cables are re-tensioned once again starting with the proximal cable.

Once the femur (1) and the GT (2) are placed in the test bed, as illustrated in Figure 2, forces (P1) and (P2) can be independently controlled with an accuracy of ±3N in static mode[12] in accordance with the user needs. Measured forces (load cells 9, 11, 15) and displacements (pistons (7) positions) can then be recorded in real-time.

MOTION ANALYSIS VIDEO SYSTEM

For this study, a dedicated motion analysis video system was developed to follow in-plane and out-of-plane (gap) displacements and rotations of the GT fragment with respect to the femur under simulated physiological loading. The motion analysis system contains three video cameras as illustrated in Figure 4. Cam1 has a Field of View (FOV) on the slide plane; Cam2 and Cam3 have FOVs on the median plane of the femur in anterior and posterior views.

To identify and track targets, the motion analysis application program uses LabView 8.5's vision capabilities (National Instruments). Images are acquired by three black-and-white Grasshopper cameras (GRAS-20S4M-C, Point Grey Research, Richmond, BC, Canada) with a focal length of 35 mm lenses (MeVis-C, LINOS Photonics, Munich, Germany) are used. The cameras' resolutions are set to 1024 X 768 pixels, which corresponds to the maximum observable area without image loss at 30 Hz. To maximize the system's targets following capacity, higher speed frame grabbing is preferred to higher resolution. The resolution of the motion analysis system was determined, in previous unpublished works, to be better than 0.01 mm for a 350 mm distance between the camera and the tracked landmarks.

TESTING METHODOLOGY AND MEASUREMENT ERROR

The test bench is designed to independently apply the weight force to the femoral head (P1) and the abductor force to the GT fragment (P2). In this study, mechanical testing of the GT-femur assembly consists of simultaneous cyclic application of the abductor and weight forces from the reference loaded state to the maximum loaded state (Table 1). The peak forces P1 and P2 applied are: 2400 N (2.8 body-weight of 847 N) on the femoral head (P1), and 650 N (0.75 body-weight) on the greater trochanter (P2) (Figure 1c and Table 1). The P1 and P2 force amplitude and direction are in the range of relevant literature data when the Vasus Lateralis is not taken into account [9,10,13,14]. The amplitudes of both P1 and P2 forces are limited by the following testing bench force-related limitations: a) maximum forces that could be generated by hydraulic cylinders of the bench, and b) maximum forces that could be supported by the GT fragment attached to the bench using screw-strap fixation. Also, force vector directions are set to apply a large frontal force on the reattached GT fragment since this is what happens in a critical movement such as rising from a chair[13]. The force coordinate system corresponds to that shown on Figure 1. Maximum forces in Table 1 were adjusted to respect the test bench and GT fragment force-withstanding capabilities. The force generated by the femoral head actuator (P1) is multiplied by 1.3 to compensate for the guide-pulley (13) friction.

In this study, the two forces are applied simultaneously with the following loading sequence for each cycle: a) increase from the reference to the maximum force (three-second ramp), b) five-second dwell, and c) release from the maximum to the reference force (three-second ramp).

Note that two main approaches can be used to evaluate relative GT-femur movement during biomechanical testing: a) direct image measurement using contour or volume representations of the GT and femur bodies, and b) rigid-body analysis. Rigid-body analysis involves measuring the relative movement of at least two targets, one that belongs to the GT fragment and the other to the femur, and then the subsequent calculation of the relative positions of the bodies, without considering their deformation. Even though the direct image measurement approach is more reliable that the rigid-body one, it is much more difficult to apply to real-time measurements because of the huge amount of data to be processed. The rigid-body approach requires much less calculation and was proven to be appropriate for the majority of biomechanical studies [7-9]. In this work, an original measurement technique based on the hypothesis of rigid-body displacements and the least-squares singular value decomposition method adapted by Petit et al.[15] is used to track GT-femur movements. The use of this approach is validated in Appendix.

To perform measurement error evaluation, the femur model is prepared in conformity with the plate-cable reattachment system testing procedure (Figure1), except that the GT fragment is glued to the femur to avoid their relative movement. In this case, all calculated rigid-body displacements will result exclusively from measurement errors and femur deformation.
Two forces are applied to the femur as shown in Figure 1c, one to simulate the body weight of the subject and the other, the action of abductor muscles on the GT fragment; the latter is applied directly to the femur implant, respecting the orientation presented in Table 1. In this

test, six 4.76 mm diameter white-ball landmarks (pin heads) for each camera are dipped into hot adhesive on the proximal zone of the femur and on the GT fragment.

By grouping landmarks, two rigid bodies are defined, one for the GT fragment and one for the femur. Four out of the six landmarks defining each rigid body were used to create 225 different pairs of coordinate systems (CS). Five repetitions were performed with different landmarks' positions.

The discrepancy between the CS's initial and final registered positions is considered as caused by system errors (dotted lines in Figure 5). Rigid-body displacement measurement results are affected differently by the landmark positions for each camera. Table 2 summarizes the mean, standard deviation (STD) and maximum deviation of the mean (MDM) for displacement (X and Y), rotation (R), and maximum displacement on contour (Contour Max) as measured by each camera.

For CAM1, the results in Table 2 show reference point and contour movements, or offsets, of more than 2σ caused by loading. For camera 2, only X, Y displacements and contour movement are significant, whereas camera 3 shows no significant movement. Since this testing does not involve any GT-femur relative movement (GT was glued to the femur), the mean, STD and MDM displacements and rotations of Table 2 are caused by the femur deformation, and by the video system's measurement errors. It can be concluded that any result (displacement or rotation) measured during subsequent testing should be compared with the error measurement data of Table 2 in order to be considered as significant.

EXAMPLE OF EXPERIMENTATION

As an example of the testing system capabilities, a standard GT reattachment is tested (Figure 1). Simulated physiological forces represent the input variables, and GT fragment displacements and cable tensions are the output variables. Eight white spherical targets are mounted on needles, dipped into hot adhesive and positioned to obtain 4 landmarks visible by the camera on the GT and the femur (Figure 6). The landmarks are then selected on the video system and followed throughout the testing procedure. The results obtained from CAM 1 with an FOV on the osteotomy plane are presented below (see justification in Appendix).

The loading-dwell-unloading sequence of Table 1 is repeated 50 times to follow the evolution of the GT-femur assembly's behavior. Figure 7 presents the results of the first 10 loading cycles plotted as a function of time: loading sequence in Figure 7a, GT reference point displacement and rotation in Figure 7b, and cable tension in Figure 7c. For loaded (L) and unloaded (U) states, GT fragment displacements (X, Y and norm) and rotation measured at the reference point, as well as tension in cables 1, 2, 3 and 4 are collected for each cycle and presented in Figure 8a,b. Table 3 presents a summary of the reference point displacements measured after 50 cycles.

To summarize the results, fragment displacement from loaded to the unloaded state during one cycle is about 0.62 mm, and permanent displacement after 50 cycles is 1.31 mm (Figure 8a). Figure 8b shows that tension in all of the cables except cable 2, increases when they are loaded and decreases when they are unloaded and that all cables continuously lose tension during cycling.

DISCUSSION

Cable tensioning analysis shows important loosening of the first cable after initial tightening procedure. Retightening all the cables leads to a maximum deviation of only ±5 N from the recommended cable tension, highlighting the clinical need to retighten the cables

GT displacement showed an increase of up to 1.8 mm and subsequent stabilization after 50 loading cycles. Displacement at the 50^{th} loading cycle had a magnitude of 0.62 mm (essentially along Y axis) and the permanent displacement after 50-cycle testing is 1.3 mm. All of the results are significantly larger than the mean measurement errors in the Y direction (0.30 mm, see Table 2). Fragment rotation reaches 4.3 deg counterclockwise, which is also significantly larger than the mean rotational measurement error (0.28 deg, Table 2).

All cables are subject to significant loosening during the loading sequence, ranging from 15 % for the third cable to 30 % for the first. Cable tension was not completely stabilized after 50-cycle testing. Further cable loosening and increase in GT displacement can be anticipated if cycling continues.

CONCLUSIONS

This paper presents a testing system designed for the comparative evaluation of GT reattachment systems in terms of GT movement under physiological loads. The test bench was developed using previously developed hydraulic system. GT movement was simultaneously followed in three perpendicular planes of view using a custom-made motion analysis system.

In the framework of this study, it has been proven that the developed testing system applies the desired forces with sufficient accuracy considering possible biological variations in the muscle forces applied. Results from the camera monitoring the slide plane (CAM1) were consistent and allow relevant relative fragment motion estimation, especially in the framework of comparative testing. Overall, the test bench gives accurate results in the plane

of maximum displacements. No GT-femur gap or GT fragment tilting was observed in this study.

Finally, to the best of our knowledge, this test bench is the first to monitor cable tension throughout the experiment, from implantation to multiple loading cycles. This cable tension data will help provide a better understanding the biomechanics of trochanteric reattachment and of its failure.

ACKNOWLEDGEMENTS

This work was supported by the Natural Sciences and Engineering Research Council of Canada (NSERC) and the Canadian Foundation for Innovation (CFI). The authors would like to thank Ms. K. Boutin for her technical assistance on the motion analysis system.

APPENDIX: VALIDATION OF THE RIGID-BODY APPROACH APPLIED TO GT MOVEMENT MEASUREMENTS

Given that all rigid body-based methods of motion analysis neglect deformations of the bodies involved, the use of this approach can be problematic if the measured displacements become small and therefore comparable to the bodies' deformation. In this section, the applicability of the rigid body approach for GT movement analysis is evaluated.

The rigid-body calculated GT displacement vector ($\overrightarrow{\Delta GT_{calc}}$) contains three major contributions:

$$\overrightarrow{\Delta GT_{calc}} = \overrightarrow{\Delta GT_{eff}} + \left(\overrightarrow{\delta F} + \overrightarrow{\delta GT}\right)$$

where $\overrightarrow{\Delta GT_{eff}}$ represents the effective GT displacement vector, whereas $\overrightarrow{\delta F}$ and $\overrightarrow{\delta GT}$ represent, the apparent displacement vectors caused by the femur and GT deformations, respectively.

Using the tri-planar measurement system shown in Figure 4, a standard GT reattachment is tested between the reference (P1 = 150 and P2 = 50 N) and the maximum loads (P1 = 3120

and P2 = 650 N) using two approaches: a) direct image analysis and b) rigid-body GT movement evaluation (least-squares singular value decomposition method[15]). The results obtained are used to compare the effective ($\overrightarrow{\Delta GT_{eff}}$) and the rigid-body estimated ($\overrightarrow{\Delta GT_{calc}}$) GT motions using the following six-step approach:

1. Two four-landmark groups were positioned: one on the GT and one on the femur, and the rigid body approach was used to calculate the femur's local coordinate systems corresponding to its loaded and unloaded states.
2. The image of the loaded GT-femur assembly was superimposed on the unloaded image so that the loaded femur's local coordinate system fits with its unloaded coordinate system. Figure 9 presents the unloaded (solid lines) and the loaded (dotted lines) femur and GT positions.
3. The femur deformation vector $\overrightarrow{\delta F}$ was evaluated by measuring the displacement of one of the femur's contour points from its initial to its final reset position.
4. The movement of the GT contour was evaluated by measuring the displacement of one of the GT's contour points from its initial to its final reset position. Since the measured value includes the femur deformation, it can be expressed as $\overrightarrow{\Delta GT_{eff}} + \overrightarrow{\delta F}$.
5. The contour reference point displacement vector obtained by the direct image measurement was then compared to that from the rigid-body measurement, and their difference ($\overrightarrow{\Delta GT_{calc}} - \overrightarrow{\Delta GT_{eff}}$) was attributed to the GT and femur deformations ($\overrightarrow{\delta GT} + \overrightarrow{\delta F}$). Since the femur deformation ($\overrightarrow{\delta F}$) was already known, it is possible to determine the GT deformation ($\overrightarrow{\delta GT}$).

Geometric representation and quantitative evaluation of the vectors resulting from this evaluation are presented in Figure 9 (vector dimensions are magnified for clarity) and in Table 4. It can be seen that for CAM2 and CAM3, correspondence between the $\overrightarrow{\Delta GT_{eff}}$ and the $\overrightarrow{\Delta GT_{calc}}$ vectors is weak and their direction diverge significantly. This means that the deformation of the GT/femur assembly is large enough to reject the applicability of the rigid body-based measurements for these two cameras. On the other hand, with CAM1 and CAM3, the vector $\overrightarrow{\Delta GT_{eff}}$ contribution appears to be important and worth considering. However, for CAM3, $\overrightarrow{\Delta GT_{calc}}$ reflects an important GT-femur penetration, which is inconsistent with the direct image observations.

Based on the comparison of the results obtained by direct image and rigid body-based analyses, it can be asserted that the misleading results obtained with CAM2 and CAM3 are mainly due to GT and femur deformation under loading. This suggests that the rigid body-based measurement approach cannot be applied for either of these cameras as they are positioned in the testing set-up. Given these results, only data obtained with CAM1 will be used to illustrate the test bench capabilities for this set-up. It should be noted, however, that cameras 2 and 3 could provide useful data for another force setup than that presented in Table 1.

Table 4: Force vectors' definition.

			Force direction vector		
Applied forces	Reference force (N)	Maximum force (N)	x	y	z
P1	150	3120	0.16	-0.24	-0.96
P2	50	650	-0.50	0.63	0.60

Table 5: Mean, standard deviation and maximal deviation of the GT movement relative to the femur reference point for all three cameras. * highlights movement greater than 2 standard deviations (2□).

	Camera 1			Camera 2			Camera 3		
	Mean	STD	MDM	Mean	STD	MDM	Mean	STD	MDM
X (mm)	-0.38*	0.05	0.17	-0.21*	0.07	0.34	0.05	0.24	1.4
Y (mm)	0.30*	0.04	0.15	0.20*	0.05	0.18	-0.06	0.10	0.55
R (deg)	-0.28*	0.12	0.33	-0.20	0.22	0.95	0.08	0.42	2.42
Contour Max (mm)	0.52*	0.06	0.20	0.30*	0.07	0.30	0.17	0.21	1.42

Table 6: Summary of displacements and cables' tension at the 50th cycle: a) last loading sequence from the unloaded to the loaded states (amplitude) and b) cumulative displacements and rotation from the first to the last cycle.

	Displacements				Cable tensions			
	X (mm)	Y (mm)	N (mm)	R (deg)	1 (N)	2 (N)	3(N)	4 (N)
(a) Amplitude	-0,03	0,62	0,62	-1,18	6.4	-9.4	43.3	11.4
(b) Accumulative	0,76	1,08	1,31	-3,14	-79.4	-50.3	-51.5	-56.1

Table 7: Direct and indirect (rigid-body) movement evaluation.

		Movement (mm)		
Vectors	component	Cam1	Cam2	Cam3
$\overrightarrow{\Delta GT_{eff}}$	x	-0.58	0.28	1.21
	y	1.32	0.27	1.21
$\overrightarrow{\Delta GT_{calc}}$	x	-0,36	-1.37	2,41
	y	2.39	-0.32	0.56
$\overrightarrow{\delta F}$	x	-0.29	0.19	0.37
	y	0.47	0.45	0.00
$\overrightarrow{\delta GT}$	x	0.51	1.84	0.83
	y	0.6	1.04	-0.65

REFERENCES

1. Jarit G.J., Sathappan S.S., Panchal A., Strauss E., Di Cesare P.E., Fixation systems of greater trochanteric osteotomies: biomechanical and clinical outcomes, Journal of the American Academy of Orthopaedic Surgeons, 15(10), 614-624, 2007.
2. Barrack R.L., Butler R.A., Current status of trochanteric reattachment in complex total hip arthroplasty, Clinical Orthopaedics and Related Research®, 441, 237-242, 2005.
3. Hersh C.K., Williams R.P., Trick L.W., Lanctot D., Athanasiou K., Comparison of the mechanical performance of trochanteric fixation devices, Clinical Orthopaedics and Related Research®, (329), 317-325, 1996.
4. Markolf K.L., Hirschowitz D.L., Amstutz H.C., Mechanical stability of the greater trochanter following osteotomy and reattachment by wiring, Clinical Orthopaedics and Related Research®, (141), 111-121, 1979.
5. Plausinis D., Speirs A.D., Masri B.A., Garbuz D.S., Duncan C.P., Oxland T.R., Fixation of trochanteric slide osteotomies: a biomechanical study, Clinical Biomechanics, 18(9), 856-863, 2003.
6. Khanna G., Bourgeault C.A., Kyle R.F., Biomechanical comparison of extended trochanteric osteotomy and slot osteotomy for femoral component revision in total hip arthroplasty, Clinical Biomechanics, 22(5), 599-602, 2007.
7. Schoeniger R., LaFrance A., Oxland T., Ganz R., Leunig M., Does Trochanteric Step Osteotomy Provide Greater Stability Than Classic Slide Osteotomy? A Preliminary Study, Clinical Orthopaedics and Related Research®, 467(3), 775-782, 2009.
8. Bredbenner T.L., Snyder S.A., Mazloomi F.R., Le T., Wilber R.G., Subtrochanteric fixation stability depends on discrete fracture surface points, Clinical Orthopaedics and Related Research®, (432), 217-225, 2005.
9. Schwab J.H., Camacho J., Kaufman K., Chen Q., Berry D.J., Trousdale R.T., Optimal fixation for the extended trochanteric osteotomy: a pilot study comparing 3 cables vs 2 cables, Journal of Arthroplasty, 23(4), 534-538, 2008.

10. Thakur N.A., Crisco J.J., Moore D.C., Froehlich J.A., Limbird R.S., Bliss J.M., An Improved Method for Cable Grip Fixation of the Greater Trochanter After Trochanteric Slide Osteotomy A Biomechanical Study, Journal of Arthroplasty, 25(2), 319-324, 2008.
11. Heiner A.D., Structural properties of fourth-generation composite femurs and tibias, Journal of Biomechanics, 41(15), 3282-3284, 2008.
12. Chartrand M., Brailovski V., Baril Y., Test Bench and Methodology for Sternal Closure System Testing Experimental Techniques, On press for May 2010.
13. Charnley S.J., Detachement and reattachement of the greater trochanter. Low friction arthroplasty of the hip. Berlin: Sprigner-Verlag, 1979, p 140-151.
14. Heller M.O., Bergmann G., Kassi J.P., Claes L., Haas N.P., Duda G.N., Determination of muscle loading at the hip joint for use in pre-clinical testing, Journal of Biomechanics, 38(5), 1155-1163, 2005.
15. Petit Y., Aubin C.-É., Labelle H., Spinal shape changes resulting from scoliotic spine surgical instrumentation expressed as intervertebral rotations and centers of rotation, Journal of Biomechanics, 37(2), 173-180, 2004.

Figure 1: Specimen preparation: a) cuts of the femoral model; b) implantation of the femoral prosthesis; c) implantation of the abductor force application strap and simulated physiological forces P1, P2 (arrows).

Figure 2: Test bench.

Figure 3: a) Tensioning device and load washer assembly; b) Three-step cable implantation procedure: 1) positioning; 2) initial tightening; 3) retightening.

Figure 4: Field of view (FOV) of the three cameras and corresponding axes of coordinates.

Figure 5: Contour errors for the 5x225 landmark configurations relative to the initial femoral contour. Wide dotted line represents the contour error and the thin solid line represent the initial contour line for camera 1 (a), camera 2 (b), and camera 3 (c).

Figure 6: CAM1 view and selected landmarks, solid line circles are landmarks on the GT and dotted line circles are the landmarks on the femur.

Figure 7: Example of loading patterns and results obtained as a function of time: (a) femoral head and GT loading sequence; (b) GT displacements and rotation; and (c) cable tensions from proximal (1) to distal (4).

Figure 8: a) GT-femur relative displacement and rotation calculated at the reference point for CAM1; b) Tension in cables 1 to 4 from proximal to distal; solid lines give results on loading of the n^{th} cycle (L) and doted lines show results after unloading of the n^{th} cycle (U).

Figure 9: Relative in-plane GT displacements measured and calculated for CAM1 (a), CAM2 (b) and CAM3 (c). Thin solid and broken lines correspond to the initial (after unloading) and final (after loading) GT positions. Bold solid and broken lines correspond to the initial and

final contours of the femur and the center of gravity symbols indicate the mean position of the GT landmarks.

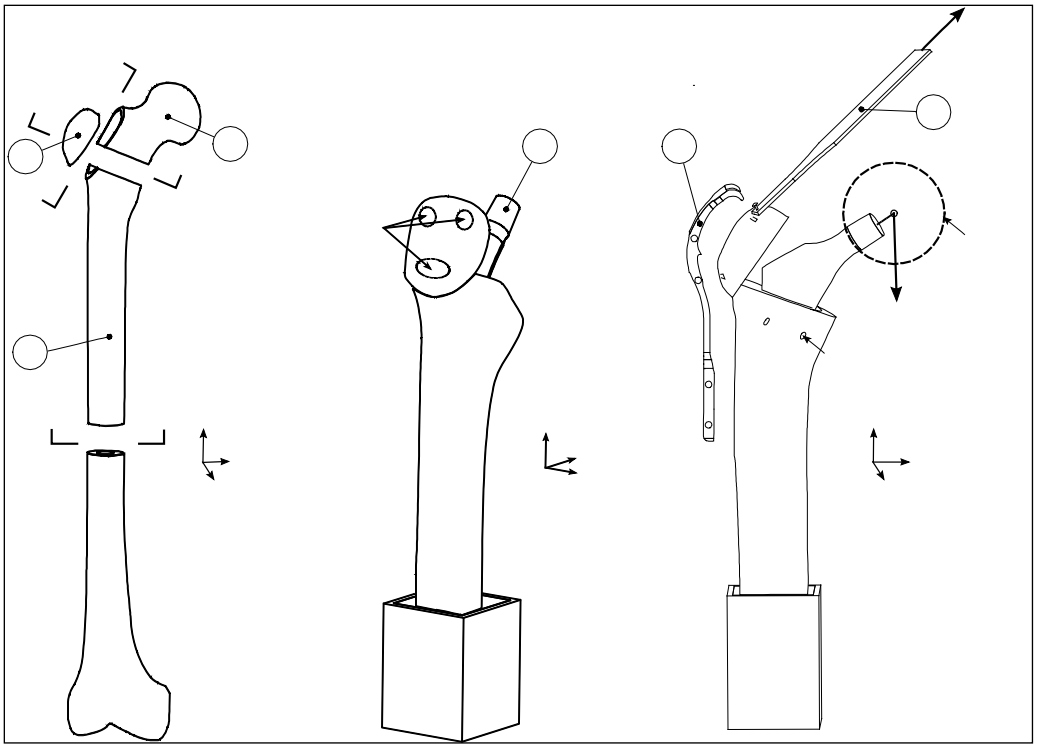

Fig 1: Specimen preparation: a) cuts of the femoral model; b) implantation of the femoral prosthesis; c) implantation of the abductor force application strap and simulated physiological forces P1, P2 (arrows).

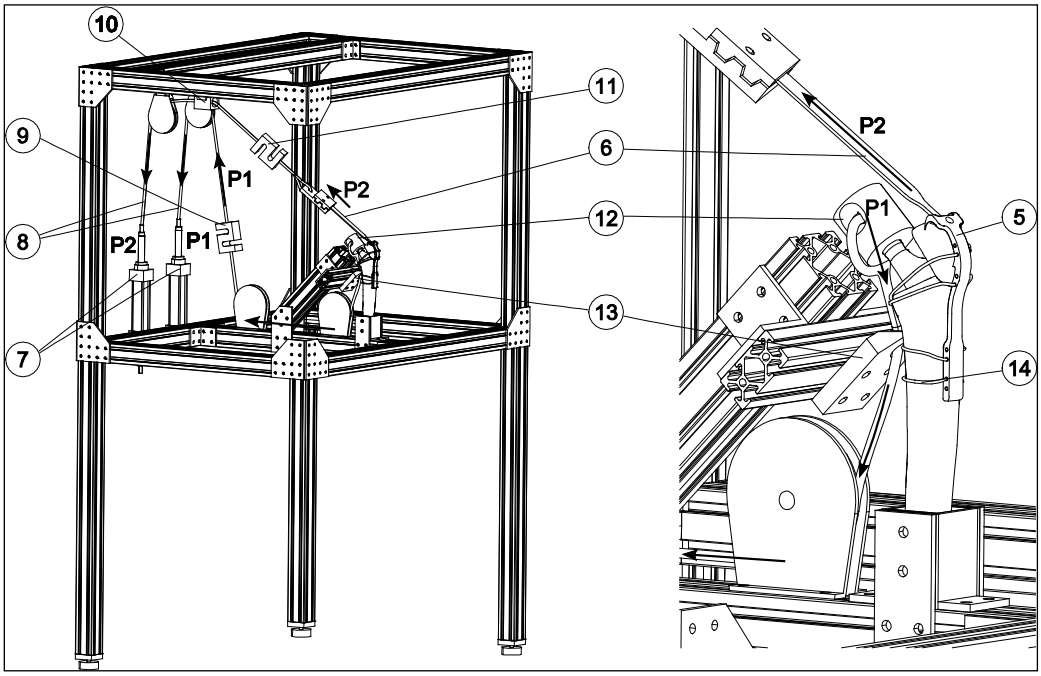

Fig 2: Test bench.

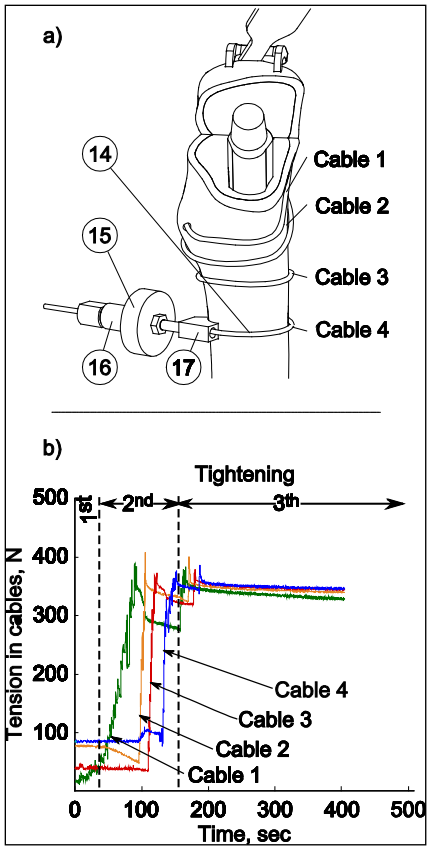

Fig 3: a) Tensioning device and load washer assembly; b) Three-step cable installation procedure: 1) positioning; 2) initial tightening; 3) retightening.

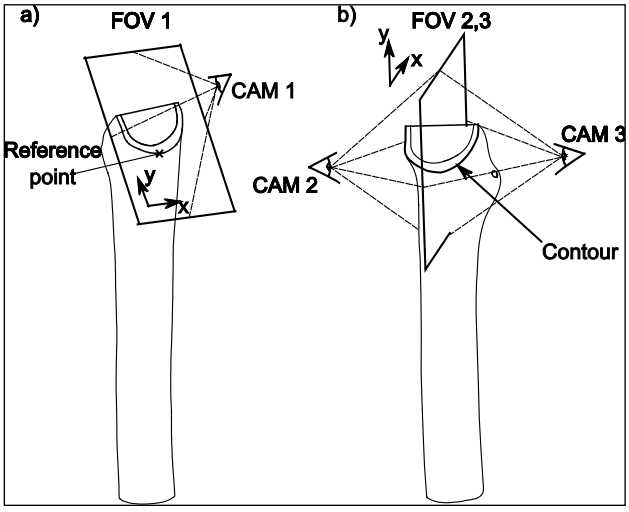

Fig 4: Field of view (FOV) of the three cameras and corresponding axes of coordinates.

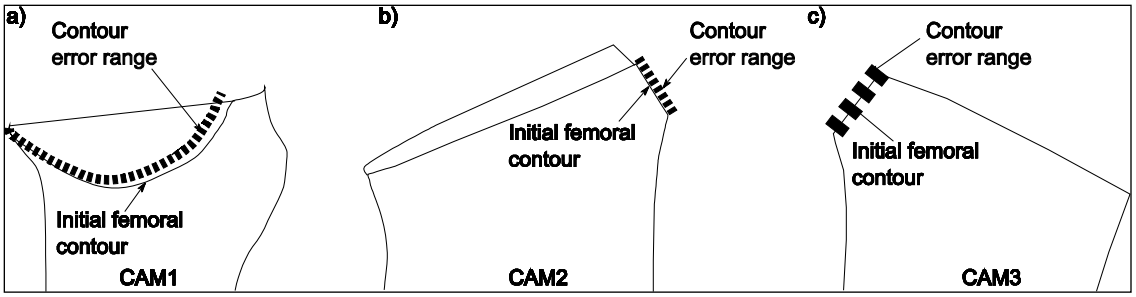

Fig 5: Contour errors for the 5x225 landmark configurations relative to the initial femoral contour. Wide dotted line represents the contour error and the thin solid line represent the initial contour line for camera 1 (a), camera 2 (b), and camera 3 (c)

Fig 6: CAM1 view and selected landmarks, solid line circles are landmarks on the GT and dotted line circles are the landmarks on the femur.

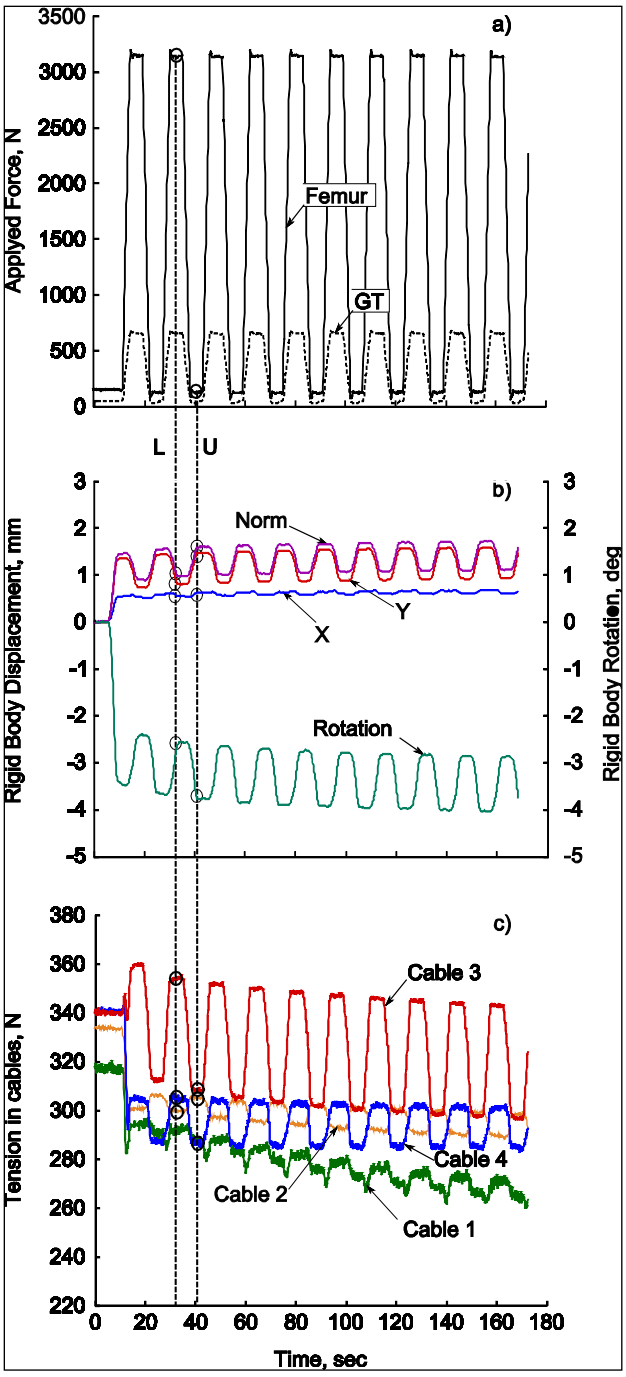

Fig 7: Example of loading patterns and results obtained as a function of time: (a) femoral head and GT loading sequence; (b) GT displacements and rotation; and (c) cable tensions from proximal (1) to distal (4).

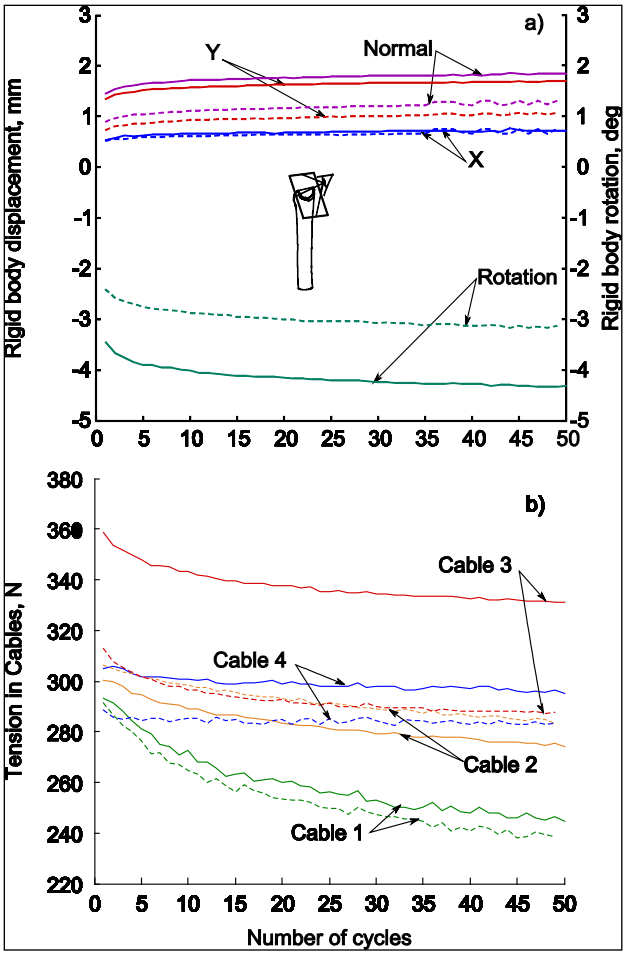

fig 8: a) GT-femur relative displacement and rotation calculated at the reference point for CAM1; b) Tension in cables 1 to 4 from proximal to distal; solid lines give results on loading of the nth cycle (L) and doted lines show results after unloading of the nth cycle (U).

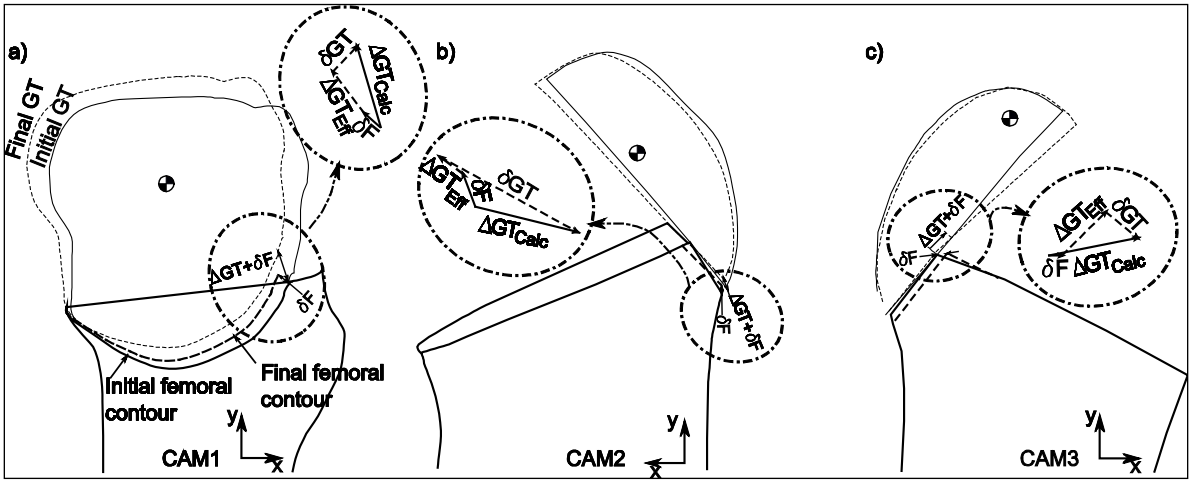

fig 9: Relative in-plane GT displacements measured and calculated for CAM1 (a), CAM2 (b) and CAM3 (c). Thin solid and broken lines correspond to the initial (after unloading) and final (after loading) GT positions. Bold solid and broken lines correspond to the initial and final contours of the femur and the center of gravity symbols indicate the mean position of the GT landmarks.

ANNEXE II

ARTICLE 4 « Improving greater trochanteric reattachment with a novel cable plate system »

Y. BARIL[1], Y. BOURGEOIS[1,3], V. BRAILOVSKI[1], K. DUKE[2], G. Y. LAFLAMME[3] AND Y. PETIT[1,3]

[1] École de technologie supérieure, Mechanical Engineering, Montréal, Québec, Canada

[2] University of Alberta, Mechanical Engineering, Edmonton, Alberta, Canada

[3] Hôpital Sacré-Coeur de Montréal, Research Center, Montréal, Québec, Canada

Cet article a été soumis à la revue : Clinical Biomechanics

RÉSUMÉ

Cette étude compare la stabilité du système de rattachement du GT « Cable Grip » de la compagnie Zimmer au nouveau système Y3. L'étude utilise un plan factoriel fractionnaire dont les modalités sont : type de plaque, type de câble, orientation de chargement du GT et les spécimens.

Les résultats montrent que le systèmeY3 est plus stable dans des conditions de chargement de lever d'une chaise alors qu'il a une stabilité comparable au « Cable Grip » dans le cas du chargement de montée d'un escalier. Le type de câble ne produit aucun effet significatif sur les déplacements. Par contre, il est possible de constater que les câbles CoCr perdent plus de tension, suite aux chargements, que les câbles superélastiques.

CONTRIBUTION

L'auteur du mémoire a contribué dans cette étude à la réalisation des essais expérimentaux, au traitement des résultats bruts et participé à leurs analyses. Il a également participé à la rédaction de l'article.

ABSTRACT

Background: Cable-Grip systems are commonly used for greater trochanteric reattachment because they have provided the best fixation performance to date, even though they have a rather high complication rate. A novel reattachment system is proposed with the aim of improving fixation stability. It consists of a Y-shaped fixation plate combined with locking screws and superelastic cables to reduce cable loosening and limit greater trochanter movement.

Methods: The novel system is compared with a commercially available reattachment system in terms of greater trochanter movement and cable tensions under different greater trochanteric abductor application angles.
A factorial design of experiments was used including four independent variables: plate system, cable type, abductor application angle, and femur model. The test procedure included 50 cycles of simultaneous application of an abductor force on the greater trochanter and a hip force on the femoral head.

Findings: The novel plate reduces the movements of a greater trochanter fragment within a single loading cycle up to 26%. Permanent degradation of the fixation (accumulated movement based on 50-cycle testing) is reduced up to 46%. The use of superelastic cables reduces tension loosening up to 24%. However this last improvement did not result in a significant reduction of the grater trochanter movement.

Interpretation: The novel plate and cables present advantages over the commercially available greater trochanter reattachment system. The plate reduces movements generated by the hip abductor. The superelastic cables reduce cable loosening during cycling. Both of these positive effects could decrease the risks related to grater trochanter non-union.
Greater trochanter reattachment, orthopaedic, cable tension, implant, slide osteotomy, locking screw

INTRODUCTION

With our aging population, the number of patients requiring hip replacement surgery is increasing rapidly. One of the common complications of hip replacement surgery (3-7%) is the fracture of the Greater Trochanter (GT) (Claus, Hopper et al. 2002). In addition, an intentional osteotomy of the GT is often performed to provide better surgical exposure during complicated primary hip arthroplasty or revision surgeries.

Stabilization of the greater trochanter continues to offer one of the greatest challenges in revision of total hip arthroplasty. Several techniques using monofilament wires were developed to achieve secure fixation of the GT fragment on the femur (Markolf et al., 1979) but the advent of the Dall-Miles cable plate system in the early 1980's (Dall and Miles, 1983) spurred a host of cable-plate systems. In today's market, the most widely used GTR systems consist of a plate, which hooks over the GT, combined with cable fixation (Zimmer Cable-Ready®, Warsaw IN & Dall-Miles Stryker, Mahwah NJ, USA) Figure 1a.

These fixation systems are considered to provide the best performance (Hersh et al., 1996, Jarit et al., 2007) but, despite the many improvements in the past few decades, they have been deemed responsible for a high rate of post-operation complications: pain, bursitis, breakage and non-union (Barrack and Butler, 2005, Keyak et al., 2001, Koyama et al., 2001, McCarthy et al., 1999, Ritter et al., 1991, Silverton et al., 1996). Some of these complications are the result of considerable post-fixation displacement.

It should be noted that the current systems essentially resist the forces generated by the hip abductor muscles acting in the superior direction. These forces are most likely to displace the GT when the hip is in a flexed position, as in the movement of rising from a chair (Charnley, 1979).

Furthermore, a high rate of cable breakage [10-19%] and non-union [9-31%] has been reported with the existing systems (Barrack and Butler, 2005, McCarthy et al., 1999). One possible source of such a high failure rate is cable loosening and its effect on system integrity. Finally, pain and bursitis can be due to irritation of the surrounding sensitive soft tissues caused by a bulky fixation system.

To sum-up, an ideal GTR system should resist forces applied by the hip abductor in all lower limb positions, contain cables that can maintain a constant compression between bone fragments, and have a low-profile geometry to reduce irritation.

A novel plate and cable system consisting of an implantable device for GT fixation protected by two complementary patent applications is studied in this work. The proposed GT system (further referred to as Y3-SMA) consists of a fixation (Y3) plate with a general Y shape which hooks over the greater trochanter (Petit et al., 2007) shown in Figure 1b. It is fixed with a combination of superelastic SMA cables (Brailovski et al., 2006) and locking screws which are inserted into the GT and into the femur.

The particular asymmetrical Y shape of the Y3 plate is designed to resist abductor and flexor muscles while having a low-profile design to reduce irritation of the surrounding soft tissues. The anterior and lateral trochanteric branches of the Y3 plate ensure a solid fixation of the greater trochanter with self-locking screws. Moreover, the anterior trochanteric branch is designed for easy intraoperative contouring to accommodate the specific geometry of a patient's femur. The femoral branch could accommodate a combination of unicortical locking screws and cables. The tubular-shaped cables are braided using NiTi superelastic filaments, a material used in numerous medical applications (Tarnita et al., 2009). The SMA cable used as a binding element provides two novel features for bone fixation. Firstly, it prevents cable loosening by maintaining near constant compression forces between bone fragments even though the cerclage geometry varies as a result of bone remodeling. Secondly, it flattens out when in contact with bones, providing a better force distribution at

the bone-cable interface and reducing the risk of cutting through the bone. Dynamic testing of these cables when used for sternal closure resulted in bone binding compression forces 20% higher than provided by standard stainless steel sutures (Baril et al., 2009). The ability of SMA cable to maintain higher compression forces on the implant should effectively stabilize the GT fragment during repetitive loading.

The objective of this study is to evaluate the overall gain of the novel Y3-SMA cable plate system over a standard cable grip system. A biomechanical testing experiment, using a Box, Hunter & Hunter fractional factorial Design of Experiment (DoE), was designed to evaluate individual impacts of the Y3 plate and the SMA cables, as well as their synergistic effect on the improvement of the GTR system stability.

MATERIALS AND METHODS

The models used for experimentation include artificial femurs and GT fragments as well as GTR systems. The models are installed in the testing rig, which applies loading and records data.

TESTING MODELS

The testing models consist of four parts to be assembled (Figure 1). These parts are the plates (3), the cables (C), the screws (S), the GT fragment (2) and the femur model (1).

Two different plates (3) were compared to reattach the GT (2) to the femur (1). The first plate is an integral long GT reattachment device of the Cable-Ready® cable grip system (Zimmer Inc., Warshaw, IN, USA). The second plate is the novel Y3 plate made of titanium alloy (Ti6Al4V) by means of electron beam melting at the IREQ (Hydro-Québec Research Institute, QC, CA) facilities. Final processing included drilling and the insertion of copper-zinc alloy inserts for the bone screws.

Two types of GTR cables (C) were also compared. The standard cables are 1.8 mm Cable-ready® Cobalt-Chrome cables. The 48-filament superelastic cables have 0.15 mm diameter filaments of BTR-BB (Ti-50.8at%Ni) alloy with 36% of cold work (Memory Corp., Bethel, CT, USA), heat treated at 350°C (15 min) in large loops and then water quenched to ambient temperature. The cables were braided from the as-drawn material using a Wardwell (Central Falls, RI, USA) braiding machine on a 3 mm diameter core. With the core in place, the braided structure was then heat treated at 350°C (15 min).

Two types of Zimmer 3.5 mm diameter screws (S) were used, depending on the Y3 plate holes' positioning: 12-20 mm locking screws (LS) and 14 mm standard cortical screws (CS) . A large left fourth-generation composite femur model (Sawbones ©, Pacific Research Laboratories, Vashon Island, WA, USA) was used to reduce specimen intervariability. The mechanical behavior of this femur model is reputed as being closer to human bone (Heiner, 2008) than the previous-generation femur model used in biomechanical studies of post-osteotomy GT fixation (Thakur et al., 2008, Khanna et al., 2007). The greater trochanter was cut according to the methodology presented in the specimen preparation section.

TESTING APPARATUS

The femur and greater trochanter fixation system assemblies were placed in a custom-made testing apparatus described in detail and validated in Baril et al. (submitted). The testing system (Figure 2) is divided into two subsystems: a test bench and a motion-analysis video system designed to record GT fragment displacements.

As shown in Figure 2a, simulated physiological forces were applied through a strap (5) on the GT (2), and through a head adaptor (6) on the femoral implant (4). Two hydraulic cylinders (7) are connected to the model by a pair of pulling cables (9), the first (P1) linked to the femoral head (6) and the second (P2), to the GT fragment (2), Figure 2b. The forces P1

and P2 were recorded in real-time by the load cells (10) (2224 N, LC101-500 and 4448 N, LC101-1k, Omega Engineering Inc, Stamford, CT, USA) installed on the pulling cables (9). The pulling cables are redirected by pulleys and guides (8, 11), and their position can be changed to modify the forces' directions.
On each GTR cable, a through-hole load cell (13) (889 N, LC8100-200-5, Omega Engineering Inc, Stamford, CT, USA), a crimping device (14) and a tensioning bracket (12) are installed to allow GTR cable tensioning and real time tension monitoring (Figure 2c).

A dedicated motion analysis video system was used to follow the GT fragment's in-cut planar displacements and rotations. This motion analysis system used one camera with the field of view (FoV) positioned in the GT cut plan, as illustrated in Figure 2a. Two groups of four 4.76 mm diameter white-ball landmarks (pin heads) installed in the proximal zones of the femur and of the GT fragment were tracked in real-time with this system. The landmark groups form two rigid bodies to measure their relative movement. This testing approach was found appropriate within the framework of a comparative study (Baril et al., submitted).

SPECIMEN PREPARATION

For the specimen preparation, similar to the method described in Bredbener et al. (2005), a customized jig and a hand saw were used to make appropriate femoral cuts (.Figure 3a). First, a transversal cut (A-A) was made medially in the femur body (1). Next, a trochanteric cut (B-B) was made at 34° from the femur axis, severing the greater trochanter fragment (2). The third cut (C-C) allows the removal of the femoral head, keeping a distance of 13 mm on the femur B-B cut. Femur (1) was than reamed to allow installation of a press-fit femoral implant (4) (Stryker, Kalamazoo, MI, USA), Figure 3b. Note that the greater trochanter and femoral head cuts were realized in a way to reproduce a fracture that could occur after a hip replacement surgery or a worst case scenario during a revision surgery were the patient is subject to severe osteopenia. Finally, the distal part of the femur was embedded in a 50 mm wide square steel tube with polyester-based body filler (Bondo, 3M, GA, USA).

Recesses were made in the GT fragment following two different patterns corresponding to the points of contact between the GT-femur assembly and those of either the Y3 or Zimmer plates, which were then filled with body filler (Figure 3b). Next, the plates (3) (Figure 3c) were imprinted in the filler before it dried to assure that the GT-femur assembly and plates would fit properly during final installation. The preparation of the specimens to be used with the Zimmer plate was completed by drilling a 2 mm diameter hole medially through the lesser trochanter in the anterior-posterior direction (Figure 3b) to reproduce a clinical practice intended to increase proximal cable stability. A strap (5) was then fixed to the proximal region of the GT fragment (Figure 3c), making the GT Application Point (AP).

For final assembly, the Cable-Ready^{tm} plate hooks were inserted into the moulded GT recesses and the plate was installed on the femur. Each of the four attachment cables were passed through the plate, around the femur, the tensioning system, the through-hole load cell and the tightening device. The first proximal cable (C1) was also passed through the lesser trochanter hole (Figure 3b). First, the cables were slightly tightened using external tools. Then, according to the manufacturer's instructions, they were initially tensioned from the proximal (C1) to the distal (C4) up to a load of 355 N (80 lb) using a tensioning bracket (Figure 2, 12). Finally, as recommended by the manufacturer, they were re-tensioned up to 355 N, using the same tensioning sequence.

The Y3 plate installation also began with its insertion into the moulded GT recesses and installation on the femur. Next, two 20 mm cortical screws (CS) were installed in the proximal femur holes S5 and S6 (Figure 1). Three cables (C1-C3) were then passed through the plate, around the femur, through the tensioning system, the through-hole load cell and the tightening device. Each cable was tensioned up to 355 N following the Zimmer plate tightening procedure. Four 12 mm long locking screws were then fixed in the GT fragment (S1-S4) and two 20 mm locking screws (S6-S7) in the femur. The installation was completed by re-tensioning all the cables up to 355 N, using the same tensioning sequence.

SPECIMEN LOADING AND OUTPUT VARIABLES

The custom test bench applied both GT muscles force and femoral head forces. Two GT force directions were set: the first direction simulated stair climbing, and the second simulated complex movement, such as rising from a chair (step-up). The stair climbing direction was inspired by the literature data (Heller et al., 2005, Schwab et al., 2008, Taylor and Walker, 2001, Thakur et al., 2008) (Table 1), and will be referred to as the Normal Angle (NA) direction. The step-up direction was set according to Charnley (1979) at 45 deg anterior to the NA and will be defined as the Wide-Angle (WA) direction. The magnitude of abductor forces was set to 650 N for both directions (5, Figure 3).

The femoral head force direction corresponds to the direction of the peak load during stair climbing (Table 1), and it was kept the same for the WA and the NA abductor force directions. The femoral head force of 3120 N includes a 1.3 compensation factor for the guide (11) friction (Figure 2).

The specimen was first slightly loaded in the desired direction to the Initial State (IS), and then cycled 50 times from the Unloaded (U) to the Loaded (L) state and back (see Figure 4a). One full cycle takes 16 seconds and contains four steps: 1) a 3-second force increase from U to L state; 2) a 5-second dwell at L state; 3) a 3-second force release from L to U state, and 4) a 5-second dwell at U state.

The output testing variables *(y)* are the GT fragment movements and the cable tensions as illustrated in Figure 4b. Two parameters of GT fragment movement are used: a) maximum displacement on the reference contour and b) rigid body rotation. The cable tensions are measured using through-hole load cells. Two differential measurements will be considered:

a) GT movement and cable tension variations corresponding to the selected single cycle: from the loaded state of the 50^{th} cycle to the unloaded state of the 49^{th} cycle (L_{50}-U_{49});
b) GT movement and cable tension variations accumulated from the 1^{st} to the 50^{th} cycle of testing: from the unloaded state of the last cycle to the initial state (U_{50}-IS).

EXPERIMENTAL PLAN

A Box, Hunter & Hunter (2005) two-level fractional factorial experimental design (2^{4-1}) was performed to evaluate the effect of four parameters: Plate Type or **PT** (Zimmer vs. Y3), Cable Type or **CT** (Co-Cr vs. SMA), GT force Application Angle or **AA** (Normal Angle, NA vs. Wide Angle, WA) and Specimen or **SP** (two different femur specimens were used for each plate modality ($SP1_Z$, $SP2_Z$, $SP1_{Y3}$, $SP2_{Y3}$). Two replications of the experiments – presented in the appendix – were performed for a total of 24 trials.

Note that the **SP** variable (specimen) is dependent on the **PT** variable (plate type), because the latter influences specimen configuration. The **SP** variable implementation was deemed necessary to ensure that specimen variations do not introduce significant variations in the results, which implies that **SP** must yield as a non-significant variable throughout the testing to allow the other input variables as to be evaluated independently.

The regression factors of the linear model with the interactions resulting from this factorial plan are presented in Table 2.

Equation [1] of the resulting model gives the estimated output variables ($\hat{y}$) as a function of the input variables' value or modality (Box, 2005).

[1]

The cable tensions in the GTR systems cannot be directly compared because of their difference in number and positions. The main experimental design was therefore divided into two 3-variable fractional factorial designs (2^{3-1}), one for each plate. The resulting design includes independent variables CT, AA and SP, and allows calculation of their independent effects.

The p-value for significance was set to p=0.01 to take into account the large number of analyses which were carried out. Statistical analysis of the results obtained was performed with the help of Statistica 7 (StatSoft, Inc., OK, U.S.A.)

RESULTS

In Figure 5 selected direct measurement data are plotted as a function of time for the first 10 loading cycles: the GT maximum contour displacements and rotations are in Figure 5a, and cables tensions are in Figure 5b.

Figure 6 corresponds to a selected trial consisting of a direct comparison of two GTR systems under Wide Angle conditions: a Zimmer plate with CoCr Cables (Zimmer system) and a Y3 plate with SMA cables (Y3-SMA system). It gives the GT fragment's maximum displacements and rotations, and the cable tensions for loaded (L) and unloaded (U) states as functions of the number of cycles. It can be seen from the distance between solid (L) and broken (U) lines (U) that during cycling, the Y3-SMA system attenuates both the fragment's movements (.Figure 6 a,b) and the cable tensions' variations.Figure 6 c,d).

ANALYSIS OF THE EXPERIMENTAL PLAN

In this section, GT movements and cable tension variations corresponding to the last loading cycle and those accumulated during 50-cycle testing are analysed. Table 3 presents a synthetic picture of this analysis; detailed figures are in the appendix. One observation is that

the use of the Y3-SMA system reduces both the GT fragment movements and the tension variation amplitude (negative signs).

GT MOVEMENT

Maximum GT displacements measured during the last cycle of the 50-cycle run range between 0.47 and 1.60 mm. The negative plate type effect (PT) indicates that the Y3 plate significantly reduces the maximal displacement as compared to the Zimmer plate. This reduction corresponds to 0.27 mm: from 1.02 to 0.75 mm (a gain of 26 %) if all other factors are set at their mean values (CT=AA=SP=0); see Table A1 in the appendix and Equation 1. Furthermore, one of the confounded interaction factors, CT×SP or PT×AA, could be selected after analysis of the main effects' impact. In this particular case, the plate type and the application angle are the only significant and important effects. PT×AA appeared to be preponderant, and CT×SP appeared to be a factor that can be neglected. It is then possible to estimate that, under WA conditions (AA=1; CT=SP=0), the GT displacements pass from 1.37 to 0.74 mm (a gain of 46 %).

Measured GT rotation ranged between 0.04 and 2.45 deg. The same trend as that for displacement can be observed: the Y3 plate significantly reduces GT rotations. However, we note that these results cannot be quantified numerically because the SP significantly affects GT rotation measurements.

The maximum accumulated GT displacement (50 cycles) ranged between 0.19 and 2.48 mm. The use of the Y3 plate as compared to the Zimmer plate resulted in a significant decrease (-0.42 mm) of GT displacement. PT×AA interaction appears to be preponderant to that of CTxSP, resulting in a gain of 57 % under WA conditions when comparing the Zimmer to the Y3 (AA=1; CT =SP=0) with a reduction in displacement from 1.16 to 0.50 mm. However, even though the CT×AA and PT×SP confounded factors are significant, it becomes impossible to discriminate one interaction from another.

The GT rotation ranged between 0.01 and 4.70 deg, and the use of the Y3 plate reduced rotation by 1.20 deg (CT=AA=SP=0). This effect was further improved by PT×AA interaction, which clearly overweighs that of CT×SP. Rotations decreased from 2.85 to 0.22 deg under WA conditions (a gain of 92 %) from Zimmer to Y3 setups (AA=1; CT =SP=0).

CABLE TENSION

Cable tension results are given in terms of tension variation amplitude for each cable during testing. These results do not include tension variations that occur during installation. The results presented below are those for the Zimmer plate assembled with SMA or CoCr cables only. No significant difference between CoCr and SMA cables was observed for the Y3 plate. A logarithmic transformation was applied ($Y=ln(|y|)$) to obtain standard deviation essentially independent from the mean (Box, 2005).

The tension variation amplitude for the last loading cycle ranged between 0.3 and 54.7 N for Cable 3, the cable most affected by cycling. The tension variation was reduced by a factor of nearly 7 (-6.4 N or 1.8 % of the installation tension) for Cable 1, and by nearly 50 (-17 N, 4.8 %) for Cable 3. The Application Angle had no effect on tension variation amplitude.

Cable loosening between the initial and final unloaded states ranged between 5 and 118 N for Cable 1, showing the largest accumulated tension losses. Cables 1 and 2 showed reduction factors of 7.5 (*from* 98 to 13 N, 23.7%) and 4.7 (*from* 58 to 12 N, 12.9 %), respectively.

DISCUSSION

According to the recent literature, trochanteric non-union rates have not shown significant improvement. Even for the second generation trochanteric systems (incorporating improved filament bundle pattern, plates and provisional fixation with retightening), there are disappointing rates of non-union (14.6%) and of cable breakage (19%). Patients with trochanteric non-union suffer from abductor pain, bursitis, weakness associated with a limp and increased dislocation rate (Frankel et al., 1993). In an attempt to restore abductor function more consistently than the cable systems available to date, a novel technique was developed with the use of locking plate technology and superelastic cables to improve GT fragment stability.

On one hand, the Y3 plate offers much greater GT fragment stability than the Zimmer plate in the flexed hip position or under wide angle loading. Important gains were recorded: from 41 % for displacement occurring during the last cycle to 91 % for accumulated rotation. The anterior branch of the Y3 combined with the GT fixation screws contribute to the stiffening of the system, which is beneficial for this position. However, under normal angle loading or in a stand-up position Y3 and Zimmer plates show comparable GT fragment displacements, because the Zimmer plate is mainly designed to resist hip forces in this direction.

It is also important to note that the Zimmer plate was more affected by cycling than the Y3 plate, especially in terms of cumulative effect (in-cycle variations of both plates were comparable). This lets us anticipate that the Y3 plate will be more suitable for preventing long-term degradation of the GTR. For both GTR systems, the application of Wide Angle (WA) loading increases GT fragment movements. This phenomenon reflects the fact that GT movements are most likely to occur when the hip is in a flexed position, as observed by (Charnley, 1979).

These results reflect clear tendencies. The Y3 plate improves stability of the GTR, the application angle increases displacement, and there is a benefit from the interaction between the plate type and the application angle. This last effect shows that the Y3 plate is nearly unaffected by the application angle. The results appear to be unaffected by the invalidated rotation analysis of the last cycle outputs. Moreover, the accumulated displacements are not seriously influenced by the possible interaction with the specimen type.

The multi-braided metallic cables offered superior mechanical properties compared to traditional stainless steel monofilament wires (Schmotzer et al., 1996), but their clinical use has been associated with an unacceptably high complication rate. Multifilament braided cable tends to fatigue and fray leading to a multitude of new problems including release of metallic particulate debris into the body (Hop et al., 1997, Silverton et al., 1996), accelerated polyethylene wear and acetabular loosening. Initial cable relaxation is also a major problem

according to Haddad et al (2004), limiting the cables' ability to maintain compression during the healing period.

The low elastic springback (the capacity to accommodate large deformations without loosening bone-fragments' compression) of multi-braided metallic cables prevents them from adjusting to bone remodeling or to micromotions associated with physiological loading. Haddad et al (2004) have shown that most of the tension in such cables (50%) is lost within the first post-operative day. In our study, Cable 1, made of CoCr, lost up to 98 N after 50-cycle testing, which correspond to 27 % of its initial load. This value does not take in account any initial loss occurring during installation. The SMA cables manifested greater tension maintaining capacity throughout cycling than CoCr cables (significant for cables 1 and 2 and non-significant for cables 3 and 4). Surprisingly, the influence of the application angle was not found to be significant.

In stating the objectives of this study, the authors had anticipated a synergetic positive impact on the stability of the GT fixation related to the combined use of a Y3 plate and SMA cables. It was reasonably supposed that the less the cables' tensions loosened, the more stable the GT fixation, especially when applied forces fluctuate. Unfortunately, this study was not sufficient to completely confirm or reject this hypothesis because the cable type was not found to significantly impact the GT movement.

As a first reaction to this conclusion, we assumed that this lack of synergy was due to the fact that the abductor application angle was kept constant during each run of testing, which is not representative of real life, and that this could have stabilized the GT fragment and cancelled the effects of the SMA cables. An exploratory test was realized to verify if GT movements would be amplified when the application angle is oscillating from NA to WA and back, and if under such conditions, SMA cables would improve GT stability. However, the average GT fragment displacements measured with alternating angles were situated between those

corresponding to each angle applied separately beforehand, and so no improvement in GT stability could be attributed to the SMA cables.

The testing methodology used in this work presents some limitations. First, the use of synthetic bone could affect the results, because GTR cables were easily placed with respect to the artificial femur because it is slick and free of muscles, periosteum, etc. This situation reduces the possible installation imperfections that may occur during surgery and therefore the conditions when a cable's type would have a greater impact on GT stability. Furthermore, both GTR systems were perfectly moulded in the GT fragment, thus idealizing the situation even further.

Also, both systems were tested using their full installation setups, which meant using 4 cables for the Cable-Grip® and 3 cables and 8 screws for the Y3. Depending on a surgeon's decision, each system could be installed using a reduced fastener configuration. In such cases, the results could be different.

CONCLUSION

The Y3 plate and SMA cables present advantages over Zimmer Cable-Ready® GTR when compared in the laboratory. The Y3 reduces displacements generated by the hip abductors, especially in the flexed position. Greater stability may translate clinically to lower non-union rates and thus yield to a better functional outcome for patients. SMA cables reduced cable loosening and thus could provide enhanced GT stability. However, this study was not sufficient to clearly verify a hypothesis that there is a synergy between the SMA cables' greater tension maintaining capacities and the improved Y3 fixation potential. Further work will be required to proof or disapprove this hypothesis.

ACKNOWLEGEMENTS

This research was funded by the Natural Science and Engineering Council (NSERC) and the Canadian Foundation for Innovation (CFI). Thanks go to Stryker (Kalamazoo, MI, USA) for providing the femoral implant used in this study and to the Hydro-Quebec's Research Institute (IREQ) for Y3 plate manufacturing.

REFERENCES

BARIL, Y., BOURGEOIS, Y., BRAILOVSKI, V., DUKE, K., LAFLAMME, G. Y. & PETIT, Y. (submitted) Testing system for the comparative evaluation of greater trochanter reattachment devices. *Experimental Techniques*.

BARIL, Y., BRAILOVSKI, V., CHARTRAND, M., TERRIAULT, P. & CARTIER, R. (2009) Median sternotomy: comparative testing of braided superelastic and monofilament stainless steel sternal sutures. *Proceedings of the Institution of Mechanical Engineers, Part H: Journal of Engineering in Medicine,* 223**,** 363-374.

BARRACK, R. L. & BUTLER, R. A. (2005) Current status of trochanteric reattachment in complex total hip arthroplasty. *Clinical Orthopaedics and Related Research®,* 441**,** 237-242.

BOX, G. E. P. (2005) *Statistics for experimenters : design, innovation, and discovery,* Hoboken, Hoboken : Wiley-Interscience.

BRAILOVSKI, V., CARTIER, R., TERRIAULT, P. & BARIL, Y. (2006) Binding component. Canada.

BREDBENNER, T. L., SNYDER, S. A., MAZLOOMI, F. R., LE, T. & WILBER, R. G. (2005) Subtrochanteric fixation stability depends on discrete fracture surface points. *Clinical Orthopaedics and Related Research®***,** 217-225.

CHARNLEY, S. J. (1979) Detachement and reattachement of the greater trochanter. *Low friction arthroplasty of the hip.* Berlin, Sprigner-Verlag.

DALL, D. M. & MILES, A. W. (1983) Re-attachment of the greater trochanter. The use of the trochanter cable-grip system. *journal of Bone and Joint Surgery Br,* 65**,** 55-9.

FRANKEL, A., BOOTH, R. E. J., BALDERSTON, R. A., COHN, J. & ROTHMAN, R. H. (1993) Complications of Trochanteric Osteotomy Long-Term Implications. *Clinical Orthopaedics and Related Research,* 288**,** 209-213.

HADDAD, F. S., BARRACK, R. L., RIES, M. D., ALLEN, W., JONES, B., TSAI, S. & SALEHI, A. (2004) Factors influencing cerclage cable tension loss during surgery. *AAOS Scientific Exhibit.* Annual Meeting ed. San Francisco, CA, American Academy of Orthopaedic Surgeons.

HEINER, A. D. (2008) Structural properties of fourth-generation composite femurs and tibias. *Journal of Biomechanics,* 41**,** 3282-3284.

HELLER, M. O., BERGMANN, G., KASSI, J. P., CLAES, L., HAAS, N. P. & DUDA, G. N. (2005) Determination of muscle loading at the hip joint for use in pre-clinical testing. *Journal of Biomechanics,* 38**,** 1155-1163.

HERSH, C. K., WILLIAMS, R. P., TRICK, L. W., LANCTOT, D. & ATHANASIOU, K. (1996) Comparison of the mechanical performance of trochanteric fixation devices. *Clinical Orthopaedics and Related Research®***,** 317-325.

HOP, J. D., CALLAGHAN, J. J., OLEJNICZAK, J. P., PEDERSEN, D. R., BROWN, T. D. & JOHNSTON, R. C. (1997) The Frank Stinchfield Award. Contribution of cable debris generation to accelerated polyethylene wear. *Clinical Orthopaedics and Related Research®***,** 20-32.

JARIT, G. J., SATHAPPAN, S. S., PANCHAL, A., STRAUSS, E. & DI CESARE, P. E. (2007) Fixation systems of greater trochanteric osteotomies: biomechanical and clinical outcomes. *Journal of the American Academy of Orthopaedic Surgeons,* 15**,** 614-624.

KEYAK, J. H., SKINNER, H. B. & FLEMING, J. A. (2001) Effect of force direction on femoral fracture load for two types of loading conditions. *J Orthop Res,* 19**,** 539-44.

KHANNA, G., BOURGEAULT, C. A. & KYLE, R. F. (2007) Biomechanical comparison of extended trochanteric osteotomy and slot osteotomy for femoral component revision in total hip arthroplasty. *Clinical Biomechanics,* 22**,** 599-602.

KOYAMA, K., HIGUCHI, F., KUBO, M., OKAWA, T. & INOUE, A. (2001) Reattachment of the greater trochanter using the Dall-Miles cable grip system in revision hip arthroplasty. *J Orthop Sci,* 6**,** 22-7.

MARKOLF, K. L., HIRSCHOWITZ, D. L. & AMSTUTZ, H. C. (1979) Mechanical stability of the greater trochanter following osteotomy and reattachment by wiring. *Clinical Orthopaedics and Related Research®***,** 111-121.

MCCARTHY, J. C., BONO, J. V., TURNER, R. H., KREMCHEK, T. & LEE, J. (1999) The outcome of trochanteric reattachment in revision total hip arthroplasty with a Cable Grip System: mean 6-year follow-up. *Journal of Arthroplasty,* 14**,** 810-814.

PETIT, Y., LAFLAMME, Y. & BOURGEOIS, Y. (2007) Orthopaedic fixation component and method. *Provisional Patent Application.*

RITTER, M. A., EIZEMBER, L. E., KEATING, E. M. & FARIS, P. M. (1991) Trochanteric fixation by cable grip in hip replacement. *journal of Bone and Joint Surgery Br,* 73**,** 580-1.

SCHMOTZER, H., TCHEJEYAN, G. H. & DALL, D. M. (1996) Surgical management of intra- and postoperative fractures of the femur about the tip of the stem in total hip arthroplasty. *The Journal of Arthroplasty,* 11**,** 709-717.

SCHWAB, J. H., CAMACHO, J., KAUFMAN, K., CHEN, Q., BERRY, D. J. & TROUSDALE, R. T. (2008) Optimal fixation for the extended trochanteric osteotomy: a pilot study comparing 3 cables vs 2 cables. *Journal of Arthroplasty,* 23**,** 534-538.

SILVERTON, C. D., JACOBS, J. J., ROSENBERG, A. G., KULL, L., CONLEY, A. & GALANTE, J. O. (1996) Complications of a cable grip system. *Journal of Arthroplasty,* 11**,** 400-404.

TARNITA, D., TARNITA, D. N., BIZDOACA, N., MINDRILA, I. & VASILESCU, M. (2009) Properties and medical applications of shape memory alloys. *Rom J Morphol Embryol.,* 50**,** 15-21.

TAYLOR, S. J. G. & WALKER, P. S. (2001) Forces and moments telemetered from two distal femoral replacements during various activities. *Journal of Biomechanics,* 34**,** 839-848.

THAKUR, N. A., CRISCO, J. J., MOORE, D. C., FROEHLICH, J. A., LIMBIRD, R. S. & BLISS, J. M. (2008) An Improved Method for Cable Grip Fixation of the Greater Trochanter After Trochanteric Slide Osteotomy A Biomechanical Study. *Journal of Arthroplasty,* 25**,** 319-324.

Figure 1: a) Zimmer Cable Ready® and b) Y3-SMA Greater Trochanter Reattachment Systems

Figure 2: Test bench with a) close-up view on the specimen; b) general view; c) GTR cables' tension applicator and measurement system.

Figure 3: Specimen preparation; a) cuts of the femoral model; b) installation of the femoral prosthesis; c) installation of the force application strap and illustration of the simulated physiological forces application.

Figure 4: a) Testing sequence used for each specimen. Loading sequence starts at an initial state (IS) and is followed by 50 cycles of loading (L) and unloading (U); b) Fragment movement measurement.

Figure 5: Example of results obtained as a function of time (Zimmer-CoCr-WA): (a) GT displacements and rotations; and (b) cable tensions from proximal (1) to distal (4). Figure adapted from Baril et al.(submitted).

Figure 6: Typical results for two experiments Zimmer-CoCr-WA (a, c) and Y3-SMA-WA (b, d); (a, b) GT-femur relative displacement and rotation; (c, d) tension in cables: solid lines correspond to the loaded (L) and broken lines to the unloaded (U) states.

Table 1: Force vectors' definition.

Table 2 : Regression factor associated with each individual variable and with their interactions.

Table 3: Influence of individual variables and their interactions on GT movements and changes in tension amplitude (Zimmer-CoCr-WA (a, c) and Y3-SMA-WA).

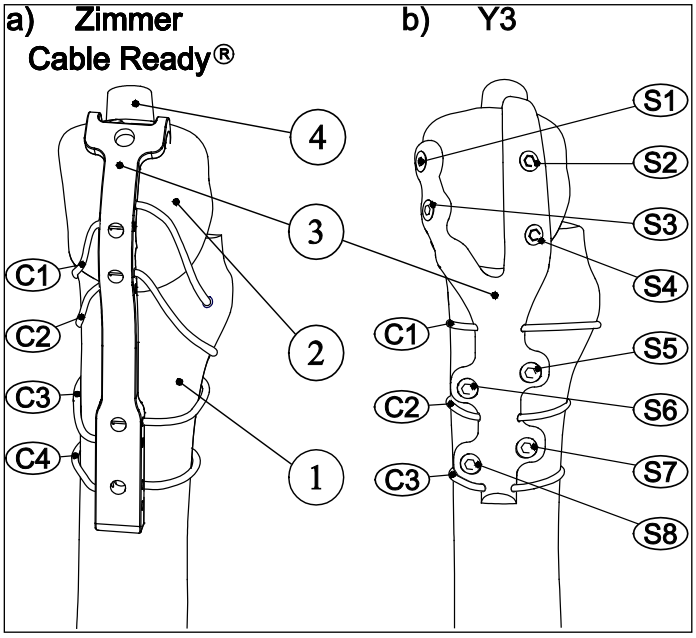

Figure 1

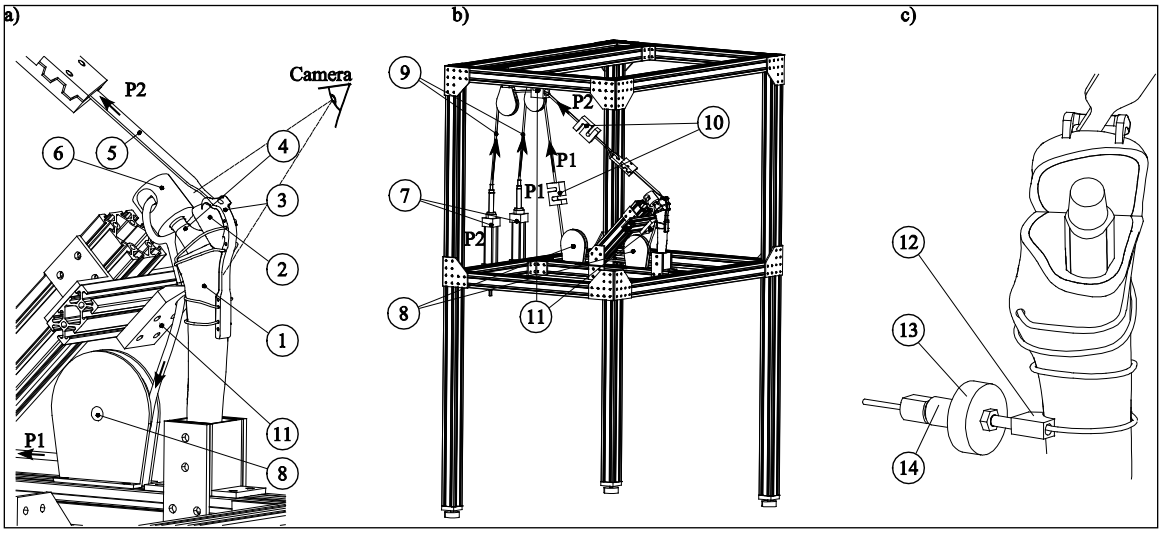

Figure 2

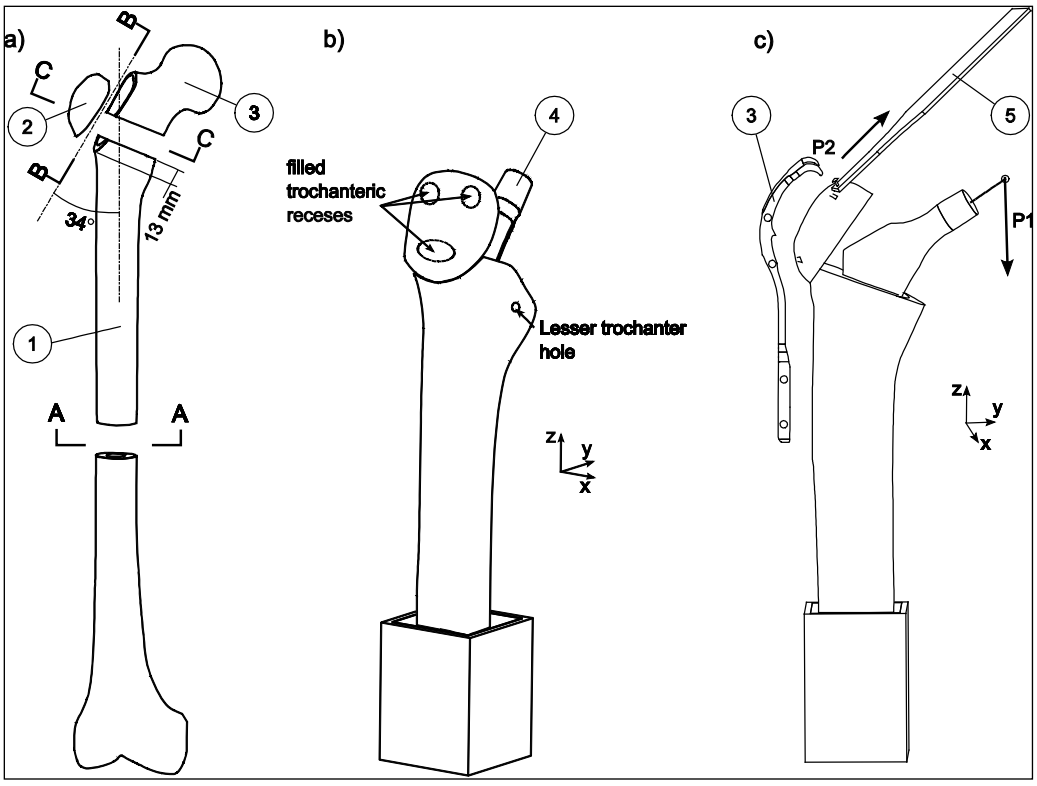
a)
b)
c)
B
C
2
3
C
B
34°
13 mm
1
A
A
4
filled
trochanteric
receses
Lesser trochanter
hole
z
y
x
3
P2
5
P1
z
y
x

Figure 3

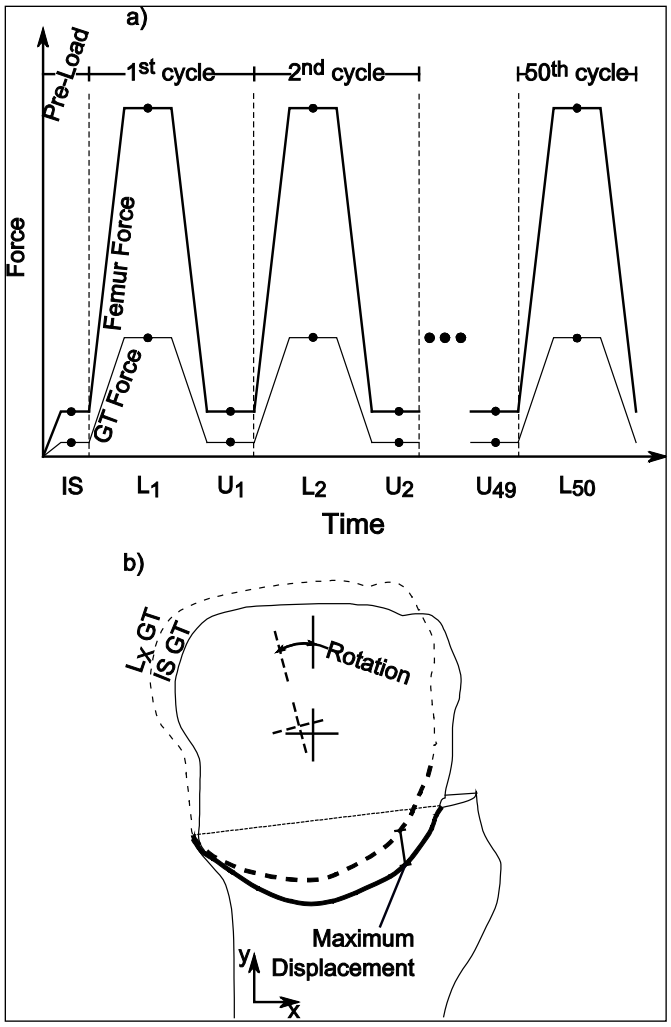
a)
Pre-Load
1st cycle
2nd cycle
50th cycle
Force
Femur Force
GT Force
IS
L1
U1
L2
U2
U49
L50
Time
b)
Lx GT
IS GT
Rotation
Maximum
Displacement
y
x

Figure 4

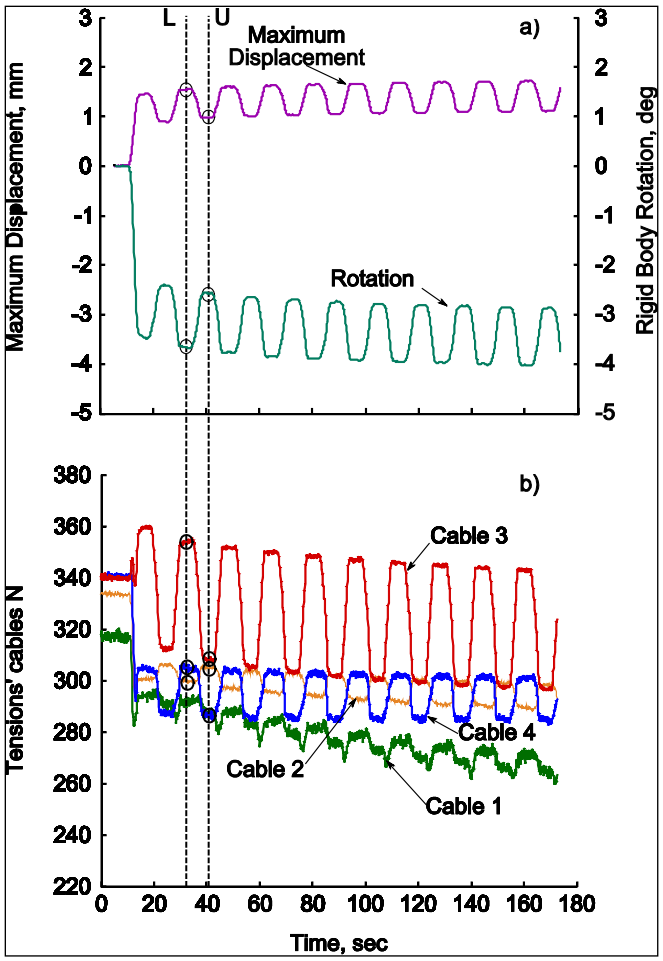
L
U
Maximum Displacement
a)
Rotation
Maximum Displacement, mm
Rigid Body Rotation, deg
b)
Cable 3
Cable 4
Cable 2
Cable 1
Tensions' cables N
Time, sec

Figure 5

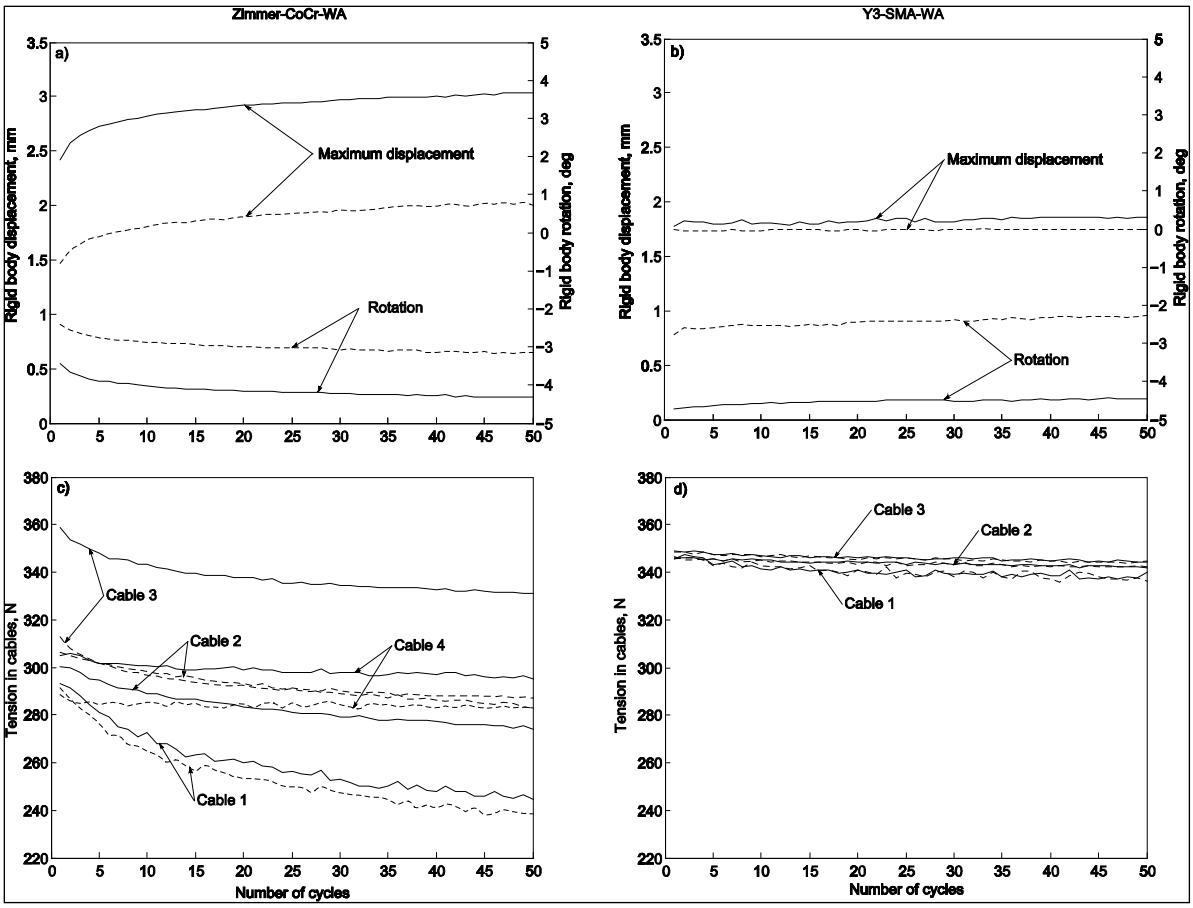
Zimmer-CoCr-WA
Y3-SMA-WA
a)
b)
c)
d)
Rigid body displacement, mm
Rigid body rotation, deg
Maximum displacement
Rotation
Tension in cables, N
Number of cycles
Cable 1
Cable 2
Cable 3
Cable 4

Figure 6

Table 1: Force vectors' definition.

			Direction vectors					
			Normal Angle (NA)			Wide Angle (WA)		
	Initial State (IS), N	Peak Load, N	x	y	z	x	y	z
P1	150	3120	0.16	-0.24	-0.96	0.16	-0.24	-0.96
P2	50	650	-0.34	0.73	0.60	-0.50	0.63	0.60

Table 2 : Regression factor associated with each individual variable and with their interactions.

	Regression factors	Individual variables and their interactions	
Individual	β1	CT	---
	β2	PT	---
	β3	AA	---
	β4	SP	---
Confounded	β5	CT×PT	AA×SP
	β6	CT×AA	PT×SP
	β7	CT×SP	PT×AA

AA: application angle; CT: Cable Type; PT: Plate Type; SP: Specimen

Table 3: Influence of individual variables and their interactions on GT movements and changes in tension amplitude (Zimmer-CoCr-WA (a, c) and Y3-SMA-WA).

		CT	PT	AA	SP	PT×AA	Note
50th cycle	Displacement	NS	-	+	NS	-	
	Rotation	NS	-	+	+	-	Invalidated (SP significant)
	Cable tension amplitude	-	X	NS	NS	X	
Accumulation	Displacement	NS	-	NS	NS	-	PT×SP significant
	Rotation	NS	-	+	NS	-	
	Loss in cable tension	-*	X	NS	NS	X	

-: effect of reduction; +: effect of augmentation; X: Not applicable; NS: Not significant. AA: Application Angle (NA vs WA); CT: Cable Type (SMA vs CoCr); PT: Plate Type (Y3 vs Zimmer); SP: Specimen (S1 vs S2); *: Only cables 1 & 2 present significant results.

APPENDIX

This appendix presents the calculated effects of the experiments using a Box, Hunter & Hunter (2005) two-level fractional factorial experimental design (2^{4-1}) methodology (Table A1). This design allows the effect of four parameters to be evaluated: Plate Type or **PT** (Zimmer vs. Y3), Cable Type or **CT** (Co-Cr vs. SMA), GT force Application Angle or **AA** (Normal Angle, NA vs. Wide Angle, WA) and Specimen or **SP** (two different femur specimens were used for each plate modality ($SP1_Z$, $SP2_Z$, $SP1_{Y3}$, $SP2_{Y3}$). Two replicates of the experiments – presented in Table A2 – were performed for a total of 24 trials.

Table A1 : Variables' modalities and descriptions for each experiment.

Experiment	PT		CT		AA		SP	
1	-1	Zimmer	-1	CoCr	1	WA	-1	$SP1_Z$
2	-1	Zimmer	1	SMA	1	WA	1	$SP2_Z$
3	1	Y3	-1	CoCr	1	WA	1	$SP2_{Y3}$
4	1	Y3	1	SMA	1	WA	-1	$SP1_{Y3}$
5	-1	Zimmer	-1	CoCr	-1	NA	1	$SP2_Z$
6	-1	Zimmer	1	SMA	-1	NA	-1	$SP1_Z$
7	1	Y3	-1	CoCr	-1	NA	-1	$SP1_{Y3}$
8	1	Y3	1	SMA	-1	NA	1	$SP2_{Y3}$

AA: Application Angle; CoCr: Cobalt-Chrome cables; CT: Cable Type; NA: Normal angle; PT: Plate Type; SP: Specimen; SPx_Z: specimen related to Zimmer plate; SPx_{Y3}: specimen related to Y3 plate; WA: Wide Angle.

Table A2 presents the calculated effects from the experimental design results for movements measured at the last loading cycle. The mean (m), the principal effects and the interaction effects are given for the maximum displacement point of the GT and the rotation of the GT fragment.

Table A2: Calculated effects for the GT movement for a single-cycle loading

	Maximum displacement		GT rotation†	
	Effect, mm	p	Effect, deg	p
m	*0.88	<0.0001	*0.84	<0.0001
CT	0.04	0.3883	0.15	0.1042
PT	*-0.27	<0.0001	*-0.85	<0.0001
AA	*0.35	<0.0001	*0.55	<0.0001
SP	0.13	0.0150	*0.30	0.0033
CT×PT | AA×SP	-0.01	0.8632	-0.07	0.4245
CT×AA | PT×SP	0.11	0.0284	0.22	0.0215
CT×SP | PT×AA	*-0.37	<0.0001	*-0.96	<0.0001

m: mean effect; AA: Application Angle; CT: Cable Type; PT: Plate Type; SP: Specimen; *significant parameters ($p<0.01$), † non-valid results, since SP is a significant factor (see explanations in the text).

Table A3 presents the calculated effects of GT displacements and rotations for permanent degradation over time (the 50-cycle experiment).

Table A3: Calculated effects of GT movement for permanent degradation over time

	Maximum displacement		GT rotation	
	Effect, mm	p	Effect, deg	p
μ	*0.91 mm	<0.0001	*1.12 deg	<0.0001
CT	-0.06	0.6940	-0.15	0.5397
PT	*-0.42	0.0081	*-1.20	0.0001
AA	0.24	0.1000	*0.83	0.0028
SP	0.13	0.3687	0.11	0.6472
CT×PT | AA×SP	0.32	0.0331	0.41	0.1057
CT×AA | PT×SP	*-0.55	0.0011	-0.65	0.0144
CT*SP | PT*AA	*-0.68	0.0002	*-1.43	<0.0001

μ: mean effect; AA: application angle; CT: Cable Type; PT: Plate Type; SP: Specimen;
* significant parameters ($p<0.01$)

For cable tension variation in the Zimmer plate, a logarithmic transformation was applied ($Y=ln(|y|)$) to obtain the standard deviation, essentially independent of the mean (Box, 2005).The model equation resulting from this transformation is:

— — — . [2]

Table A4 presents the mean (m) and the principal effects of CT, AA and SP for the cable tension amplitude of variation at the last loading cycle. Table A5 presents the results for total tension loss between the initial state and the last loading cycle.

Table A4: Calculated logarithmic effects on the cable tension during one loading cycle.

	Cable1		Cable2		Cable3		Cable4	
	Effect	p	Effect	p	Effect	p	Effect	p
μ	*1.06	0.0002	0.53	0.0565	*1.04	0.0034	0.63	0.0345
CT	*-1.91	0.0004	*-2.83	*0.0003	*-3.64	0.0001	*-3.90	<0.0001
AA	-0.18	0.5995	0.67	0.1977	0.07	0.8984	0.21	0.6876
SP	0.59	0.1106	0.48	0.3435	0.07	0.8932	0.05	0.9239

μ: mean effect; AA: application angle; CT: Cable Type; PT: Plate Type; SP: Specimen; * significant parameters ($p<0.01$)

Table A5: Calculated logarithmic effects of the variation of cable tension amplitude for the degradation accumulated during cycling.

	Cable1		Cable2		Cable3		Cable4	
	Effect	p	Effect	p	Effect	p	Effect	p
μ	*3.58	<0.0001	*3.29	<0.0001	*2.67	<0.0001	*3.05	<0.0001
CT	*-2.01	<0.0001	*-1.55	0.0008	-0.83	0.1534	-0.95	0.0241
AA	-0.22	0.3970	0.30	0.3334	0.34	0.5386	0.54	0.1536
SP	0.28	0.2893	-0.48	0.1423	-0.68	0.2363	0.36	0.3253

μ: mean effect; AA: application angle; CT: Cable Type; PT: Plate Type; SP: Specimen; * significant parameters ($p<0.01$)

RÉFÉRENCES BIBLIOGRAPHIQUES

Amstutz, H. C., L. L. Mai et I. Schmidt. 1984. « Results of interlocking wire trochanteric reattachment and technique refinements to prevent complications following total hip arthroplasty ». *Clin Orthop Relat Res*, n° 183 (Mar), p. 82-9.

Archibeck, Michael J., Aaron G. Rosenberg, Richard A. Berger et Craig D. Silverton. 2003. « Trochanteric Osteotomy and Fixation During Total Hip Arthroplasty ». *J Am Acad Orthop Surg,* vol. 11, p. 163-173.

ASM-International, et Granta-Design. 2010. *Materials for Medical Devices Database*, 2010. ASM International. <http://products.asminternational.org/meddev/index.aspx>.

Bal, B. S., P. Kazmier, T. Burd et T. Aleto. 2006. « Anterior trochanteric slide osteotomy for primary total hip arthroplasty. Review of nonunion and complications ». *J Arthroplasty,* vol. 21, n° 1 (Jan), p. 59-63.

Bal, B. S., B. T. Maurer et W. H. Harris. 1998. « Trochanteric union following revision total hip arthroplasty ». *J Arthroplasty,* vol. 13, n° 1 (Jan), p. 29-33.

Baril, Y., Y. Bourgeois, V. Brailovski, K. Duke, Y. G. Laflamme et Y. Petit. 2010a. « Improving greater trochanteric reattachment with a novel cable plate system ». In *Journal of Clinical Biomechanics* (Summited).

Baril, Y., Y. Bourgeois, V. Brailovski, K. Duke, Y. G. Laflamme et Y. Petit. 2010b. « Testing system for the comparative evaluation of greater throchanter reattachment devices
». *Experimental Techniques*, (Summited).

Barrack, R. L., et R. A. Butler. 2005. « Current status of trochanteric reattachment in complex total hip arthroplasty ». *Clin Orthop Relat Res,* vol. 441, (Dec), p. 237-42.

Berry, D. J., et M. E. Muller. 1993. « Chevron osteotomy and single wire reattachment of the greater trochanter in primary and revision total hip arthroplasty ». *Clin Orthop Relat Res*, n° 294 (Sep), p. 155-61.

Bourgeois, Y., Y. Petit et Y. G. Laflamme. 2010. « Finite Element Model of a Greater Trochanteric Reattachment System ». In *32nd Annual International Conference of the IEEE EMBS* (August 31 - September 4). Buenos Aires, Argentina.

Box, George E. P. (320-324). 2005. *Statistics for experimenters : design, innovation, and discovery*. Hoboken: Hoboken : Wiley-Interscience.

Brown, TD, ME Way et AB Jr Ferguson. 1981. « Mechanical characteristics of bone in femoral capital aseptic necrosis ». *Clin Orthop Relat Res,* vol. 156, p. 240-7.

Cegonino, J, JM Garcia Aznar, M Doblare, D Palanca, B Seral et l F Sera. 2004. « A comparative analysis of different treatments for distal femur fractures using the finite element method
». *Comput Methods Biomech Biomed Engin,* vol. 7, n° 5, p. 245-56.

Charnley, Sir John (140-151). 1979. *Low friction arthroplasty of the hip*. Berlin: Sprigner-Verlag, 393 p.

Chen, W. M., J. P. McAuley, C. A. Engh, Jr., R. H. Hopper, Jr. et C. A. Engh. 2000. « Extended slide trochanteric osteotomy for revision total hip arthroplasty ». *J Bone Joint Surg Am,* vol. 82, n° 9 (Sep), p. 1215-9.

Chen, W. P., C. L. Tai, C. H. Shih, P. H. Hsieh, M. C. Leou et M. S. Lee. 2004. « Selection of fixation devices in proximal femur rotational osteotomy: clinical complications and finite element analysis ». *Clin Biomech (Bristol, Avon),* vol. 19, n° 3 (Mar), p. 255-62.

Chin, K. R., et G. W. Brick. 2000. « Reattachment of the migrated ununited greater trochanter after revision hip arthroplasty: the abductor slide technique. A review of four cases ». *J Bone Joint Surg Am,* vol. 82, n° 3 (Mar), p. 401-8.

Dall, D. M., et A. W. Miles. 1983. « Re-attachment of the greater trochanter. The use of the trochanter cable-grip system ». *J Bone Joint Surg Br,* vol. 65, n° 1 (Jan), p. 55-9.

Elkholy, AH. 1995. « Design optimization of the hip nail-plate-screws implant ». *Comput Methods Programs Biomed,* vol. 48, n° 3, p. 221-7.

Ganesh, VK, K Ramakrishna et DN Ghista. 2005. « Biomechanics of bone-fracture fixation by stiffness-graded plates in comparison ». *Biomed Eng Online,* vol. 4, p. 46.

Heiner, A. D. 2008. « Structural properties of fourth-generation composite femurs and tibias ». *J Biomech.,* vol. 41, n° 15, p. 3282-4. Epub 2008 Oct 1.

Heller, M. O., G. Bergmann, J. P. Kassi, L. Claes, N. P. Haas et G. N. Duda. 2005. « Determination of muscle loading at the hip joint for use in pre-clinical testing ». *J Biomech,* vol. 38, n° 5 (May), p. 1155-63.

Hersh, C. K., R. P. Williams, L. W. Trick, D. Lanctot et K. Athanasiou. 1996. « Comparison of the mechanical performance of trochanteric fixation devices ». *Clin Orthop Relat Res*, n° 329 (Aug), p. 317-25.

Hillman, S. K. 2003. *Interactive functional anatomy*. London: Primal Pictures Ltd.

Huang, TJ, RW Hsu, CL Tai et WP Chen. 2003. « A biomechanical analysis of triangulation of anterior vertebral double-screw ». *Clin Biomech,* vol. 18, n° 6, p. S40-5.

Institut canadien d'information sur la santé. 2009. *Arthroplasties de la hanche et du genou au Canada — Rapport*
annuel de 2008-2009 du Registre canadien des remplacements articulaires (RCRA). Coll. « ICIS ». Ottawa (Ont.).

Jarit, Gregg J., Sathappan S. Sathappan, Anand Panchal, Eric Strauss et Paul E. Di Cesare. 2007. « Fixation Systems of Greater Trochanteric Osteotomies: Biomechanical and Clinical Outcomes ». *Journal of the American Academy of Orthopaedic Surgeons,* vol. 15, p. 614-624.

Koyama, K., F. Higuchi, M. Kubo, T. Okawa et A. Inoue. 2001. « Reattachment of the greater trochanter using the Dall-Miles cable grip system in revision hip arthroplasty ». *J Orthop Sci,* vol. 6, n° 1, p. 22-7.

Lakstein, D., D. Backstein, O. Safir, Y. Kosashvili et A. E. Gross. 2009. « Modified Trochanteric Slide for Complex Hip Arthroplasty Clinical Outcomes and Complication Rates ». *J Arthroplasty,* vol. 19, p. 19.

Mann, K.A., D.L. Bartel, T.M. Wright et A.H. Burstein. 1995. « Coulomb frictional interfaces in modeling cemented total hip replacements: a more ». *J Biomech,* vol. 28, n° 9, p. 1067-78.

Mann, K.A., D.L. Bartel, T.M. Wright et A.R. Ingraffea. 1991. « Mechanical characteristics of the stem-cement interface ». *J Orthop Res,* vol. 9, n° 6, p. 798-808.

Markolf, K. L., D. L. Hirschowitz et H. C. Amstutz. 1979. « Mechanical stability of the greater trochanter following osteotomy and reattachment by wiring ». *Clin Orthop Relat Res*, n° 141 (Jun), p. 111-21.

McCarthy, J. C., J. V. Bono, R. H. Turner, T. Kremchek et J. Lee. 1999. « The outcome of trochanteric reattachment in revision total hip arthroplasty with a Cable Grip System: mean 6-year follow-up ». *J Arthroplasty,* vol. 14, n° 7 (Oct), p. 810-4.

Netter, F. H. 2007. *Atlas of human anatomy*, Elsevier-Masson. Paris, 548 p.

Nicholson, P., D. Mulcahy et G. Fenelon. 2001. « Trochanteric union in revision hip arthroplasty ». *J Arthroplasty,* vol. 16, n° 1 (Jan), p. 65-9.

Noorda, RJ, et PI Wuisman. 2002. « Mennen plate fixation for the treatment of periprosthetic femoral fractures: a ». *J Bone Joint Surg Am*, p. 2211-5.

Nutton, R. W., et R. G. Checketts. 1984. « The effects of trochanteric osteotomy on abductor power ». *J Bone Joint Surg Br,* vol. 66, n° 2 (Mar), p. 180-3.

Pacific Research Laboratories. 2009. « Composite Bones ». <http://www.sawbones.com/products/bio/composite.aspx>.

Pappas, C. A., P. G. Young et A. J. Lee. 2006. « Development of the mennen 3 peripro fixation plate for the treatment of periprosthetic fractures of the femur ». *Proc Inst Mech Eng [H],* vol. 220, n° 7 (Oct), p. 775-85.

Peleg, E, R Mosheiff, M Liebergall et Y Mattan. 2006. « A short plate compression screw with diagonal bolts: a biomechanical evaluation performed experimentally and by numerical computation
». *Clin Biomech,* vol. 21, n° 9, p. 963-8.

Petit, Y., C.-É. Aubin et H. Labelle. 2004. « Spinal shape changes resulting from scoliotic spine surgical instrumentation expressed as intervertebral rotations and centers of rotation ». *Journal of Biomechanics,* vol. 37, n° 2, p. 173-180.

Petit, Y., G. Y. Laflamme et Y. Bourgeois. Summited (2008). *Orthopaedic fixation component and method*.

Plausinis, D., A. D. Speirs, B. A. Masri, D. S. Garbuz, C. P. Duncan et T. R. Oxland. 2003. « Fixation of trochanteric slide osteotomies: a biomechanical study ». *Clin Biomech (Bristol, Avon),* vol. 18, n° 9 (Nov), p. 856-63.

Poitout, D. 2004. « Fracture Healing and Stability of Fixation ». In *Biomechanics and Biomaterials in Orthopedics*, sous la dir. de Springer. p. 654. London: Springer-Verlag London Limited 2004.

Polgar, K., M. Viceconti et J. J. O'Connor. 2001. « A comparison between automatically generated linear and parabolic tetrahedra when used to mesh a human femur ». *Proceedings of the Institution of Mechanical Engineers, Part H (Journal of Engineering in Medicine),* vol. 215, n° H1, p. 85-94.

Pritchett, J. W. 2001. « Fracture of the greater trochanter after hip replacement ». *Clin Orthop Relat Res*, n° 390 (Sep), p. 221-6.

Schutzer, S. F., et W. H. Harris. 1988. « Trochanteric osteotomy for revision total hip arthroplasty. 97% union rate using a comprehensive approach ». *Clin Orthop Relat Res,* vol. 227, (Feb), p. 172-83.

Tai, C. L., W. P. Chen, H. H. Chen, C. Y. Lin et M. S. Lee. 2009. « Biomechanical optimization of different fixation modes for a proximal femoral L-osteotomy ». *BMC Musculoskelet Disord,* vol. 10, p. 112.

Takahira, N., M. Itoman, K. Uchiyama, S. Takasaki et K. Fukushima. 2010. « Reattachment of the greater trochanter in total hip arthroplasty: the pin-sleeve system compared with the Dall-Miles cable grip system ». *International Orthopaedics,* vol. 34, n° 6 (Aug), p. 793-797.

Tonino, AJ, CL Davidson, PJ Klopper et LA Linclau. 1976. « Protection from stress in bone and its effects. Experiments with stainless steel ». *J Bone Joint Surg Br,* vol. 58, n° 1, p. 107-13.

Tudor-Locke, C., T. L Hart et T. L. Washington. 2009. « Expected values for pedometer-determined physical activity in older populations ». *Int J Behav Nutr Phys Act,* vol. 6, p. 59.

Viceconti, M., L. Bellingeri, L. Cristofolini et A. Toni. 1998. « A comparative study on different methods of automatic mesh generation of human femurs ». *Medical Engineering & Physics,* vol. 20, n° 1, p. 1-10.

Von Fraunhofer, J. A., L. A. Schaper et D. Seligson. 1985. « The rotational friction characteristics of human long bones ». *Surface Technology,* vol. 25, n° 4, p. 377-383.

Zarin, J. S., D. Zurakowski et D. W. Burke. 2009. « Claw plate fixation of the greater trochanter in revision total hip arthroplasty ». *J Arthroplasty,* vol. 24, n° 2 (Feb), p. 272-80.